MODIFICATIONS OF EPOXY RESINS FOR IMPROVED MECHANICAL AND TRIBOLOGICAL PERFORMANCES AND THEIR EFFECTS ON CURING KINETICS

Wunpen Chonkaew, B.S., M.S.

Dissertation Prepared for the Degree of

DOCTOR OF PHILOSOPHY

UNIVERSITY OF NORTH TEXAS

May 2008

APPROVED:

Witold Brostow, Major Advisor
Kevin P. Menard, Co-Major Advisor
Thomas Scharf, Committee Member
Mohamed El Bouanani, Committee Member
Rick Reidy, Interim Chair of the Department of Materials Science and Engineering
Oscar Garcia, Dean of the College of Engineering
Sandra L. Terrell, Dean of the Robert B. Toulouse School of Graduate Studies

Chonkaew, Wunpen, Modifications of epoxy resins for improved mechanical and tribological performances and their effects on curing kinetics. Doctor of Philosophy (Materials Science), May 2008, 172 pp., 17 tables, 49 illustrations, references, 167 titles.

A commercial epoxy, diglycidyl ether of bisphenol-A, was modified by two different routes. One was the addition of silica to produce epoxy composites. Three different silane coupling agents, glycidyloxypropyl trimethoxy silane (GPS), γ-methacryloxypropyl trimethoxy silane (MAMS) and 3-mercaptopropyltriethoxy silane (MPS), were used as silica-surface modifiers. The effects of silica content, together with the effects of chemical surface treatment of silica, were studied. The results indicate that epoxy composites with silica exhibit mechanical and tribological properties as well as curing kinetics different than the pure epoxy. The optimum silica content for improved mechanical and tribological properties (low friction coefficient and wear rate) was different for each type of silane coupling agent. An unequivocal correlation between good mechanical and improved tribological properties was not found. Activation energy of overall reactions was affected by the addition of silica modified with MAMS and MPS, but not with GPS.

The second route was modification by fluorination. A new fluoro-epoxy oligomer was synthesized and incorporated into a commercial epoxy by a conventional blending method. The oligomer functioned as a catalyst in the curing of epoxy and polyamine. Thermal stability of the blends decreased slightly at a high oligomer content. Higher wear resistance, lower friction coefficient and higher toughness were found with increasing oligomer content; thus in this case there was a correlation between good

mechanical and improved tribological properties. The results indicated that increasing toughness and formation of a transfer film contribute to improved tribological performances.

ACKNOWLEDGEMENTS

I would like to greatly thank the Royal Thai Government for all their financial support provided to me throughout my studies. I wish to extend my gratitude to all the people whose help and encouragement motivated me throughout the dissertation process. First, I am deeply grateful for my advisor, Dr. Kevin P. Menard, for open access to all Perkin Elmer's instruments, but more importantly, for his guidance and expertise throughout my doctoral program. I thank my co-major advisor, Dr. Witold Brostow for encouraging me to constantly improve my writing. Dr. Brostow not only provided me opportunities to work with his worldwide colleagues but also encouraged and supported financially my international travels. I thank my committee members, especially Dr. Thomas Scharf, not only for their time and kindness but also for their valuable suggestions. I greatly appreciate all the help from Mr. John Sawyer and Ms Joan Jolly. I wish to express my heartfelt thanks to Dr. Tea Datashvili, and Ms. Angkana Onbun-uea for their true friendship, encouragement and reassurance. I thank my English writing tutors and Dr. Connie Menard for editing assistance. Last but not least, I wish to express my sincere gratitude to my parents for their unconditional love, patience and moral support.

TABLE OF CONTENTS

Page

ACKNOWLEDGEMENTS iii

LIST OF TABLES vii

LIST OF ILLUSTRATIONS viii

Chapter

1. OVERVIEW 1

1.1 References 4

2. EPOXY COMPOSITES FILLED WITH SILICA PARTICLES 5

2.1 Introduction 5

2.2 Polymer Composites 6

2.2.1 Polymer Matrix: Epoxy Resin 6

2.2.2 Inorganic Filler: Silica 8

2.2.3 Silane Coupling Agent 10

2.2.4 Inorganic-Organic Hybrid Materials 10

2.2.5 Advantages of Combining Inorganic–Organic Materials 12

2.2.6 Post-Synthetic Modification 15

2.3 Tribological Properties of Polymers 15

2.4 Experimental 17

2.4.1 Materials 17

2.4.2 Preparation of Silica and Silane Modified Silica Particles 19

2.4.3 Preparation of Epoxy Composites Filled with Silica 19

2.4.4 Infrared Spectroscopy 20

2.4.5 Thermogravimetric Analysis 20
2.4.6 Dynamic Mechanical Analysis 20
2.4.7 Scratch Resistance Testing 20
2.4.8 Pin on Disc Tribometer 21
2.4.9 Profilometer 22
2.4.10 Scanning Electron Microscopy and Optical Microscope 22
2.5 Results and Discussion 23
2.5.1 Characterization of Surface-Treated Silica 23
2.5.2 TGA Analysis 24
2.5.3 Dynamic Mechanical Analysis 33
2.5.4 Tensile Testing 46
2.5.5 Scratch Resistance Testing 51
2.5.6 Friction and Wear 54
2.6 References 77
3. MODIFICATION OF EPOXY RESIN WITH FLUORO-EPOXY OLIGOMER 81
3.1 Introduction 81
3.2 Experimental 84
3.2.1 Materials 84
3.2.2 Synthesis of Diglycidyl of Trifluoromethyl Aniline (DGTFA) Epoxy Oligomer 85
3.2.3 Determination of Epoxy Equivalent Weight 85
3.2.4 Preparation of DGEBA + DGTFA Epoxy Resin 86
3.2.5 Determination of Gel Content 86
3.2.6 Fourier Transform Infrared Spectroscopy (FTIR) 87

3.2.7 Thermogravimetric Analysis (TGA) 87
3.2.8 Dynamic Mechanical Analysis (DMA)..... 87
3.2.9 Mechanical Properties of DGEBA + DGTFA Epoxy 87
3.2.10 Pin on Disc Tribometer..... 87
3.2.11 Profilometer..... 88
3.2.12 Scanning Electron Microscope (SEM) and Optical Microscope 89
3.3 Results and Discussion..... 89
3.3.1 Characterization of Fluoro-Epoxy Oligomer 89
3.3.2 Thermogravimetric Analysis 91
3.3.3 Dynamic Mechanical Analysis..... 92
3.3.4 Mechanical Testing of the DGEBA + DGTFA Epoxy Resins 96
3.3.5 Friction and Wear..... 99
3.4 References..... 110
4. CURING KINETICS OF EPOXY-AMINE SYSTEMS..... 113
4.1 Introduction 113
4.2 Cure Mechanisms of Epoxy-Amine Systems 113
4.3 Kinetic Equations 114
4.4 Determination of Cure Kinetics 117
4.4.1 Cure Kinetics from Dynamic Tests 117
4.4.2 Cure Kinetics from Isothermal Tests 121
4.5 Effects of Additives and Fillers on Curing Kinetics..... 123
4.6 Experimental..... 125
4.6.1 Materials..... 125

4.6.2 Preparation of Epoxy + Silica Composites 125

4.6.3 Preparation of the Fluorinated Modified Epoxy 125

4.6.4 Instrumentation 126

4.7 Results and Discussion 127

4.7.1 Curing of DGEBA + DGTFA Epoxy with Polyamine 127

4.7.2 Kinetics of Epoxy + Silica Composites 137

4.8 References 156

5. CONCLUDING REMARKS 159

APPENDIX

A. CONTACT AREA, MAXIMUM CONTACT PRESSURE AND AVERAGE CONTACT PRESSURE 163

B. MOVING HEAT SOURCE 166

C. FLASH TEMPERATURE IN CIRCULAR CONTACT 169

D. AVERAGE ROUGHNESS PARAMETERS 171

LIST OF TABLES

Page

2.1 TGA data of pure epoxy, silica powder and epoxy composites 32

2.2 DMA data of epoxy composites filled with neat silica 42

2.3 DMA data of epoxy composites filled with surface-treated silica 43

2.4 Activation energy for relaxation of epoxy + silica hybrids 45

2.5 Interfacial shear stress of epoxy + silica composites 70

3.1 TGA data the cured DGEBA + DGTFA epoxy resins 92

3.2 DMA data of DGEBA + DGTFA epoxies curing with polyamine 94

3.3 Data from flexural testing of DGEBA + DGTFA epoxy resins at 25°C 98

3.4 Surface roughness of DGEBA + DGTFA epoxy resins 100

3.5 Interfacial shear stress of DGEBA + DGTFA epoxy resins 104

4.1 The E_a and n values of DGEBA blended with various amounts of DGTFA curing with polyamine obtained from Pyris 7 software 130

4.2 Exothermic peak maxima T_p and total heat of reaction ΔH_{rxn} of DGEBA + DGTFA curing with polyamine 133

4.3 Kinetic parameters of DGEBA + DGTFA epoxy curing with polyamine from multiple scanning rate methods 135

4.4 Activation energy E_a of pure epoxy resin and epoxy composites filled with different types of silica at the 10 phr 138

4.5 Time at maximum rate of reaction t_p and maximum rate of reaction r_p at different curing temperatures 147

4.6 Kinetic parameters k_1, k_2, m and n as determined from the autocatalytic kinetic model for epoxy + 10.0 phr silica at various curing temperatures 152

4.7 Activation energy from isothermal scan method for pure epoxy resin and epoxy composites filled with different types of silica at 10 phr 153

LIST OF ILLUSTRATIONS

Figure Page

2.1 FTIR spectra of (a) neat silica, (b) silica-MAMS, (c) silica-MPS and (d) silica-GPS 23

2.2 TGA thermograms of different types of silica powder under air atmosphere 27

2.3 TGA thermograms of epoxy composites filled with (a) neat silica and (b) silica-GPS under N_2 atmosphere 28

2.3 TGA thermograms of epoxy composites filled with (c) silica-MAMS and (d) silica-MPS under N_2 atmosphere 29

2.4 TGA thermograms of epoxy composites filled with (a) neat silica and (b) silica-GPS under air atmosphere 30

2.4 TGA thermograms of epoxy composites filled with (a) silica-MAMS and (b) silica-MPS under air atmosphere 31

2.5 (a) Storage modulus, (b) loss modulus and (c) tan δ of epoxy + neat silica composites 38

2.6 (a) Storage modulus, (b) loss modulus and (c) tan δ of epoxy + silica-GPS composites 39

2.7 (a) Storage modulus, (b) loss modulus and (c) tan δ of epoxy + silica-MAMS composites 40

2.8 (a) Storage modulus, (b) loss modulus and (c) tan δ of epoxy + silica-MPS composites 41

2.9 Tan δ of pure epoxy as a function of temperature at frequency 1, 5, 10 and 20 Hz 44

2.10 Calculation of activation energy for relaxation process of pure epoxy 45

2.11 Data from tensile testing at room temperature 47

2.12 SEM micrograph of epoxy composites filled with (a) 5.0 phr of neat silica, (b) 20.0 phr of neat silica, (c) 5.0 phr of silica-GPS and (d) 20.0 phr of silica-GPS 50

2.13 Penetration depth R_p and residual depth R_h as a function of of silica content at applied forces of 5.0 N and 10.0 N 51

2.14 Percent elastic recovery as a function of silica content for (a) epoxy + neat silica, (b) epoxy + silica-GPS, (c) epoxy + silica-MAMS and (d) epoxy + silica-MPS 54

2.15 Profilometer cross section of wear traces for (a) pure epoxy, (b) epoxy + neat silica, (c) epoxy + silica-GPS, (d) epoxy + silica-MAMS and (e) epoxy + silica-MPS after sliding against Si_3N_4. Silica content: 20.0 phr; sliding speed: 200 rpm; normal load: 5.0 N; revolution: 10,000 turns 55

2.16 Wear rate of the epoxy composites filled with (a) neat silica, (b) silica-GPS, (c) silica-MAMS, (d) silica-MPS. Sliding speed: 200 rpm; normal load: 5.0 N; revolution: 10,000 turns 56

2.17 Optical image (100x) and Raman mapping of worn surface for pure epoxy. Condition of sliding wear tests: (a, b) normal load of 3.0 N; sliding speed of 200 rpm; revolution of 10,000 turns (c, d) normal load of 10.0 N; speed of 200 rpm; revolution of 10,000 turns 60

2.18 The SEM micrographs of the worn surface for (a, b, c) pure epoxy, (d, e, f) epoxy + neat silica and (g, h, i) epoxy + silica-GPS. Silica content: 15.0 phr. Condition of sliding wear tests: normal load of 5.0 N; sliding speed of 200 rpm; revolution of 10,000 turns. Magnification: 260x for (a, d, g), 1600x for (b, e, h) and 5800x for (c, f, i) 64

2.18 The SEM micrographs of the worn surface for (j, k, l) epoxy + silica-MAMS and (m, n, o) epoxy + silica-MPS. Silica content: 15.0 phr. Condition of sliding wear tests: normal load of 5.0 N; sliding speed of 200 rpm; revolution of 10,000 turns. Magnifications: 260x for (j, m), 1600x for (k, n) and 5800x for (l,o) 65

2.19 Evolution with time of the friction coefficient under a normal load of 5.0 N and sliding speed of 200 rpm against Si_3N_4 ball for (a) epoxy + neat silica and (b) epoxy + silica-GPS 73

2.19 Evolution with time of the friction coefficient under a normal load of 5.0 N and sliding speed of 200 rpm against Si_3N_4 ball for (c) epoxy + silica-MAMS and (d) epoxy + silica-MPS 74

2.20 Steady state friction coefficient of (a) epoxy + neat silica, (b) epoxy + silica-GPS, (c) epoxy + silica-MAMS and (d) epoxy + silica-MPS systems. Normal load: 5.0 N; sliding speed: 200 rpm; revolution: 10,000 turns 75

2.21 Optical image (100x) of transfer film formed on the surface of Si_3N_4 counterface after sliding against (a) pure epoxy, (b) epoxy + neat silica, (c) epoxy + silica-GPS, (d) epoxy + silica-MAMS and (e) epoxy + silica-MPS. Normal load: 5.0 N; sliding speed: 200 rpm; revolution: 10000 turns 76

3.1 FT-IR spectrum of DGTFA 90

3.2 TGA thermograms of the cured DGEBA + DGTFA epoxy resins 91

3.3 (a) Storage modulus, (b) loss modulus and (c) tan δ of DGEBA + DGTFA epoxies curing with polyamine 93

3.4 Percent extraction as a function of DGTFA content 96

3.5 Flexural stress vs percent flexural strain for DGEBA + DGTFA epoxy resins measured at 25.0^{o}C 98

3.6 Evolution of the friction coefficient with time for DGTFA epoxy resins blending with various amounts of DGTFA 100

3.7 Steady state friction coefficient of DGEBA + DGTFA epoxy resins as a function of DGTFA content 101

3.8 Profilometer cross section of wear traces for (a) pure DGEBA epoxy resin, DGEBA epoxy resin blending with (b) 2.5 phr of DGTFA, (c) 5.0 phr of DGTFA, (d) 10.0 phr of DGTFA, (e) 15.0 phr of DGTFA and (f) 20.0 phr of DGTFA after sliding against Si_3N_3. Sliding speed: 200 rpm; normal load: 5.0 N; revolution: 5,000 turns 102

3.9 Wear rate of DGEBA + DGTFA epoxy resins as a function of DGTFA content 103

3.10 The SEM micrographs of the worn surface for (a, b, c) pure DGEBA epoxy resin, (d, e, f) DGEBA epoxy blended with 5.0 phr of DGTFA and (g, h, i) DGEBA epoxy blended with 15.0 phr of DGTFA. Condition of sliding wear tests: normal load of 5.0 N; sliding speed of 200 rpm revolution of 5,000 turns. Magnification: 120x for (a, d, g), 2000x for (b, e, h) and 5000x for (c, f, i) 108

3.11 Wear rate as a function of the product of flexural strength and strain at deflection point for DGEBA + DGTFA epoxy resins 109

3.12 Optical image (200x) of transfer film formed on the surface of Si_3N_4 counterface after sliding against (a) pure DGEBA epoxy and DGEBA epoxy blended with (b) 5.0 phr

of DGTFA and (c) 20.0 phr of DGTFA. Normal load: 5.0 N; sliding speed: 200 rpm; revolution: 5000 turns 109

4.1 Dynamic DSC thermograms at 10.0°C/min for unreacted DGEBA + DGTFA curing with polyamine 128

4.2 Dynamic DSC thermograms at different heating rates for the unreacted (a) pure epoxy DGEBA, (b) DGEBA + 2.5 phr of DGTFA, (c) DGEBA + 5.0 phr of DGTFA, (d) DGEBA + 10.0 phr of DGTFA, (e) DGEBA + 15.0 phr of DGTFA and (f) DGEBA + 20.0 phr of DGTFA curing with polyamine 131

4.3 Plot of $ln\ (\beta/T_p^2)$ versus $1/T_p$ (Kissinger) and $ln\ \beta$ versus $1/T_p$ (Ozawa) for (a) pure epoxy DGEBA,(b) DGEBA + 2.5 phr of DGTFA, (c) DGEBA+ 5.0 phr DGTFA, (d) DGEBA + 10.0 phr DGTFA, (e) DGEBA + 15.0 phr DGTFA and (f) DGEBA + 20.0 phr DGTFA curing with polyamine 134

4.4 Dynamic DSC thermograms at different heating rates for the unreacted (a) pure epoxy (b) epoxy DGEBA + 10.0 phr of neat silica, (c) epoxy DGEBA + 10.0 phr of silica-GPS, (d) epoxy DGEBA + 10.0 phr of silica-MAMS and (e) epoxy DGEBA + 10.0 phr of silica-MPS 139

4.5 Plot of $ln\ (\beta/T_p^2)$ versus $1/T_p$ (Kissinger) and $ln\ \beta$ versus $1/T_p$ (Ozawa) for (a) pure epoxy, (b) epoxy DGEBA+ 10.0 phr of neat silica, (c) epoxy DGEBA+ 10.0 phr of silica-GPS, (d) epoxy DGEBA+ 10.0 phr of silica-MAMS and (e) epoxy DGEBA + 10.0 phr of silica-MPS 140

4.6 Conversion as a function of time for pure epoxy curing with cycloaliphatic amine at different curing temperatures 143

4.7 Conversion as a function of time for (a) epoxy + neat silica, (b) epoxy+silica-GPS, (c) epoxy+silica-MAMS and (d) epoxy+silica-MPS curing with cycloaliphatic amine at different curing temperatures 144

4.8 Reaction rate as a function of time for (a) pure epoxy, (b) epoxy + neat silica, (c) epoxy + silica-GPS, (d) epoxy + silica-MAMS and (e) epoxy+silica-MPS curing with cycloaliphatic amine 146

4.9 Comparison of experimental data with model predictions: rate versus conversion at 90°C for (a) pure epoxy, (b) epoxy + 10.0 phr of neat silica, (c) epoxy + 10.0 phr of silica-MAMS, (d) epoxy + 10.0 phr of silica-GPS and (e) epoxy + 10.0 phr of silica-MPS curing with cycloaliphatic amine 150

4.10 Temperature dependence of rate constant k_1 and k_2 in Kamal's equation (Equation 4.4) for (a) pure epoxy, (b) epoxy + 10.0 phr neat silica, (c) epoxy + 10.0 phr silica-GPS, (d) epoxy + 10.0 phr silica-MAMS and (e) epoxy + 10.0 phr silica-MPS curing with cycloaliphatic amine 151

A.I Contact between a sphere and a flat surface 165

A.II Schematic of a surface profile 172

CHAPTER 1

OVERVIEW

Epoxy resins are considered to be one of the most important classes of thermosetting polymers. They are widely used in a variety of technical applications such as adhesives, protective coatings, sealants, and matrices for composite materials in aerospace and leisure industries [1, 2]. This wide range of applications arises from characteristics of epoxy resins including high chemical and corrosion resistance, good mechanical and thermal properties, outstanding adhesion to various substrates, low shrinkage upon cure, flexibility, good electrical properties, and easy processability [2, 3]. However, despite these advantages, there are also some drawbacks: high water uptake [1], moisture absorption [4] and brittle nature owing to their highly cross-linked structures [5], low wear resistance and high friction coefficient [6].

Several methods have been used to lessen the friction and wear of polymeric materials. Basic concepts applied to achieve such an improvement are reduction of their adhesion to the counterpart materials and enhancement of mechanical properties such as hardness, modulus and compressive strength. These effects can be done by adding certain fillers. To reduce adhesion, internal lubricants such as polytetrafluoroethylene (PTFE) or perfluoropolyether (PFPE) are frequently used. The presence of fluorine atoms in their respective molecular backbones is believed to be responsible for their low surface energy. Considerable efforts have been expended in the past to improve tribological properties of epoxies by incorporation of fluorine atoms into the systems. Fluoropolymers [7, 8] or fluoro epoxy monomers [9-12] were blended with epoxy resins. The fluorination of the epoxy resins by physical [4] or chemical

methods [13] has been used. However, lower friction coefficient sometimes has to be sacrificed for the phase separation [7] or even for the reduction in wear resistance. To enhance the mechanical properties, fillers in forms of particulates and fibers are often used to reinforce polymeric matrices. Fillers such as carbon fibers [14, 15], titanium oxide [16], silica [17, 18], alumina [19-21] and others were reported to improve the wear resistance. However, the deterioration of wear resistance was reported as well, when short carbon fibers [22], quartz and glass particles [23] or silica and dolomite [24] were added to polymers.

Because tribological properties are not material properties but environmentally dependent, their understanding is not sufficient. Therefore, in this dissertation, tribological properties, together with thermal and mechanical properties of fluoro-modified epoxy resins and epoxy + silica composites and their correlation were investigated. Diglycidyl ether of bisphenol-A cured with two different kinds of amines, namely polyamines and cycloaliphatic amines, was selected as the model for the studies. Two different ways for the modification were investigated. The first was the addition of silica particles to the epoxy system. The effects of silica loading, as well as the effect of chemical surface treatment of silica, were studied. Three silane coupling agents, glycidyloxypropyl trimethoxy silane (GPS), γ-methacryloxypropyl trimethoxy silane (MAMS) and 3-mercaptopropyltriethoxy silane (MPS), were used to treat silica particles. The second was the addition of fluoro-functionalized epoxy oligomer to the epoxy system. A new epoxy oligomer, diglycidyl of trifluoromethyl aniline (DGTFA), was synthesized and blended with a commercial epoxy resin. The effects of DGTFA content were studied.

Thus, this work includes 3 main chapters (Chapters 2 to 4) in which the experimental procedures and results are discussed. Chapter 2 reports on a study of epoxy composites filled with neat silica and surface-treated silica. A conventional blending method was selected as a mean for incorporating different types of silica particles into the systems. Effects of silica loading, together with chemical surface treatments on the thermal and mechanical properties, as well as tribological properties, are evaluated. A brief review of epoxy + silica composites and effects of fillers on tribological properties of epoxies are provided as well. Chapter 3 reports on a study of a commercial epoxy blended with a novel fluoro-functionalized epoxy (DGTFA). Synthesis and characterization of fluoro-functionalized epoxy oligomers are provided. The effects of DGTFA on the thermal and mechanical, as well as tribological properties are demonstrated. The possibility of mechanical-tribological property correlation is discussed. Lastly, curing kinetics of epoxy resins is studied and reported in chapter 4. The effects of fillers, both DGTFA and silica, on kinetic and curing mechanisms are discussed. Moreover, a brief review of curing kinetic techniques both in isothermal and in non-isothermal methods is given. The dissertation then closes with some concluding remarks (chapter 5).

1.1 References

[1] Lee LH. Adhesives, sealents and soatings for space and harsh environments, New York: Plenum Press, 1988.

[2] Distasio JI. Epoxy resin technology: development since 1979, New Jersey: Noyes Data, 1982.

[3] May CA. Epoxy resins: chemistry and technology, New York: Marcel Dekker, 1988.

[4] Han HS, Tan KL, Kang ET. J Appl Polym Sci 2000;76(3):296-304.

[5] Pascault JP, Sautereau H, Verdu J, Williams RJJ. Thermosetting polymers, New York: Marcel Dekker, 2002.

[6] Brostow W, Cassidy PE, Macossay J, Pietkiewicz D, Venumbaka S. Polym Internat 2003;52:1498-1505.

[7] Brostow W, Cassidy PE, Hagg HE, Jaklewicz M, Montemartini PE. Polymer 2001;42(19):7971-7977.

[8] Kasemura T, Oshibe Y, Uozumi H, Kawai S, Yamada Y, Ohmura H, Yamamoto T. J Appl Polym Sci 1993;47(12):2207-2216.

[9] Hu HP, Gilbert RD, Fornes RE. J Polym Sci Polym Chem 1987;25(5):1235-1248.

[10] Lee JR, Jin FL, Park SJ, Park JM. Surf Coat Technol 2004;180-181:650-654.

[11] Sangermano M, Bongiovanni R, Malucelli G, Priola A, Pollicino A, Recca A. J Appl Polym Sci 2003;89(6):1524-1529.

[12] van de Grampel RD, Ming W, van Gennip WJH, van der Velden F, Laven J, Niemantsverdriet JW, van der Linde R. Polymer 2005;46(23):10531-10537.

[13] Park SJ, Jin FL, Shin JS. Mater Sci Eng 2005;390(1-2):240-245.

[14] Lee HG, Hwang HY, Lee DG. Wear 2006;261:453-459.

[15] Zhang H, Zhang Z, Friedrich K. Compos Sci Technol 2007;67:222-230.

[16] Chang L, Zhang Z, Breidt C, Friedrich K. Wear 2005;258:141-148.

[17] Xing XS, Li RKY. Wear 2004;256:21-26.

[18] Zhang MQ, Rong MZ, Yu SL, Wetzel B, Friedrich K. Macromol Mater Eng 2002;287:111-115.

[19] Shi G, Zhang MQ, Rong MZ, Wetzel B, Friedrich K. Wear 2004;256:1072-1081.

[20] Vassileva E, Friedrich K. J Appl Polym Sci 2006;101:4410-4417.

[21] Wetzel B, Haupert F, Zhang MQ. Compos Sci Technol 2003;63:2055-2067.

[22] Lancaster JK. Friction and wear. In: Jenkins AD, editor. Polymer science, a material science handbook, Amsterdam: North-Holland, 1972.

[23] Prasad SV, Calvert PD. J Mater Sci 1980;15:1746-1754.

[24] Xu YM, Mellor BG. Wear 2001;251:1522-1531.

CHAPTER 2

EPOXY COMPOSITES FILLED WITH SILICA PARTICLES

2.1 Introduction

Epoxy resins, being organic in nature, have their limitations for high performance applications because they are both mechanically weak and thermally unstable. Inorganic materials are brittle, but have a high thermal resistance. It has been found that inorganic polymers have high heat resistance and good mechanical and optical properties [1, 2].

Incorporating inorganic materials can provide enhancement in mechanical and thermal properties. The formation of organic-inorganic composites provides a feasible approach to simultaneously improving thermal properties, mechanical properties, flame retardant properties and resistance to scratching, as well as dimensional stability of epoxy resins [3]. The combination of epoxy and inorganic composites, thus, has drawn considerable attention.

Several metal oxides can be used as fillers, in particular SiO_2, TiO_2, ZnO and CeO_2 [4]. Silica (SiO_2) containing composites are the most extensively studied due to a wide variety of applications, including structural materials, adhesives and coating materials. They show remarkable barrier properties to gas and moisture, as well as resistance to stain [5, 6].

However, the success of their applications depends on a good understanding of the nature of composites and the structure-property relation. Besides the mechanical properties, understanding their tribological response, including wear and friction, is essential. In particular, the understanding of wear behavior of inorganic + epoxy

composites is still limited. This work looks at the preparation of silica reinforced epoxy resins and studies their structure-property relationships by looking at the chemical structure and morphology of silica + epoxy composites, as well as the interaction between a matrix phase and a dispersed phase, that affect properties of epoxy composites.

2.2 Polymer Composites

Polymer composites or polymer matrix composites (PMCs) are used increasingly for engineering applications. One part of composite materials here is represented by epoxy resin. Because of the demand for the applications to withstand high mechanical and tribological loads, this matrix is necessarily reinforced with fillers. Silica is usually chosen as filler because it stiffens the matrix materials. It is also able to increase the strength under a certain load condition, but it may also cause detrimental effects at the same time. For more detail about each component, a brief description of the polymer matrix and the filler used in the present studies follows.

2.2.1 Polymer Matrix: Epoxy Resin

Epoxy resins [7] are characterized by a three-membered ring known as the epoxy, epoxide, oxirane, or ethoxyline group:

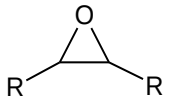

where R represents alkyl groups or a hydrogen atom

Scheme 2.1. Chemical structure of epoxy resins.

Commercial epoxy resins contain aliphatic, cycloaliphatic, or aromatic backbones. The capability of the epoxy ring to react with a variety of reagents imparts versatility to

the resins. Reacting with curing agents gives it a three dimensional, insoluble, and infusible network. The choice of which curing agent to use depends on processing methods, curing conditions and physical and chemical properties desired. Curing agents are either catalytic or coreactive. Catalytic curing agents, including lewis bases, lewis acids and photoinitiated cationic cures, function as initiators for epoxy resin homopolymerization. Coreactive curing agents, including amines and acid anhydride, act as comonomers in the polymerization process. In this study, only amine types of coreactive curing agents were used. Descriptions of amines are described below:

A. Aliphatic amines and amidoamines.

These curing agents gel rapidly at room temperature, but a complete through cure at room temperature will take about five to seven days. Heating the material can reduce this time to a few hours.

Typical cure cycles for these curing agents are 60^{o}C to 110^{o}C for 2 to 4 hours. A higher temperature is not recommended since some of these curing agents contain plasticizers intended to remain in the thermosets and they may volatilize during the cure.

B. Cycloaliphatic amines.

These curing agents gel rapidly at room temperature but a complete through cure at room temperature is not possible. The gelled materials appear hard, but the formulation will be brittle and cured less than 60%. Heating the material is necessary for optimum properties. Typical cure cycles for these curing agents are staged at 70^{o}C to 90^{o}C for 30 minutes followed by 150^{o}C to 170^{o}C for 2 to 3 hours.

C. Aromatic amines.

These curing agents gel very slowly at room temperature, but like cycloaliphatic amines a complete cure at room temperature is not possible. The gelled materials appear to be hard, but again the formulation will be brittle and weak with a low percent cure conversion. Heating the material is necessary for optimum properties.

Typical cure cycles for these curing agents are staged at 80^{o}C to 90^{o}C for 2 hours followed by 150^{o}C to 170^{o}C for 2 to 3 hours. Curing at high temperature initially is not recommended because the potential exists to establish a tightly crosslinked network so rapidly that remaining unreacted sites will be sterically hindered and will not completely cure even if exposed to higher temperatures. This will lead to less than optimum mechanical properties. In general, characteristics such as stiffness, strength, and glass transition temperature increase with increased cross-link, but toughness decreases. Thus, other constituents: fillers, solvents, diluents, plasticizers and accelerators were used to facilitate processing and modify the cured resin properties.

2.2.2 Inorganic Filler: Silica

Silica is one of the most abundant oxide materials in the earth's crust. It is commonly found naturally in sandstone, silica sand and quartzite. It is used as the starting material for production of silicate glasses and ceramics. Silica can exist either in an amorphous form, known as vitreous silica, or in a crystalline form. There are three crystalline forms of silica: quartz, tridymite and cristobalite. Each of these particular crystalline forms can be differentiated into two different forms—the high temperature form and the low temperature form—depending on the processing temperature and pressure. The high temperature polymorph consists of different arrangements of

undistorted SiO_4 tetrahedra linked together by shared corners. The lower temperature polymorph has a similar structure but is distorted [8].

Besides the silica occurring in nature, synthetic silica can be produced by a carbon arc, plasma arc, gas fired continual extrusion or carbon electrode fusion. By these methods, a high purity grade of silica with silica content of 99.4-99.9% can be produced. Fused silica is primarily used in the electronics industry where its good dielectric and insulating properties are exploited; it may, however, also be used as a refractory material or in investment casting.

Another interesting and popular process for obtaining silica is through the sol-gel process. This process allows synthesizing ceramic materials with high purity and homogeneity. The process occurs in liquid solution organometallic precursors. The typical precursors used to prepare silica are tetramethyl orthosilicate (TMOS) and tetraethyl orthosilicate (TEOS). The process is conducted through hydrolysis and condensation of silicon alkoxide in the presence of a mixture of water and alcohol at a low temperature [9]. General chemical reactions of the process can be demonstrated as:

$$\text{M-O-R} + H_2O \rightarrow \text{M-OH} + \text{R-OH} \text{ (hydrolysis)}$$

$$\text{M-OH} + \text{HO-M} \rightarrow \text{M-O-M} + H_2O \text{ (water condensation)}$$

$$\text{M-O-R} + \text{HO-M} \rightarrow \text{M-O-M} + \text{R-OH} \text{ (alcohol condensation)}$$

During the hydrolysis and condensation processes, the silicate monomer nucleates in a supersaturated solution and grows to dimeric, cyclic, spherical particles or gel networks [10]. One important characteristic of silica, compared to other oxides, is that the condensation of $Si(OH)_4$ forms a very stable amorphous SiO_2 instead of a crystalline

SiO_2 [11]. Thus, SiO_2 in variable sizes and shapes, but with a constant chemical composition, can be prepared through controlling parameters such as the concentration of alkoxide, amount of water, concentration of catalyst, solvent, aging time and electrolyte additive [12].

2.2.3 Silane Coupling Agents

Silane coupling agents are silicon-based chemicals that contain both inorganic and organic reactivity in the same molecule. They act as bridges at the interface between the inorganic and organic parts. Thus, the two dissimilar materials can be bonded or coupled. The general structure of silane coupling agents is:

$$(RO)_3SiCH_2CH_2CH_2\text{-}X$$

where RO is a hydrolyzable group, such as methoxy, ethoxy, or acetoxy, and X is an organofunctional group, such as methacryloxy or epoxide groups.

2.2.4 Inorganic-Organic Hybrid Materials

Hybrid materials can be classified in several ways, depending on the relative composition of the constituent components, on the chemical interaction between the constituent species, and on the various functionalities that can be attained. Novak [13] classified the types of hybrids into five major classes based on their macromolecular structures and phase connectivity as follows:

Type 1: Soluble, preformed organic polymers embedded in an inorganic network.

Type 2: Embedded, preformed organic polymer possessing covalent bonds to the inorganic network.

Type 3: Mutually interpenetrating organic-inorganic network.

Type 4: Mutually interpenetrating networks with covalent bonds between the organic and inorganic phases.

Type 5: Non-shrinking sol-gel composite materials.

The classification commonly adopted by the scientific community is based on the nature of chemical bonding between the organic and inorganic components [11]. Hybrid materials can be classified into two main classes:

Class I: Systems in which one of the components, either inorganic or organic, is embedded in a network of the other one and is linked by weak forces such as van der Waals or hydrogen bonds.

Class II: Systems in which the two components are chemically linked to each other by strong, covalent bonds.

Hybrids can be created by mixing polymers and inorganic materials at a molecular level, and several methods have been used to prepare inorganic-organic materials. They can be produced by the interpenetration, inclusion or dispersion of an inorganic component. Interactions, such as hydrophilic-hydrophobic interaction, coordinative or covalent bonding, provide stabilization of the incompatible phases with a large interface area. Three main synthetic routes for creating hybrid materials can be identified. One involves the polymerization of organic functional groups from a preformed sol-gel network [14]. Alternatively, the sol-gel hydrolysis and condensation are carried out from the preformed functional organic polymers or oligomers, where a trialkoxysilane group is usually the reactive functionality. In both cases, if trialkoxysilane derivatives are used as the sol-gel precursor, the polyhedral oligomeric silsesquioxane (POSS) can arise. This method is tedious due to the difficulties in the compatibilization of the two

components [15]. Moreover, the formation of a true hybrid is still elusive because the interactions between the inorganic and organic components are still low. One way of increasing the interaction, thereby enhancing the inorganic–organic interfacial compatibility, is to use silane coupling agents as crosslinkers [16, 17]. With such systems, the inorganic and organic networks are formed together to achieve homogeneous phase morphologies which are difficult to produce by other methods.

2.2.5 Advantages of Combining Inorganic–Organic Materials

Organic polymers usually have some superior characteristic with respect to their flexibility and processabilty. On the other hand, inorganic polymers have high heat resistance and good mechanical and optical properties. By combining them together, one can favorably obtain the combination of superior properties of both components in one material. There are many possible combinations of components to invent a new set of hybrids with a large spectrum of known and as yet unknown properties. One of the examples is the incorporation of silica particles into polymer matrices. The resulting silica containing nanocomposites show remarkable barrier properties to gases and moisture as well as a very good resistance to staining. Ochi et al. [17] synthesized epoxy+silica hybrids from a diglycidyl ether of bisphenol A (DGEBA) epoxy resin and a γ-glycidoxyproppyltrimethoxysilane (GPTMS) and from the epoxy and tetramethylorthosilicate (TMOS) by utilizing a sol-gel process. They found that the silica networks dispersed uniformly in the hybrids. The hybrids with GPTMS showed a very high adhesion strength with the silicone rubber, while it was not found in the hybrids with TMOS. Lin et al. [15] prepared epoxy DGEBA + SiO_2 and polyimide + SiO_2 nanocomposites based on phosphorus-containing triethoxysilane. The resulting epoxy

+ SiO_2 nanocomposites exhibit a better char yield, higher glass transition temperature, higher flame retardancy and lower dielectric constant than those of the neat epoxy system. The glass transition temperature in polyimide+SiO_2 nanocomposites decreased slightly with the content of the triethoxysilane due to the plasticizing effect of aliphatic bonds. Wang et al. [18] prepared polyimide + silica hybrid materials via a sol-gel process using silicic acid oligomer extracted from water glass. A γ-aminopropyltriethoxysilane (APTES) was used as a coupling agent. They found a very good dispersion of inorganic particles within the polyimide matrix, and the coefficients of thermal expansion of the hybrids were lower than those of pure polyimide. Jensen et al. [14] prepared the hybrids by diffusing an uncured epoxy DGEBA and a bis (p-aminocyclohexyl) methane curing agent into the spherical particles of condensed and crosslinked 3-glycidoxypropyltrimethoxysilane (GPS).

Even though there are several advantages reported, the hybrids prepared by the in situ sol-gel process still have some disadvantages due to the nature of the method itself. In the epoxy + silica hybrids formed by the sol-gel process, the evaporation of solvent, curing reaction of epoxy and condensation reaction of the hydrolyzed alkoxysilane occur simultaneously. Lui et al. [19] pointed out several interesting drawbacks to the preparation of hybrids by the sol-gel process. One problem was that the solution process of sol-gel technique was not practical in the manufacturing processes of epoxy molding compounds. Moreover, the simultaneously released volatiles from the condensation of alkoxysilane sol would certainly bring about undesirable effects to the resins and present difficulties in processing during the epoxy curing reaction. Another drawback was the deterioration of the thermal stability due to

the residual of the silanoxy groups in the resulting hybrid. These silanoxy groups might undergo a dehydration reaction under the high temperature in the processing and during the using period of the nanocomposites.

In addition to the sol-gel process, blending inorganic fillers and organic polymeric materials in molecular scale to form inorganic-organic composites has been frequently chosen, including in the present studies. The word “composites” and “hybrids” therefore were used interchangeably in this work. Basically, inorganic fillers can be layered clay, nanoparticles, nanofibers and other synthetic materials. For the hybrids formed by this method, the interaction between the inorganic and the organic parts is low. Phase separation often occurs, usually detrimental to one or more of the properties of the resulting hybrids. To avoid those problems, Lui et al. [19, 20] prepared epoxy + silica nanocomposites by directly blending DGEBA with nanoscale colloidal silica and then curing with 4,4-diaminodiphenylmethane. They found that the hybrids showed a good transparency and miscibility. Moreover, the thermal stability of the epoxy resin was improved with incorporation of the colloidal silica.

Recently, several authors demonstrated that the composites of polymers [21], in particular epoxies, with nanoparticles can significantly improve mechanical strength and wear. Jiguet et al. [22] studied the effect of silica nanoparticles on the wear and frictional behavior of SU8, a negative tone epoxy. They reported that SU8 composites produced in the form of thin films exhibit similar or even better tribological properties than the bulk epoxies. The composites exhibit reduced friction coefficient and wear rate, compared to the neat epoxy. Interestingly, the reinforcement of polymers with conventional micrometer sized inorganic particles was reported to cause a deleterious

effect on a wear resistance [23]. On the other hand, Xing and Li [24] reported that the uniform sub-micron spherical silica particles could improve wear resistance of the epoxy matrix. They, however, found the effect of particle size on wear resistance—the smaller sized particles seemed to be more effective in improving the wear resistance.

2.2.6 Post-Synthetic Modification

A post synthetic modification is a process where the clusters or nanoparticles are formed in the first step, and the functionalization with organic groups is applied in the second step. Reactive surface functionalities are required to allow a chemical reaction with the surface modifier. There are several ways to attach functional groups to the surface of nanoparticles: nucleophilic substitution reactions, ligand exchange reactions on surface groups, a layer by layer deposition and others. In the case of silica particles, the nucleophilic substitution reactions with silane coupling agents are usually used. Silanol groups are reacted with silane coupling agents to form a stable covalent as shown in scheme 2.2. These molecules contain alkoxy reactive groups Si-OR, which can react with hydroxyl groups on the surface of silica to form Si-O-Si bonds.

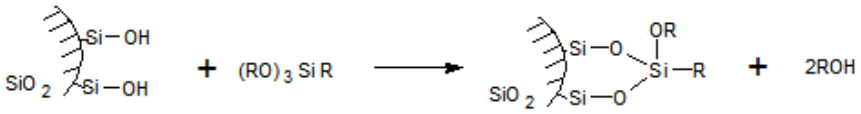

Scheme 2.2 A general reaction of surface silanol-groups at the surfaceof a silica particle with a silane coupling agent.

2.3 Tribological Troperties of Polymers

The word tribology is derived from the Greek word *tribos* meaning rubbing and *logy* meaning study of, or science. Thus, the literal meaning is the science of rubbing. Friction, wear and lubricant science are all included in this meaning. *The American*

Heritage Dictionary of the English Language defines tribology as “the science of the mechanisms of friction, lubrication, and wear of interacting surfaces that are in relative motion”. Therefore tribological characterization of materials deals with friction coefficient, wear resistance and design of interactive surfaces in relative motion. The use of a liquid-lubricant for reducing the friction coefficient in ancient times provides the evidence for use of such knowledge before its definition was given. However, it was quoted in the book of Rabinowicz [25] that the first landmark report, recorded about the economic importance of tribology, was started in 1996 by Jost. The use of the term has become widespread ever since.

Tribology in polymers is crucial to many applications. Plastic bearings and bushing, cams and gears, seal and slides and a number of others parts vital in rolling and sliding are now standard in cars, washing machines, airplanes, computer, etc. Thus, the control of friction and wear of polymers is of importance. Solid lubricants, reinforcing fibers [26, 27] and inorganic particulates have been normally used to enhance those properties. Solid lubricants are added to a polymer to decrease adhesion or form a transfer film with a low interfacial shear stress on the counterface, thus reducing the friction coefficient and wear rate of the polymer matrix. Fillers in the form of particulates and fibers are often embedded into a polymeric matrix to improve its mechanical properties and aid in creating transfer films by tribochemical reactions. Fillers, whose hardness and modulus are greater than those of the polymer, will increase the strength and initial modulus of the mixture, at least in the case of good adhesion [28] and, hence, are effective in reducing wear in dry sliding conditions involving adhesion and fatigue. Zhang et al. [29-33] reported the reduction in wear resistance and friction coefficient

when nanosilica and nanoalumina were incorporated into the epoxy matrix. Xu and Mellor [34] studied the effects of fillers on the wear resistance of thermoplastic polymeric coatings. They found that silica and dolomite filled polymeric coatings had a higher wear rate than an unfilled polymer. Friedrich [35] reported that wear rate is not improved by adding short fibers if the wear mechanism is highly abrasive in nature. Larson et al. [36] reported that addition of CuO increases wear relative to the neat epoxy. When nano-CuO is added to epoxy with PTFE incorporated, the wear rate decreased slightly.

Based on the literature reported, the effect of filler on the abrasive wear is not, by any means, predictable. Embedded fillers can either enhance or degrade other properties because a performance depends strongly on the type of test, on the type of reinforcement, upon the nature of the interface and on the strength of the adhesion between the phases.

Thus in this chapter, the effects of inorganic silica content, together with surface treatment of silica particles, on the tribological properties of epoxy resin were studied.

2.4 Experimental

2.4.1 Materials

Epoxy resin diglycidyl ether of bisphenol A (DGEBA) was purchased from System Three. The epoxy equivalent weight is 210 g/eq. Bis-(p-aminocyclohexyl) methane used as a curing agent (AMICURE ® PACM) was kindly supplied from Air Products and Chemicals, PA. Colloidal silica in methyl isobutyl ketone (MIBK) with 30-31 % amorphous silica and particle size of 17-23 nm was kindly supplied from Nissan Chemical Houston Corporation. Glycidyloxypropyl trimethoxy silane (GPS), γ-

methacryloxypropyl trimethoxy silane (MAMS) and 3-mercaptopropyltriethoxy silane (MPS) used as silane coupling agents were kindly supplied from Struktol company. The chemical structures of the chemicals used are shown in Scheme 2.3.

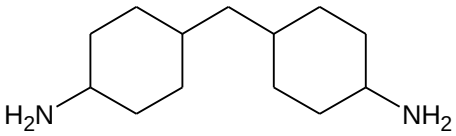

Bis-(p-aminocyclohexyl) methane

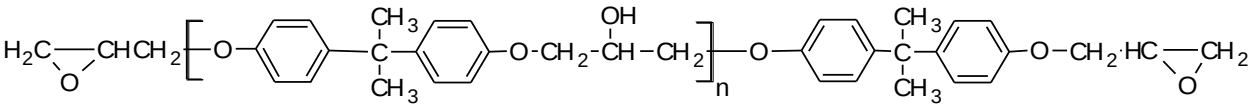

diglycidyl ether of bisphenol A (DGEBA)

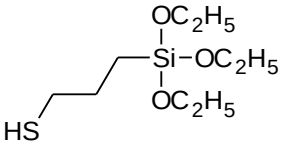

3-mercaptopropyltriethoxy silane (MPS)

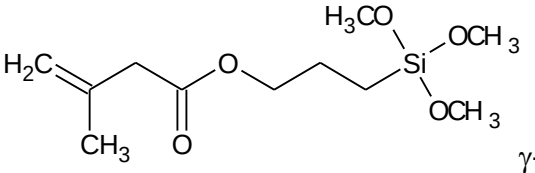

γ-methacryloxypropyl trimethoxy silane (MAMS)

Con't

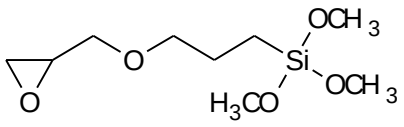

glycidyloxypropyl trimethoxy silane (GPS)

Scheme 2.3. The chemical structures of chemicals used.

2.4.2 Preparation of Silica and Silane Modified Silica Particles

Colloidal silica was left at room temperature to evaporate the MIBK solvent. The obtained silica was then ground and dried in a conventional oven at 60^{o}C to eliminate all the residue solvent. To prepare the γ-glycidyloxypropyl trimethoxy modified silica (silica-GPS), 10 parts per hundreds (phr) of glycidyloxypropyl trimethoxy silane (GPS) was added to the silica powder in the presence of toluene solvent. The mixture was then refluxed at 80 ^{o}C for 24 hours. The slurry was obtained and dried at room temperature for 24 hours. The powder was then dried further to eliminate the residual solvent in a conventional oven at 80^{o}C for 24 hour. The same procedure was used to prepare γ-methacryloxypropyl trimethoxy modified silica and 3-mercaptopropyltriethoxy modified silica, but the silane coupling agents used were γ-methacryloxypropyl trimethoxy silane and 3-mercaptopropyltriethoxy silane, respectively.

2.4.3 Preparation of Epoxy Composites Filled with Silica

Epoxy hybrids with 10 phr silica powder were prepared. The silica powder either neat or silane modified silica was mixed with DGEBA. The silica and epoxy mixtures were ultrasonicated for 3 hours. The 1:1 stoichiometric amount of AMICURE®PACM

was then added, with continuous gentle stirring, to the DGEBA + silica mixture. The mixtures were then poured into silicone molds, and were cured in a conventional oven at 80^{o}C for 2 hours and 150^{o}C for 2 hours.

2.4.4 Infrared Spectroscopy [37]

The silica powders were mixed with KBr and then pelletized under hydraulic pressure. The obtained disks were characterized using FTIR, Perkin Elmer.

2.4.5 Thermogravimetric Analysis [38]

Thermal stability of samples was determined using Pyris 1 TGA, Perkin Elmer. Cure samples were performed at a heating rate of 20^{o}C/min from 30 to 950^{c}C both in N_2 atmosphere and in air.

2.4.6 Dynamic Mechanical Analysis [39]

Dynamic mechanical analysis (DMA) was performed using DMA 8000 from Perkin Elmer with single cantilever configuration. The storage modulus, loss modulus and tan δ of each cured sample were determined with a displacement control of 0.05 mm at constant frequency of 1, 5, 10 and 20 Hz and a scan rate of 5^{o}C/min.

2.4.7 Scratch Resistance Testing

Generally, there are two types of surface damage—mar and scratch [40]. A mar is a shallow mark that is too minor to be perceived by the naked human eye alone, but nevertheless does become visible when present in large quantities. A scratch is a mark that forms surface damage or a visible groove. There are numerous factors influencing the response of polymers to the scratch, including the amount and types of fillers or additives used, the scratch loads and speeds, and the geometry and number of scratches. Several methods have been used to determine the scratch resistance

varying from using simplistic methods, like the pencil hardness test, to employing more sophisticated device like a scratch machine, taber testing machine and pin on disc tribometer.

In the present studies, scratch resistance of samples were performed using a Swiss micro-scratch tester (MST) from CSEM Instrument using a diamond conical indenter. The Rockwell, a type of indenter, with the size of 200 microns, was used. A single scratch pass was performed with at least 5 repeats. The indenter was applied normal to the surface with an applied force of 5.0 and 10.0 N. The tests were carried out at a speed of 5 mm/min and scratch length of 5.0 mm.

The indenter passed three times over the surface for each test. A first pass, called a pre-scan, is performed at the force 0.03 N to determine the topography of the surface. The second pass was an actual scratch; the desired load is applied on the sample surface to determine the penetration depth, R_p. The third scan, called a post-scan, is performed at the force 0.03 N to determine the residual depth R_h or called the after-healing depth. The shallower the final depth, R_h is, the better the scratch resistance.

2.4.8 Pin on Disc Tribometer

Tests were carried out using Nanovea pin-on-disk tribometer from Micro Photonics Inc. The pin was a silicon nitride (Si_3N_4) ball with the diameter of 3.2 mm. The pin was fixed in a holder on a loading lever arm. The load applied to the level arm during the test was 5.0 N which is equivalent to the initial Hertzian contact radius of 151 μm with maximum and mean contact pressures of 105 MPa and 70 MPa, respectively (see APPENDIX A). The rotation speed of the disc was 200 rpm and the radius of wear track was 2.0 mm. The equivalent sliding speed was 4.19 mm/s. The test was performed for

10,000 revolutions under ambient conditions (at temperature of 22^{o}C and % RH of 35-45 %). The friction coefficient (μ) was obtained by using Amonton's first law of friction [41, 42], i.e. $\mu = F_f / W$, (where F_f is tangential force and W is normal force) and is reported as an averaged value based on data points in the steady state regime.

In order to investigate the effects of normal loading on wear resistance, different loads (3.0 and 10.0 N), were used and tested under similar conditions.

Before testing, the two sliding surfaces were cleaned using Kimwipes® soaked in isopropanol.

2.4.9 Profilometer

Cross-section areas of wear track remaining after each pin-on-disc friction test were determined with a Veeco Dektak 150 Profilometer. A stylus with tip radius of 12.5 μm was used. The force applied to the sample was 1 mg, and scan rate was 26.7 μm/sec. The profilometer amplifies and records the vertical motions of a stylus displaced at a constant speed by the surface to be measured [41]. As the stylus moves, the stylus rides over the sample surface detecting surface deviations.

All samples were cleaned by high pressure air to eliminate all debris before each test. At least 5 scans were run for each sample, and the average value of the area was used to calculate the wear rate.

2.4.10 Scanning Electron Microscopy and Optical Microscope

Morphology of fracture surfaces and worn surfaces of composites were observed with environmental scanning electronic microscope (FEI Quanta E-SEM). All samples were mounted on stubs and coated with a thin layer of gold to avoid electrostatic charging during examination. Before coating with gold, the worn surface samples were

cleaned using high pressure air to eliminate all debris. The silicon nitride ball, after sliding against the sample surface, was investigated for traces of the transfer film using the optical microscope, Nikon Eclipse ME600.

2.5 Results and Discussion

2.5.1 Characterization of Surface-Treated Silica

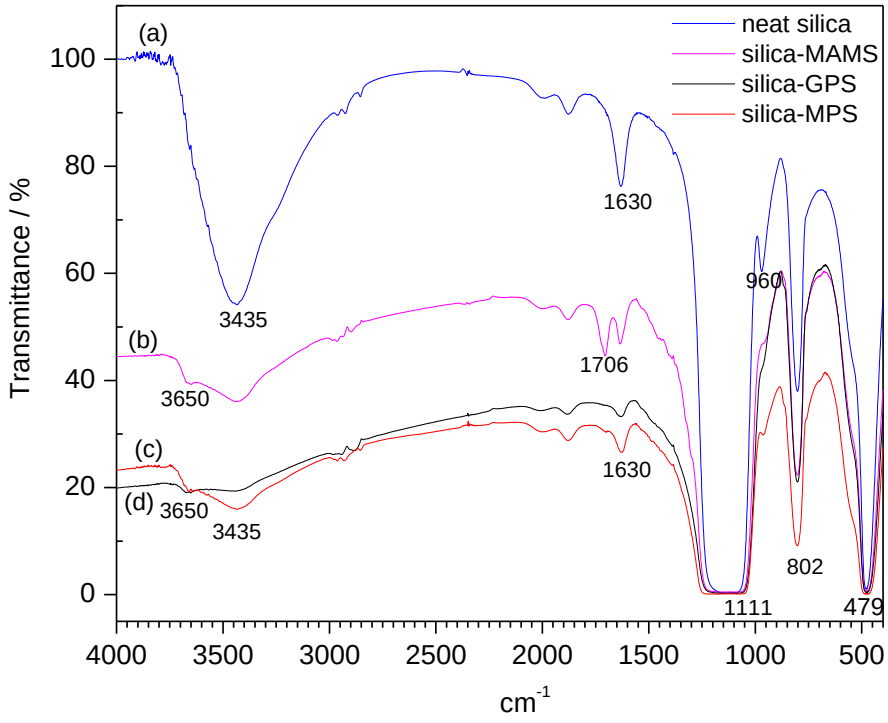

Figure 2.1. FTIR spectra of (a) neat silica, (b) silica-MAMS, (c) silica-MPS and (d) silica-GPS.

Figure 2.1 shows the FTIR spectra of (a) neat silica (b) silica-MAMS (c) silica-MPS and (d) silica-GPS, respectively. The broad hydrogen-bonded O-H stretching band over 3700-2700 cm^{-1} is due to both water and SiOH groups, and a peak at 1630 cm^{-1} is due to water. A strong absorption band between 1300 and 1000 cm^{-1} related to the asymmetry stretching of Si-O-Si bonds both in linear and cyclic forms, and the peak at

960 cm^{-1} is due to Si-OH. In spectra of the surface-treated silica (Figures 2.1 (b), (c) and (d)), hydrogen-bonded OH band at 3700-2700 cm^{-1} is weaker than that is found in the neat silica. The peak observed at 3650 cm^{-1} is due to an isolate O-H in SiOH. The peak at 1630 cm^{-1} due to water still existed, but is weaker than that is found in neat silica. This means that there are definably much fewer silanol groups remaining. The characteristic band related to Si-O-Si at 1300 to 1000 cm^{-1} is still present; however, the peak at 960 cm^{-1} due to Si-OH groups changes from a sharp peak for neat silica to a shoulder peak for all of the surface-treated silica. These indicate that some of the hydroxyl groups on the silica surface are substituted by the organofunctional groups. In the case of silica-MAMS, the characteristic peak for C=O at 1706 cm^{-1} was observed, confirming the presence of acrylate groups on the surface of silica. However, in the case of silica-GPS and silica-MPS, it is quite difficult to identify other functional groups by IR spectroscopy due to the strong and broad peaks of Si-O (1300-1000 cm^{-1}) and –O-H (3700-2700 cm^{-1}) groups having polar bonding.

2.5.2 TGA Analysis

The thermal stability of neat silica powder and surface-treated silica powder are shown in Figure 2.2. The neat silica shows only a small change in total weight loss on heating, compared to the surface-treated silica. The weight loss below 100^{o}C is due to the dehydration at which all the physisorbed water is removed. The weight loss at about 600^{o}C is due to the dehydroxylation at which most of silanol groups are removed. On the other hand, two distinct weight losses are observed for all the surface-treated silica. A gradual decrease in the weight loss is found below 250^{o}C instead of a sudden change found in neat silica. The weight loss due to a carbonaceous decomposition is at

about 500^{o}C. The initial temperature degradation, ITD, and the temperature of the maximum rate of weight loss, T_{max}, and the residual weight at 700^{o}C for silica-MPS, silica-MAMS and silica-GPS are tabulated in Table 2.1. The silica-MPS shows the highest thermal stability among any other surface-treated sililca.

Figures 2.3 and 2.4 show TGA thermograms of the epoxy composites filled with the different types of silica. The relevant data are tabulated in Table 2.1 as well. Patterns of TGA curves of the epoxy + silica systems are similar to that of the pure epoxy resin, obtained by testing under either nitrogen or air atmosphere. This similarity appears because only organic components contribute to the thermal weight loss of the hybrid materials.

Thermal decomposition of the pure epoxy and all the epoxy + silica composite samples in nitrogen shows only one stage of weight loss. Incorporation of epoxy with all types of silica causes the ITD and T_{max} to shift to a higher temperature. At the same time, the residuals at 700^{o}C increase with the increase in silica contents. The residuals of resins at high temperature come from the inorganic silica filler and carbonaceous products or char. The higher char residuals denote that relatively fewer amounts of volatile small molecules were released under thermal decomposition. The char could have helped to protect the substrate by interfering with the access of oxygen [43]. Thus, the char formed on the polymer surface could be postulated to act as a heat shield for the base materials.

Figure 2.4 shows TGA thermograms of the composite samples in air. The thermal degradation of composites in air could be divided into two stages—about at 300^{o}C and 500^{o}C. Becker et al. [44] showed that the weight loss of epoxy resin in the first stage

was attributed to decomposition of the ends of the epoxy network while the second stage was attributed to degradation of the main chain.

As shown in Table 2.1, all composites at all compositions show higher ITD, T_{max} and percent residuals than the pure epoxy resin either in inert atmosphere or oxidative atmosphere, which implies an improvement in the thermal stability. In the case of epoxy + neat silica, the expected results were observed; ITD and T_{max} as well as percent residuals increased with increasing neat silica contents either in N_2 or in air atmosphere. This is attributed to a good thermal stability and heat resistance of silica particles, which retard the thermal degradation rate of an organic part of the hybrid materials. Moreover, silica can function as the insulating barriers to the residuals [20]. Hsiue et al. [45] explained that, due to the low surface potential energy of silicon, the silicon element, as in the form of silica, migrated to the surface of materials and served as a heat barrier to protect the inner layer of the polymer. The similar results are observed only in the case of epoxy + silica-GPS (see Table 2.1). The changes in ITD and T_{max}, as a function of silica content for epoxy + silica-MAMS and epoxy + silica-MPS, are complex and periodic, especially in oxidative atmosphere. These periodical changes can be explained by the competition effects of lower cross-link density of the epoxy hybrids and higher content of inorganic silica content. Silica-GPS, silica-MAMS and silica-MPS can react with amine and epoxy, but only silica-MAMS and silica-MPS somehow change the cure mechanism and obstruct the network formation between epoxy and amine. A detail explanation is given later (see chapter 4). Thus, even though the thermal stability of silica-MAMS and silica-MPS themselves are higher than that of silica-GPS, the epoxy composites filled with silica-GPS shows higher thermal stability.

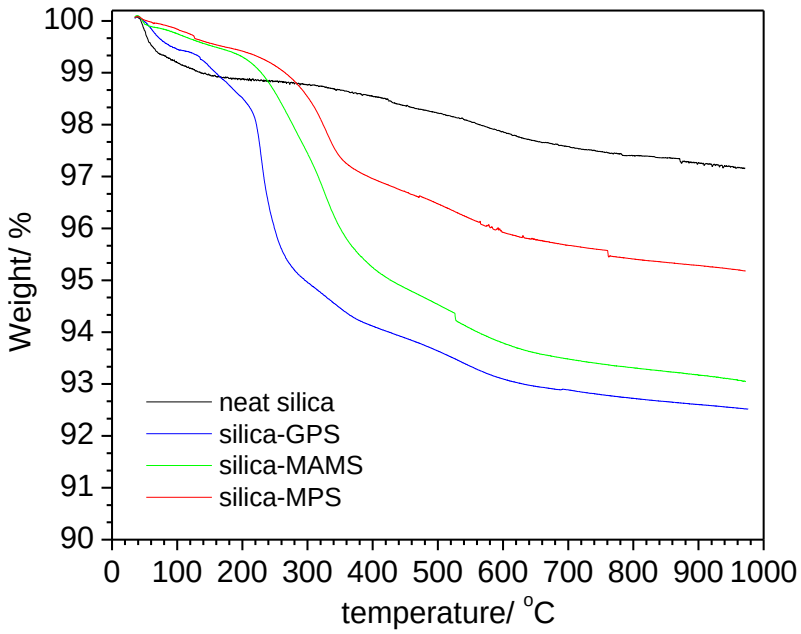

Figure 2.2. TGA thermograms of different types of silica powder under air atmosphere.

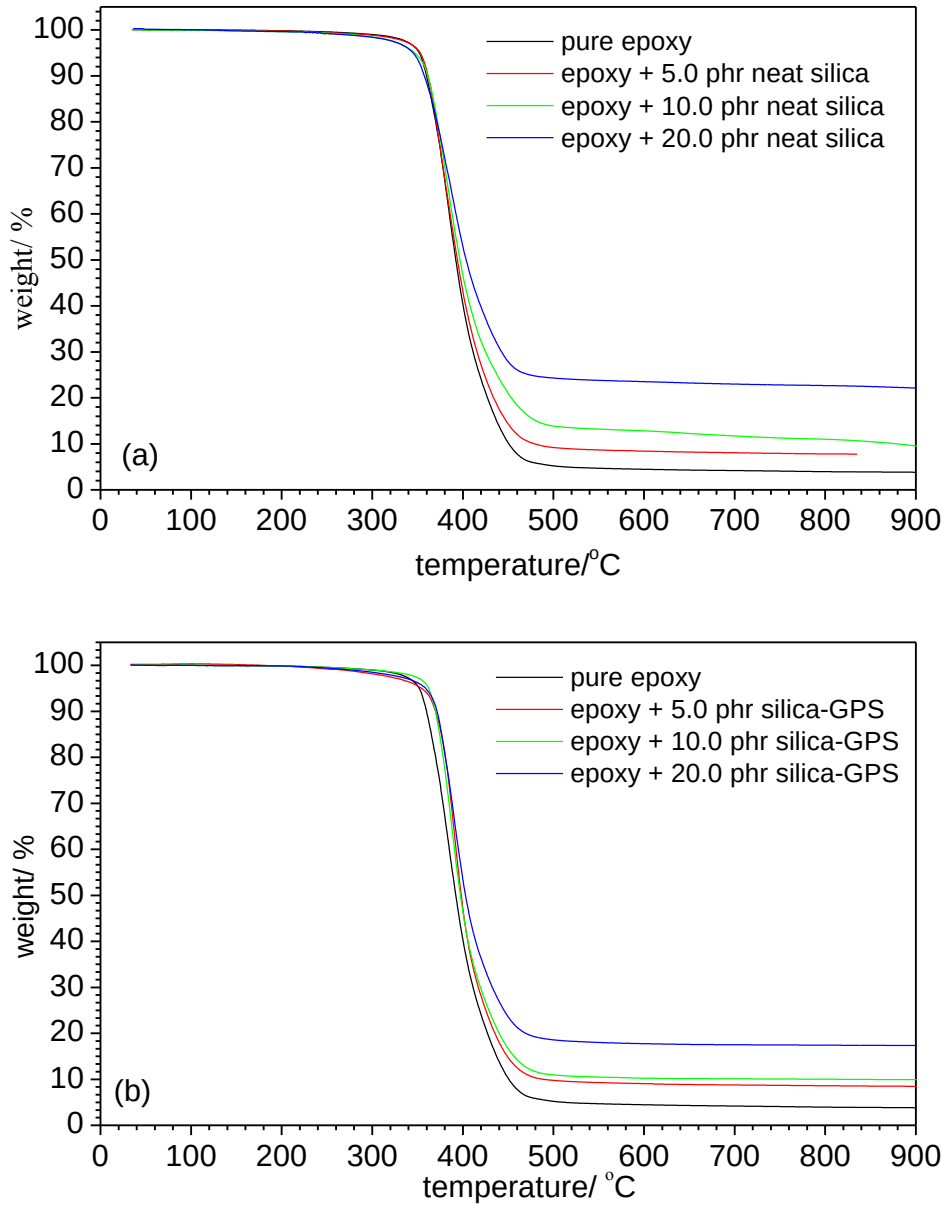

Figure 2.3. TGA thermograms of epoxy composites filled with (a) neat silica and (b) silica-GPS under N_2 atmosphere.

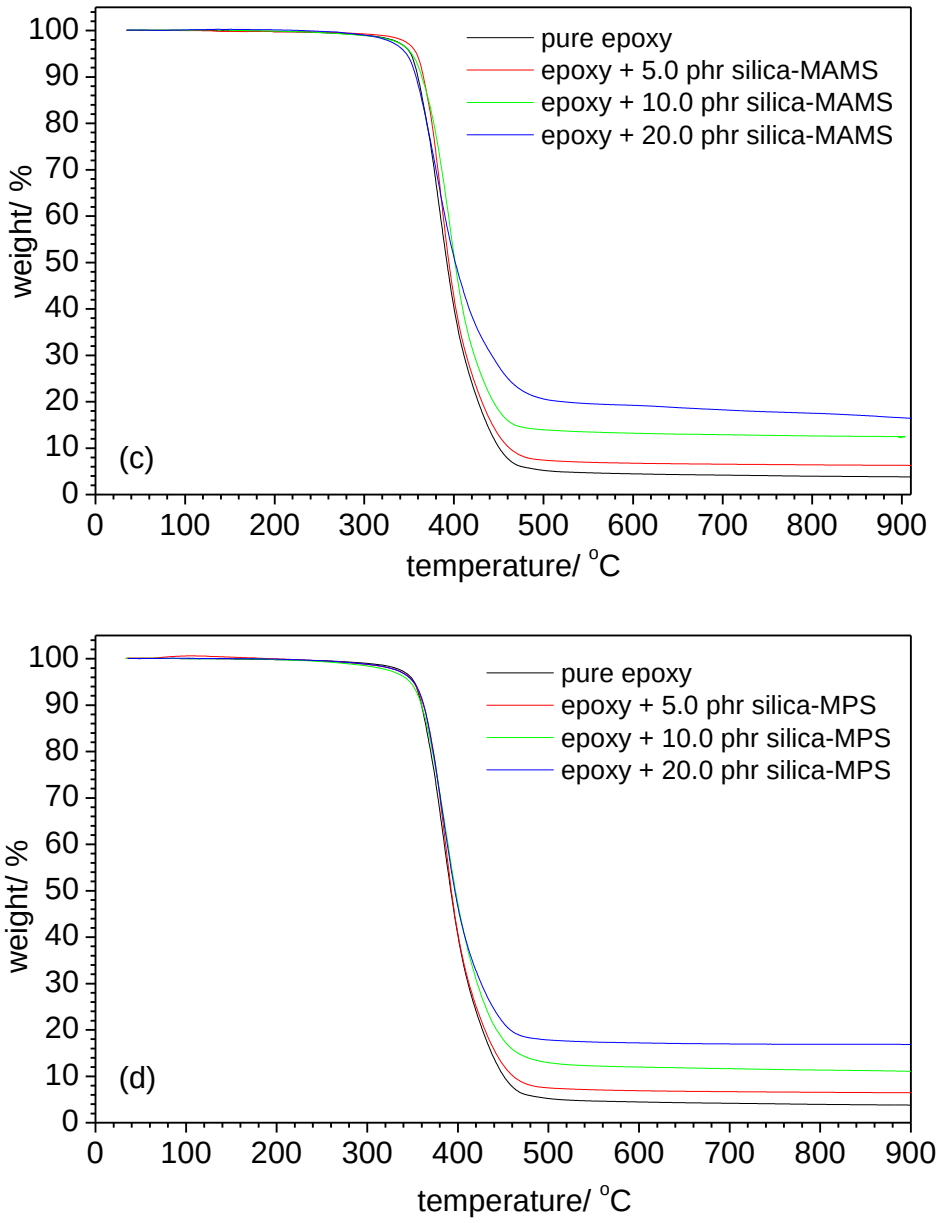

Figure 2.3. TGA thermograms of epoxy composites filled with (c) silica-MAMS and (d) silica-MPS under N_2 atmosphere.

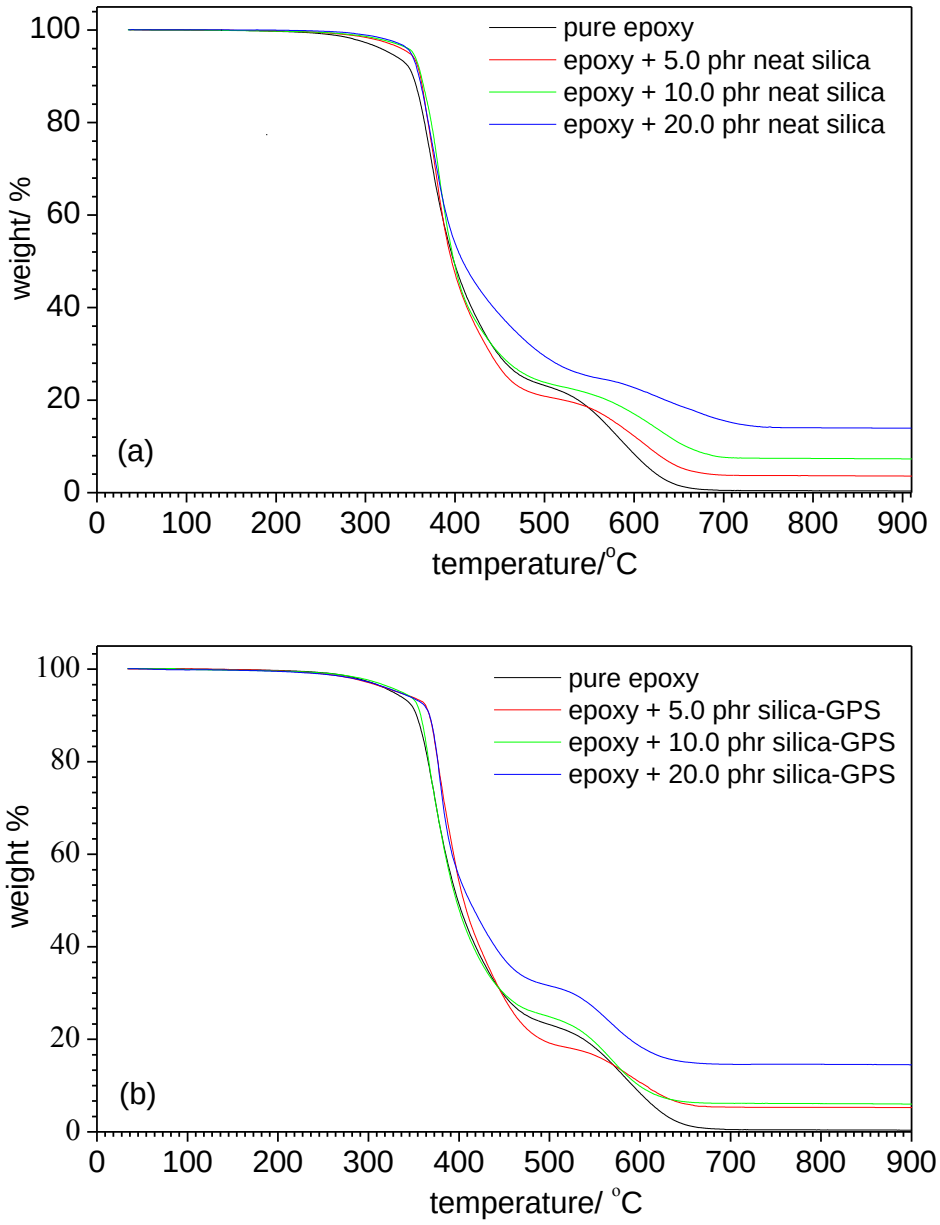

Figure 2.4. TGA thermograms of epoxy composites filled with (a) neat silica and (b) silica-GPS under air atmosphere.

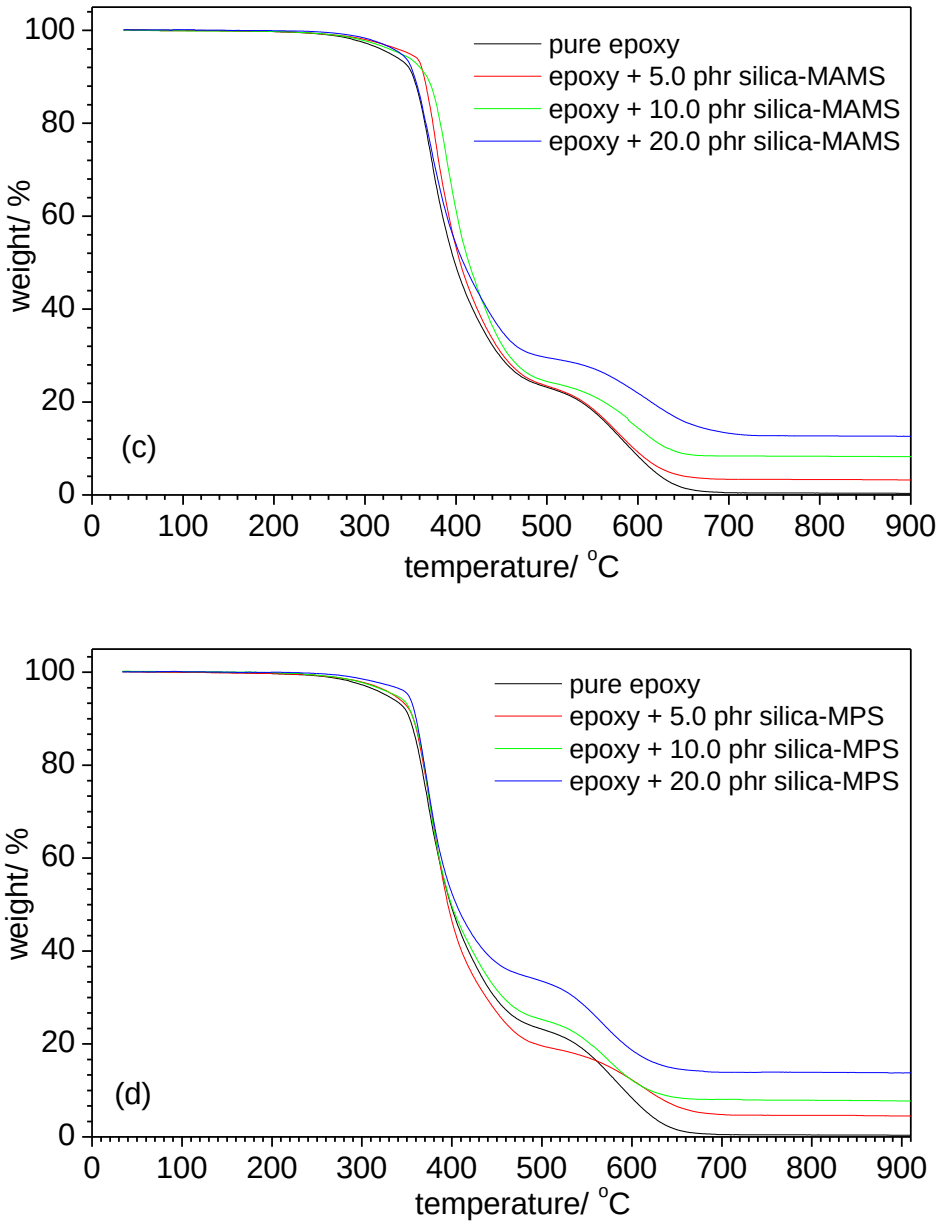

Figure 2.4. TGA thermograms of epoxy composites filled with (c) silica-MAMS and (d) silica-MPS under air atmosphere.

Table 2.1. TGA data of pure epoxy, silica powder and epoxy composites.

Sample	ITD/ ^{o}C		T_{max}/ ^{o}C			Char yield at 700^{o}C/ %	
	N_2	Air	N_2	Air-1	Air-2	N_2	Air
silica-GPS	-	116.6	-	228.1	538.3	-	92.90
silica-MAMS	-	165.0	-	324.6	537.6	-	93.48
silica-MPS	-	187.5	-	331.3	539.8	-	95.70
pure epoxy	350.5	346.7	380.0	373.3	587.2	4.20	0.00
epoxy + 5 phr neat silica	352.4	353.5	381.0	380.2	614.9	8.04	3.53
epoxy + 10 phr neat silica	354.7	358.2	382.4	380.6	629.6	11.60	7.53
epoxy + 20 phr neat silica	351.9	349.7	390.4	380.9	643.3	22.70	14.53
epoxy + 5 phr silica-GPS	363.9	351.7	390.6	378.3	591.7	8.56	5.21
epoxy + 10 phr silica-GPS	364.8	358.9	389.7	376.9	567.2	10.15	6.00
epoxy + 20 phr silica-GPS	368.6	363.2	390.6	378.3	567.6	17.28	14.32
epoxy + 5 phr silica-MAMS	357.1	357.6	385.4	378.5	577.0	6.49	3.23
epoxy + 10 phr silica-MAMS	356.6	364.8	393.9	388.4	587.6	12.83	8.38
epoxy + 20 phr silica-MAMS	351.5	358.4	383.7	377.5	566.4	18.37	13.29
epoxy + 5 phr silica-MPS	355.7	347.1	368.7	380.8	621.1	6.52	4.78
epoxy + 10 phr silica-MPS	355.3	349.7	388.4	376.9	573.7	11.67	7.95
epoxy + 20 phr silica-MPS	357.7	351.4	389.7	375.8	568.9	16.82	13.89

2.5.3 Dynamic Mechanical Analysis

Temperature dependence of dynamic mechanical properties of epoxy + silica composites, containing different amount of silica at frequency of 1 Hz, is shown in Figures 2.5 to 2.8. For epoxy composites filled with neat silica (Figure 2.5(a)), a change in the storage modulus $E^{/}$ at a glassy region of epoxy + silica composites is not significant. The reinforcement is observed only if more than 10.0 phr of neat silica is added. The storage modulus $E^{/}$ at the glassy region of the composites is increased about 22 % when 20 phr of neat silica is added (see Table 2.2). At high temperature and low frequency, epoxy resin is rubbery-like. Unlike when in glassy state, epoxy + neat silica in rubbery state shows remarkable increases in the storage modulus $E^{/}$ as the neat silica content increases. About 122 % improvement of the storage modulus is observed when 20 phr of neat silica is added. The increase in the storage modulus $E^{/}$ is attributed to a high stiffness of silica particles. In Table 2.2, epoxy + neat silica composites show more significant improvement of the storage modulus in a rubbery plateau region than in a glassy region. Similar results are observed in other studies [46-49].

Figure 2.5 (b) shows the loss modulus $E^{//}$ at temperature range of -120 to 200^{o}C. From Figure 2.5 (b), two relaxation peaks are observed. The lower temperature relaxation, known as β-relaxation, caused by the short-range motion, is about -46 to -57^{o}C while the higher temperature α-relaxation, known as the glass transition temperature or T_g, caused by a long-range motion, is about 117 to 121^{o}C. Similar results are observed by Jensen et al. [14]. They explained that a board lower

temperature β-relaxation was caused by the localized chair- to boat-conformation changes, experienced in the cyclohexyl ring of the PACM curing agent.

The variation of T_β and T_g as a function of neat silica content is shown in Table 2.2. Many investigators reported an increase in T_g values [50, 51] whereas others found a slight decrease or no change in values [46, 52-54]. It is shown in Table 2.2 as well, that no significant improvement in T_g is achieved in epoxy + neat silica composites. Only slight increases in T_g and T_β are found when silica content is at 10 and 15 phr.

It is well known that a cure epoxy resin shows a clearly large tan δ peak in the glass transition region. It was observed by Ochi et al. [17] that the area of the tan δ peak decreased tremendously with the hybridization of the silica network in the epoxy resin. In Figure 2.5(c), the studied epoxy systems also show a large tan δ peak in the glass transition region, but the area of the tan δ peak decreases only slightly. The steric hindrance due to the presence of silica contributes to the decrease. Unlike the in situ polymerization process of the organic-inorganic hybrid whose motion of network is more strongly restricted [17, 55-57], the relaxation process of the epoxy composites filled with neat silica rarely changes. In other words, the incorporation of neat silica to the epoxy system by the blending method does not interfere with the network formation of epoxy resin. The surface of neat silica powder is inert [58], so reactions with epoxy and/or curing agent at the silica surface are difficult. The constant T_g implies that the motion of the network is not affected by the addition of neat silica powder.

Figures 2.6 to 2.8 show dynamic mechanical parameters of epoxy + surface-treated silica curing with cycloaliphatic amines. Like the epoxy + neat silica system, there is no significant improvement in the storage modulus E' in the glassy region for all epoxy +

surface-treated silica systems. To facilitate the comparison among those surface-treated silica systems, the values of $E^{/}$ at three different temperatures are given in Table 2.3. Results similar to that for the epoxy + neat silica system are found only in the case of epoxy + glycidyl modified silica (silica-GPS). The storage modulus $E^{/}$ both in the glassy and rubbery region tend to increase as the silica-GPS content increases to a certain concentration and then starts to drop. The effect of silica particles on the storage modulus $E^{/}$ at the rubbery region seems to be less than that observed in the epoxy + neat silica system. No significant improvement in T_g is observed either. The constant T_g implies that the silica-GPS does not affect the network formation of the epoxy resin.

In the case of epoxy + acrylate modified silica (silica-MAMS) as well as epoxy + mercaptan modified silica (silica-MPS), changes in the glass transition temperature T_g and storage modulus are complex. A significant lowering in the glass transition temperature T_g, compared to that for the pure epoxy, is observed when a certain silica content is added. A decrease in T_g of the epoxy as a result of the presence of silica was also reported by others [19, 30], for which a plasticizing effect of colloid silica was believed to contribute. In the present work, silica particles are chemically treated with γ-methacryloxypropyl trimethoxy silane and 3-mercaptopropyltriethoxy silane coupling agents to form γ-methacryloxypropyl trimethoxy modified silica (silica-MAMS) and 3-mercaptopropyltriethoxy modified silica (silica-MPS). Epoxy reacts with a mercaptan group on the surface of silica instead of reacting with an amine curing agent to form the epoxy network, whereas this curing agent reacts with an acrylate group on the surface of silica instead of reacting with the epoxy. Park et al. [2] evaluated the effect of

additives on the cross-link density of the epoxy using a shift of T_g obtained from DMA technique. Fox and Loshaek [59] described the linear relationship between the glass transition temperature and the cross-link density using the following equation:

$$T_{gx} = T_{g\alpha} + \frac{\zeta}{M_c} \quad (2.1)$$

where T_{gx} is the glass transition temperature, $T_{g\alpha}$ is the glass transition temperature of the linear polymer backbone at infinite molecular weight, ζ is a constant dependent on the molecular weight of the unreacted resin and M_c, which defines cross-link density, is the molar mass between cross-link. Thus, it can be inferred from the results in Figures 2.7(b) and 2.8(b) and in Table 2.3 that the cross-link density of epoxy reduces when silica-MAMS and silica-MPS are added. Hard particles cause the stiffness at the same time. All the factors together are the reasons why periodical changes in T_g are found in epoxy + silica-MAMS and epoxy + silica-MPS. In addition, it is observed that antiplasticization manifests itself in this study. The decrease of the T_g, usually known as plasticization, is accompanied by the increase in the glassy modulus at the temperature range between T_β and T_g; the effect is known as antiplasticization [60]. However, it is impossible to suppress totally viscoelastic effects through antiplasticization. The decrease in the glassy modulus $E^/$ is thus observed again at silica-MPS content of 10 and 15 phr.

In Figures 2.7(a) and 2.8 (a), the $E^/$ at rubbery region for all the epoxy + silica-MPS and the epoxy + silica-MAMS at silica content of 2.5 phr are lower than that of the pure epoxy system. It is well known that the length of the modulus and its value at the rubbery plateau are dependent upon the molecular weight between entanglements or cross-links [39]. According to the rubber elasticity theory, the inverse of the plateau

modulus at a given temperature above T_g relates to either the number of cross-links or the chain length between entanglements as follows:

$$E'_{pl} \approx (3\rho RT)/M_c \qquad (2.2)$$

where E'_{pl} is the modulus of the plateau region at a specific temperature, ρ is the polymer density and M_c is the mean molecular mass between cross-links. Thus it can be inferred from the reduction in values of rubbery E' as well, that the cross-link density is reduced when the silica-MPS is added. However, the unpredictable tendency of the rubbery E' as a function of silica content is observed. It should be noted that change in the rubbery E' here is due to the stiffness of inorganic silica together with the lowering in cross-link density.

Lastly, it is essential to discuss homogeneities of the epoxy composites filled with surface-treated silica. The area or the width under the primary relaxation α band in the tan δ curve can be used to characterize the network inhomogeneties [60]. As mentioned previously, the neat silica does not hinder the network formation of epoxy + cycloaliphatic amine systems. There is no change in the width of α band (T_g peak). Only a slight change in the peak area is observed. This implies that the epoxy network is homogenous. A similar observation is found for epoxy + silica-GPS as well. On the other hand, the width of the α band is increased when silica-MAMS is added to the systems. Only a single relaxation band is observed due to the superimposition of peaks. It can be inferred from the broadening of the tan δ peak that the addition of silica-MAMS causes the reduction in the degree of homogeneity of the spatial distribution of the cross-link density. For the epoxy composites filled with silica-MPS,

not only the broadening but also the presence of a new α peak is found. It implies that the size of a new heterogeneous phase with a lower cross-link density is so large that a doublet peak of tan δ is detected.

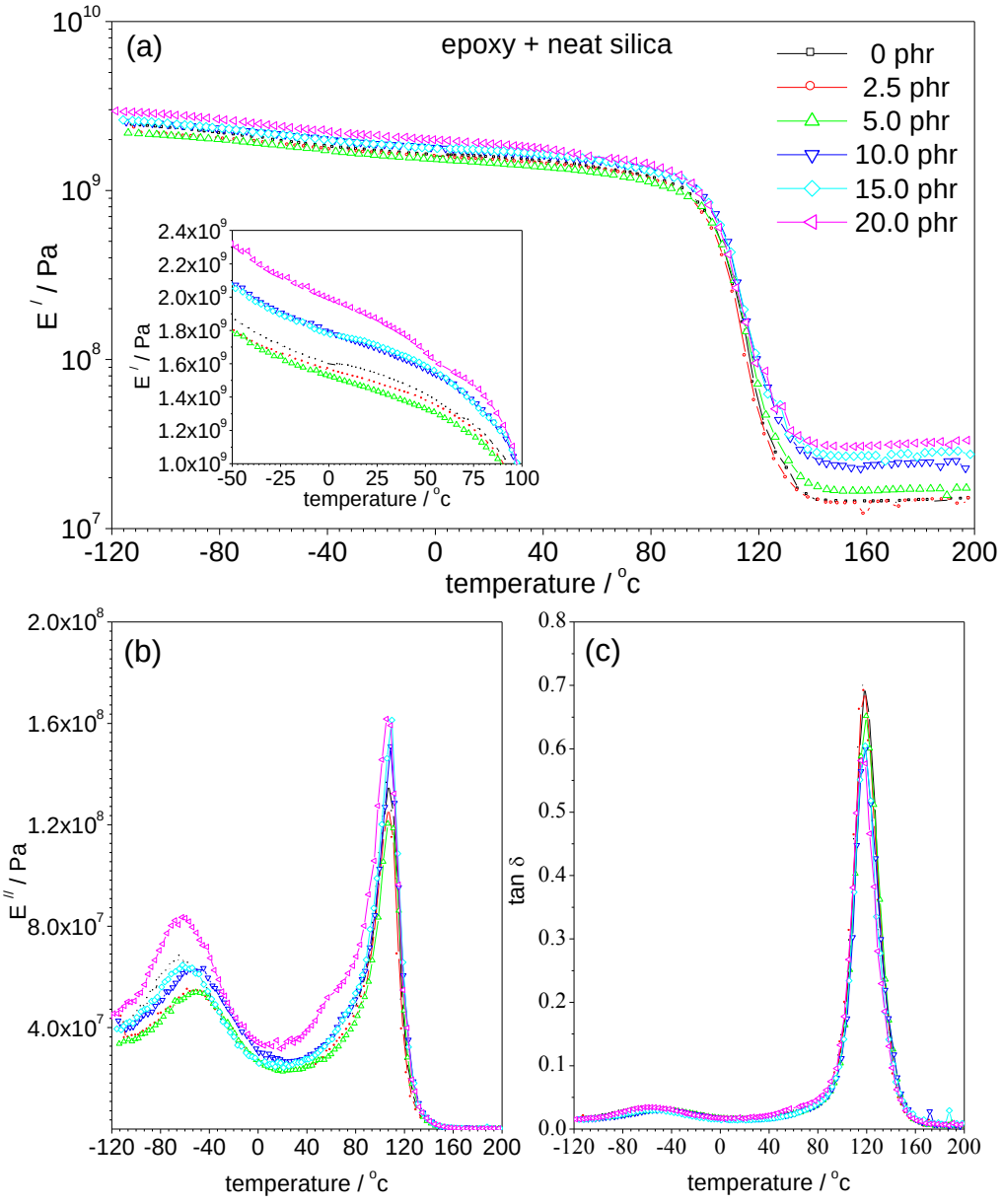

Figure 2.5. (a) Storage modulus, (b) loss modulus and (c) tan δ of epoxy + neat silica composites.

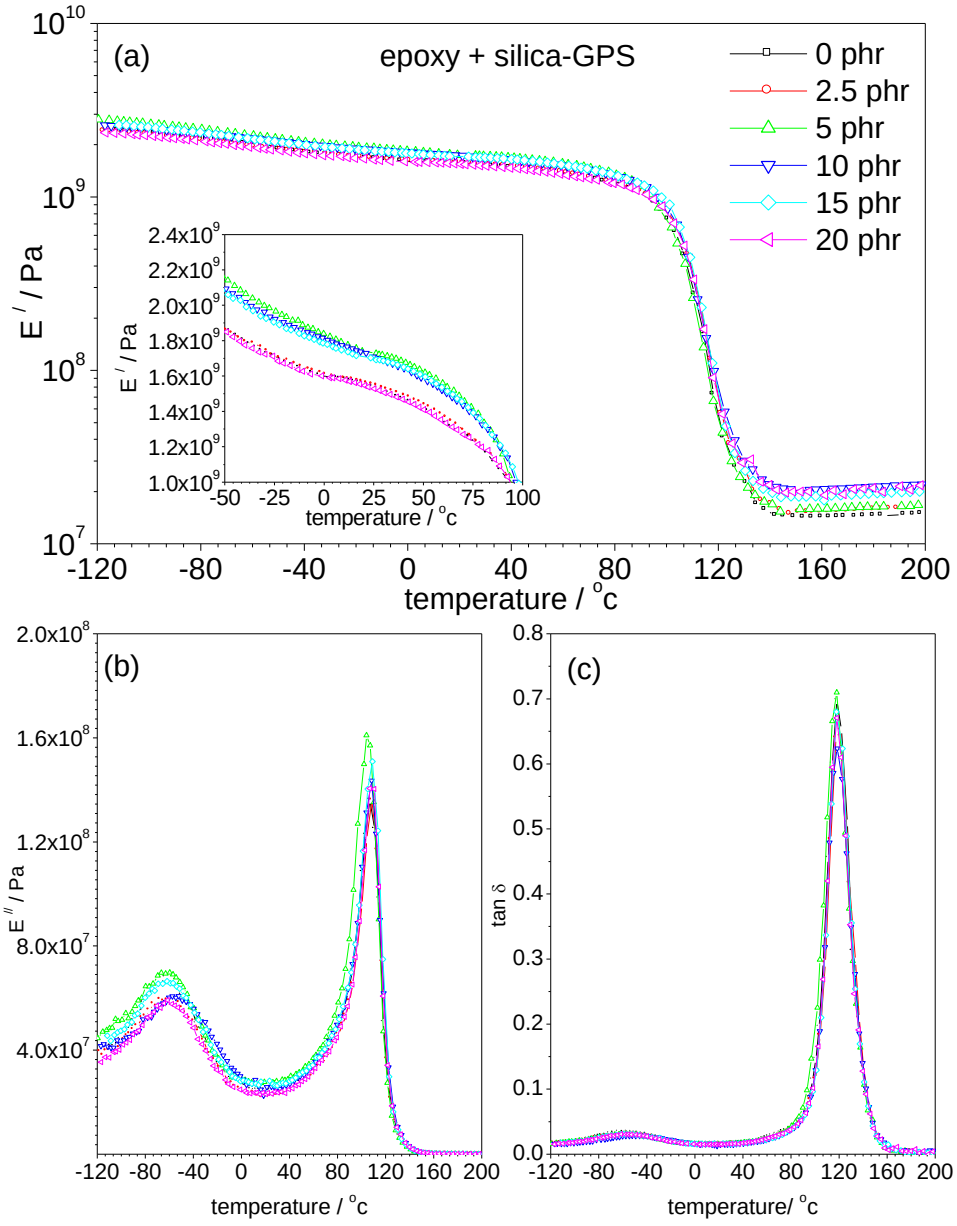

Figure2.6. (a) Storage modulus, (b) loss modulus and (c) tan δ of epoxy + silica-GPS composites.

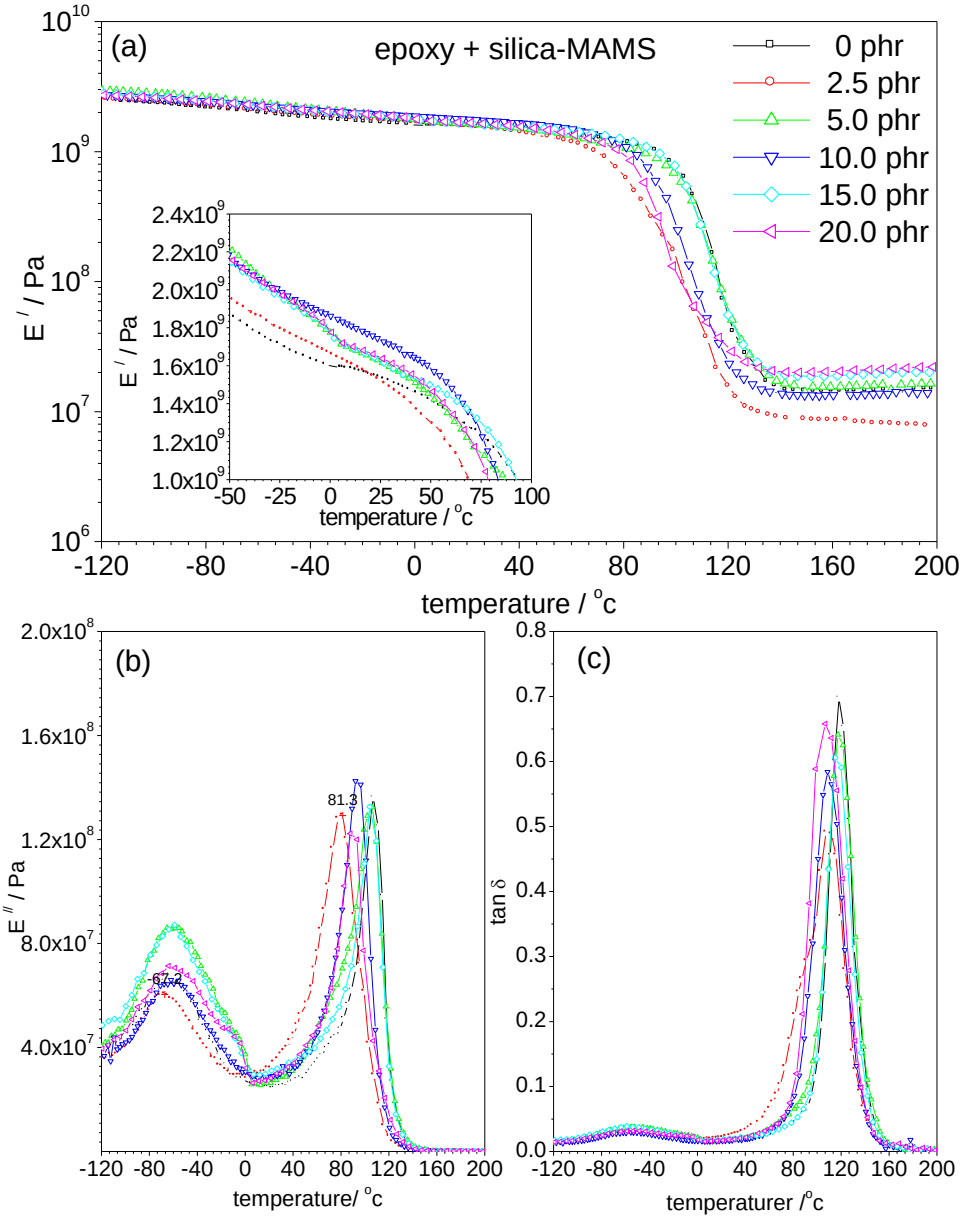

Figure 2.7. (a) Storage modulus, (b) loss modulus and (c) tan δ of epoxy + silica-MAMS composites.

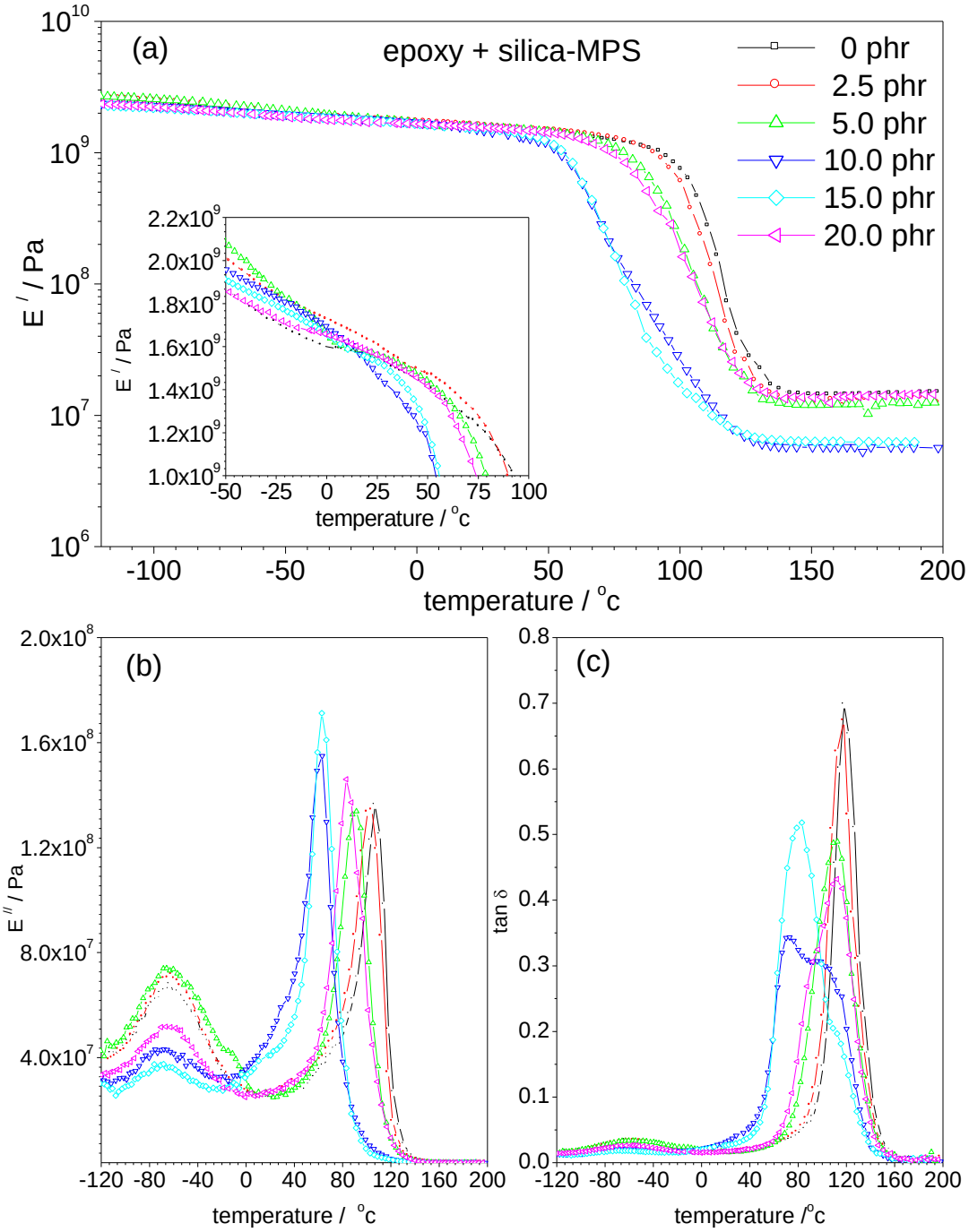

Figure 2.8. (a) Storage modulus, (b) loss modulus and (c) tan δ of epoxy + silica-MPS composites.

Table 2.2. DMA data of epoxy composites filled with neat silica.

Sample	Storage modulus at 25°C (glassy state) / MPa	Storage modulus at 180°C (rubbery state) / MPa	T at peak of loss modulus / °C		T at peak of tan δ / °C	
			at low T region	at high T region	at low T region	at high T region
pure epoxy	1536.8	14.5	-63.4	106.8	-56.1	118.2
epoxy + 2.5 phr neat silica	1482.8	14.5	-56.9	106.9	-47.1	119.2
epoxy + 5.0 phr neat silica	1437.4	17.1	-51.1	106.4	-46.6	120.7
epoxy + 10.0 phr neat silica	1689.5	24.7	-53.8	108.6	-47.5	119.8
epoxy + 15.0 phr neat silica	1710.1	28.0	-61.9	109.7	-56.2	119.7
epoxy + 20.0 phr neat silica	1873.5	32.2	-62.8	105.3	-57.2	117.6

Table 2.3. DMA data of epoxy composites filled with surface-treated silica.

Sample	Storage modulus at 25°C (glassy state) / MPa	Storage modulus at 180°C (rubbery state) / MPa	T at peak of loss modulus / °C		T at peak of tan δ / °C	
			at low T region	at high T region	at low T region	at high T region
epoxy + 2.5 phr silica-GPS	1550.4	15.7	-55.6	108.5	-54.0	121.3
epoxy + 5 phr silica-GPS	1732.6	16.4	-59.6	104.1	-57.1	117.9
epoxy + 10 phr silica-GPS	1710.1	21.4	-52.1	108.4	-50.3	119.7
epoxy + 15 phr silica-GPS	1698.3	19.5	-61.9	109.1	-56.3	120.8
epoxy + 20 phr silica-GPS	1530.2	21.0	-61.3	106.9	-56.4	119.6
epoxy + 2.5 phr silica-MAMS	1525.5	8.0	-67.2	81.3	-61.1	107.7
epoxy + 5 phr silica-MAMS	1742.8	15.9	-65.2	106.2	-52.6	119.6
epoxy + 10 phr silica-MAMS	1734.6	13.7	-61.9	103.9	-55.9	110.4
epoxy + 15 phr silica-MAMS	1623.8	19.7	-61.8	103.9	-55.2	117.4
epoxy + 20 phr silica-MAMS	1644.4	21.2	-64.0	87.9	-52.3	109.8
epoxy + 2.5 phr silica-MPS	1608.8	13.5	-61.5	104.3	-57.5	116.7
epoxy + 5 phr silica-MPS	1563.5	12.5	-65.8	91.5	-56.6	108.9
epoxy + 10 phr silica-MPS	1472.1	5.7	-65.4	63.0	-64.5	80.5
epoxy + 15 phr silica-MPS	1528.5	6.2	-67.0	62.8	-65.1	81.6
epoxy + 20 phr silica-MPS	1564.0	14.2	-66.5	88.0	-58.1	109.4

Figure 2.9 shows the frequency dependency for tan δ of pure epoxy as a function of temperature. It is observed that the temperature at the relaxation peak is shifted when the frequency is increased from 1 to 20 Hz. Thus it could be possible to relate the temperature at which the relaxation process is observed with the frequency by the Arrhenius equation.

$$f = f_o exp\left[\frac{-E_a}{RT}\right] \quad (2.3)$$

where f_o is a constant, f is the test frequency, R is the gas constant and E_a is the activation energy for relaxation process. The activation energy can be calculated directly from $-R$ × slope of the plot of $ln\, f$ as a function of 1000/T shown in Figure 2.10. The activation energies calculated at both low and high temperature ranges for all epoxy + silica composites are demonstrated in Table 2.4.

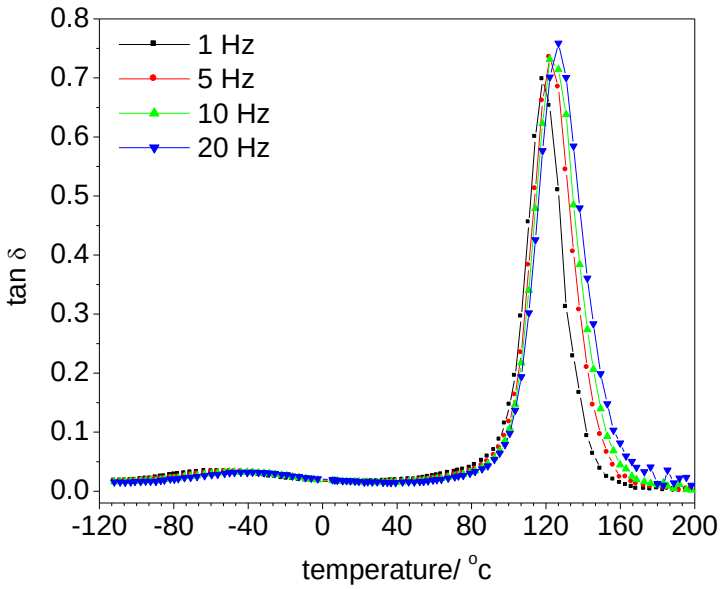

Figure 2.9. Tan δ of pure epoxy as a function of temperature at frequency 1, 5, 10 and 20 Hz.

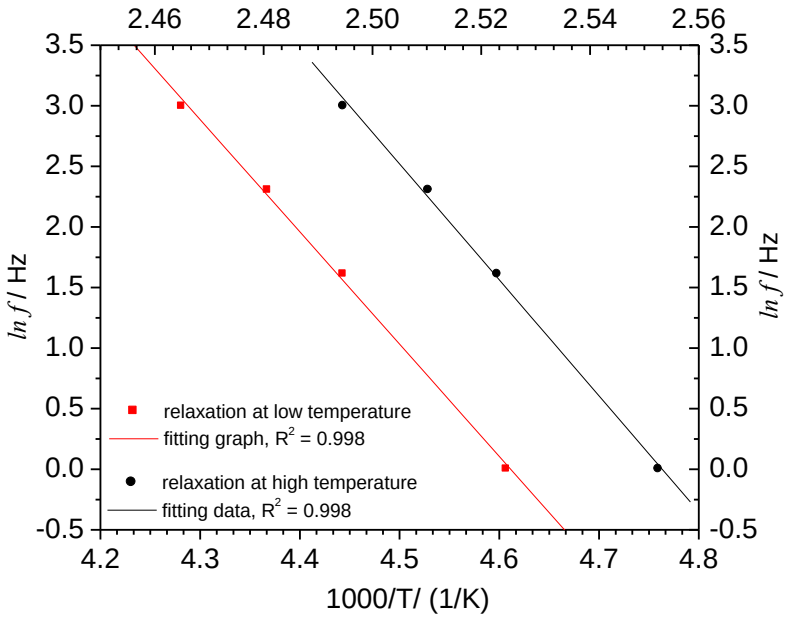

Figure 2.10. Calculation of activation energy for relaxation process of pure epoxy.

Table 2.4. Activation energy for relaxation of epoxy + silica composites.

silica content	E_a / kJmol^{-1}							
	epoxy + neat silica		epoxy + silica-GPS		epoxy + silica-MAMS		epoxy + silica-MPS	
	at high T	at low T	at high T	at low T	at high T	at low T	at high T	at low T
0	434.1	77.1	434.1	77.1	434.1	77.1	434.1	77.1
2.5	513.0	81.3	539.8	75.6	379.0	70.5	423.8	74.0
5.0	523.2	73.8	440.0	72.1	481.9	75.4	407.3	80.5
10.0	466.3	75.2	448.9	72.4	436.6	69.7	221.8	66.5
15.0	429.4	70.5	495.9	79.3	408.1	89.0	322.8	64.1
20.0	432.3	70.5	492.8	74.8	382.1	76.1	458.9	87.3

It is well known that the activation energy E_a for the relaxation process is the energy for molecules to move from one equilibrium position to another equilibrium position. Thus E_a is a measure of the difficulty of chains move to a different state. In the author's opinion, a change in the activation energy should be related to a change in the values of the relaxation temperature, thus the explanation similar to that for T_g should be applicable. It is found in Table 2.4 that the values of E_a at low temperature for all the systems are about 60-90 kJ/mol, indicating β transition, whereas those at high temperature are about 200-530 kJ/mol, indicating α transition. These values are expected for amine-crosslinked epoxies: E_a for β transition is about 70 ± 30 kJ/mol [60], while E_a for α transition is greater than 100 kJ/mol [14].

2.5.4 Tensile Testing

Figure 2.11 (a) shows Young's modulus of epoxy + silica hybrids curing with cycloaliphatic amine systems at room temperature. A tendency similar to that for DMA results is observed. For neat silica, a change in Young's modulus is not significant when small amounts of silica are added. The increase in Young's modulus, which is attributed to the stiffness of silica particles, is observed at a high silica content (> 5 phr). Unlike the flexural storage modulus, a slight decrease in Young's modulus is observed again at load of 20 phr. The decrease in Young's modulus at a high content of silica is possibly due to the agglomeration of particles (see Figures 2.12 (a) and (b)).

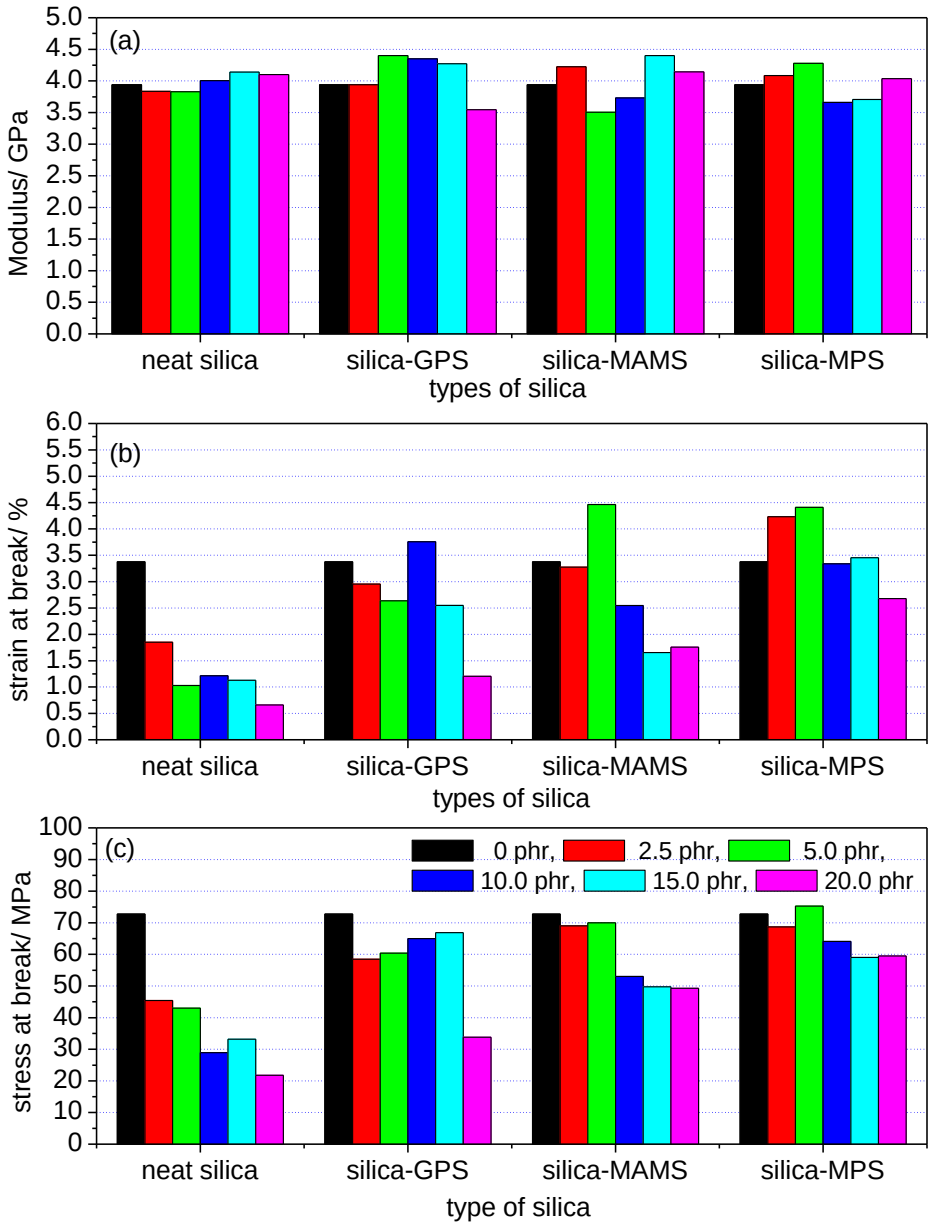

Figure 2.11. Data from tensile testing at room temperature.

For epoxy + surface-treated silica systems, the obtained results are more complex. Only the epoxy + silica-GPS showed the tendency similar to that of the epoxy + neat silica system, but the effect of silica on the values of Young's modulus is more

pronounced. The reduction in Young's modulus at a high content of silica-GPS is observed due to the agglomeration (see Figures 2.12 (c) and (d)).

As discussed earlier in sections 2.5.3, a variety of factors could affect the properties of the final products, especially the epoxy resin containing several components. The following factors affect changes in the mechanical properties: cross-link density, stiffness of the final products, interfacial interaction between epoxy and silica particles, dispersion and agglomeration of particles in epoxy matrix. For the epoxy + silica-MAMS and epoxy + silica-MPS systems, interesting phenomena are observed. It is well known that Young's modulus of polymer in the presence of inorganic fillers increases as the amounts of inorganic contents in the polymer matrix increase. The agglomeration due to the excess load of particles causes the reduction in the modulus. Nevertheless, an increase, then a decrease and followed by an increase of Young's modulus are observed in the case of epoxy+ silica-MAMS and epoxy + silica-GPS systems. An explanation similar to that for DMA results seems applicable. Silica-MAMS and silica-MPS can react with an amine curing agent and epoxy monomer, respectively, which cause a reduction in cross-link density. At low silica content, the antiplasticization effect and/or the stiffness of silica cause the improvement in Young's modulus. After adding silica-MAMS and silica-MPS above a certain critical value, the antiplasticization effect cannot suppress the liquid-like behavior due to a very low cross-link density of the network; the modulus goes down. Thus, viscoelasticity plays a dominant role in the decrease of Young's modulus. On the other hand, due to chemical interactions, the compatibility between the epoxy organic phase and the silica inorganic phase is enhanced when a higher amount of silica is added. Regardless of the existing

agglomeration, the stiffness of loaded silica together with the interfacial interaction between the inorganic and organic phases is believed to be the cause of the improvement in Young's modulus at high silica content in the case of epoxy + silica-MAMS and silica-MPS.

Figure 2.11 (b) shows strain at break of epoxy + silica hybrids at various concentrations and different surface treatments of silica. Except for systems with silica-MAMS and silica-MPS, the expected results are observed for almost all epoxy + silica systems. Strain at break decreases with increasing the amount of silica. For the epoxy + silica-MAMS and epoxy + silica-MPS, the optimum contents, providing the strain at break higher than pure epoxy, are about 5.0 phr. Values of strain at break of the epoxy + silica-MAMS and epoxy + silica-MPS composites are higher than those of epoxy + neat silica and epoxy + silica-GPS systems. The results imply that the latter systems are more brittle. A similar explanation involving the reduction in cross-link density and the interfacial interaction applies. In Figure 2.11 (c), stress at break, defined as strength, for all epoxy composites is lower than that of pure epoxy. The strength of epoxy composites filled with neat silica decreases as the amount of silica increases. However, the strength of all epoxy composites filled with the surface-treated silica is improved, compared to that of the epoxy composites filled with neat silica. This probably occurs because of the improvement of interfacial interaction between the surface-treated silica particles and epoxy matrix.

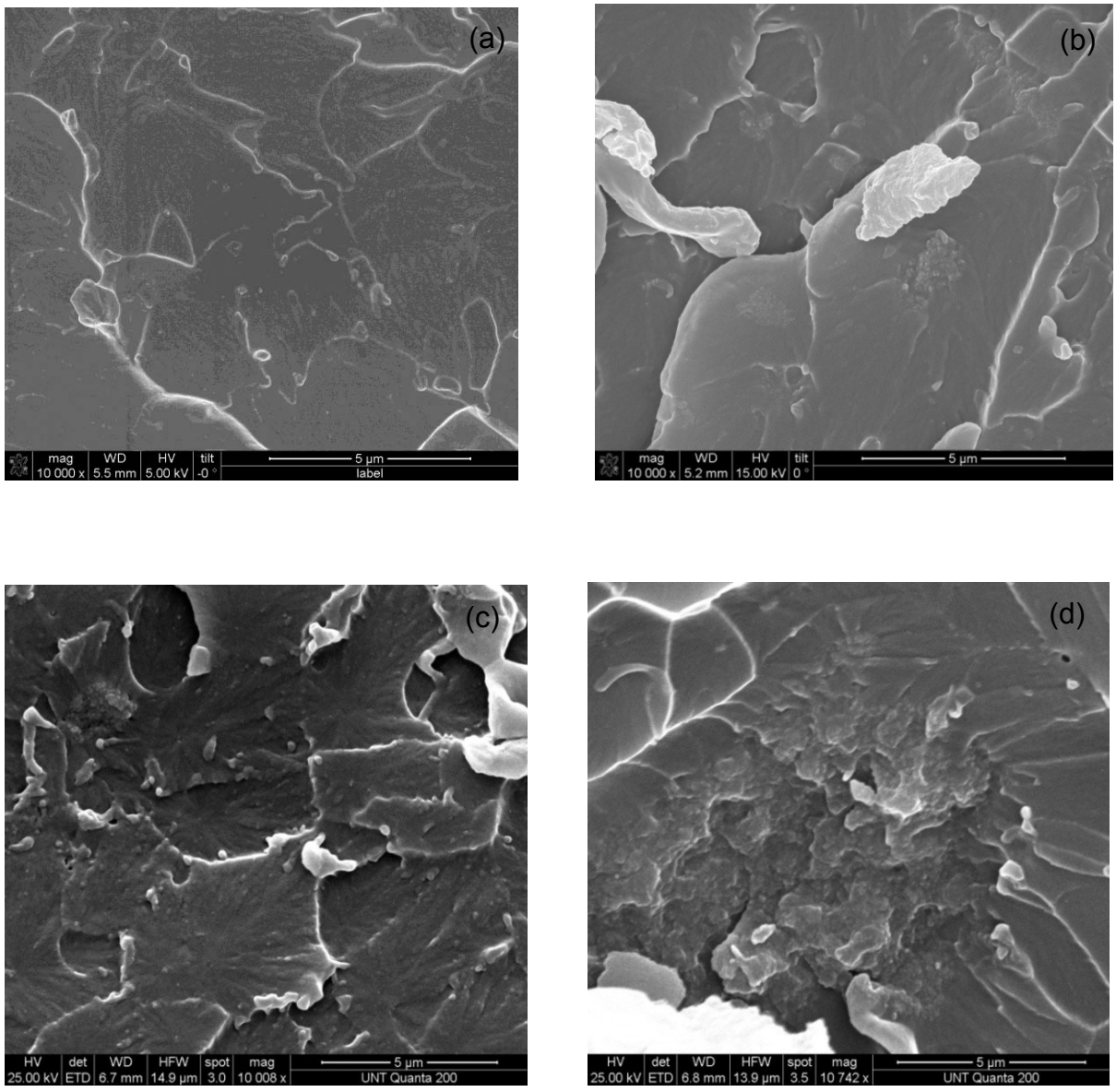

Figure 2.12. SEM micrograph of epoxy composites filled with (a) 5.0 phr of neat silica, (b) 20.0 phr of neat silica, (c) 5.0 phr of silica-GPS and (d) 20.0 phr of silica-GPS.

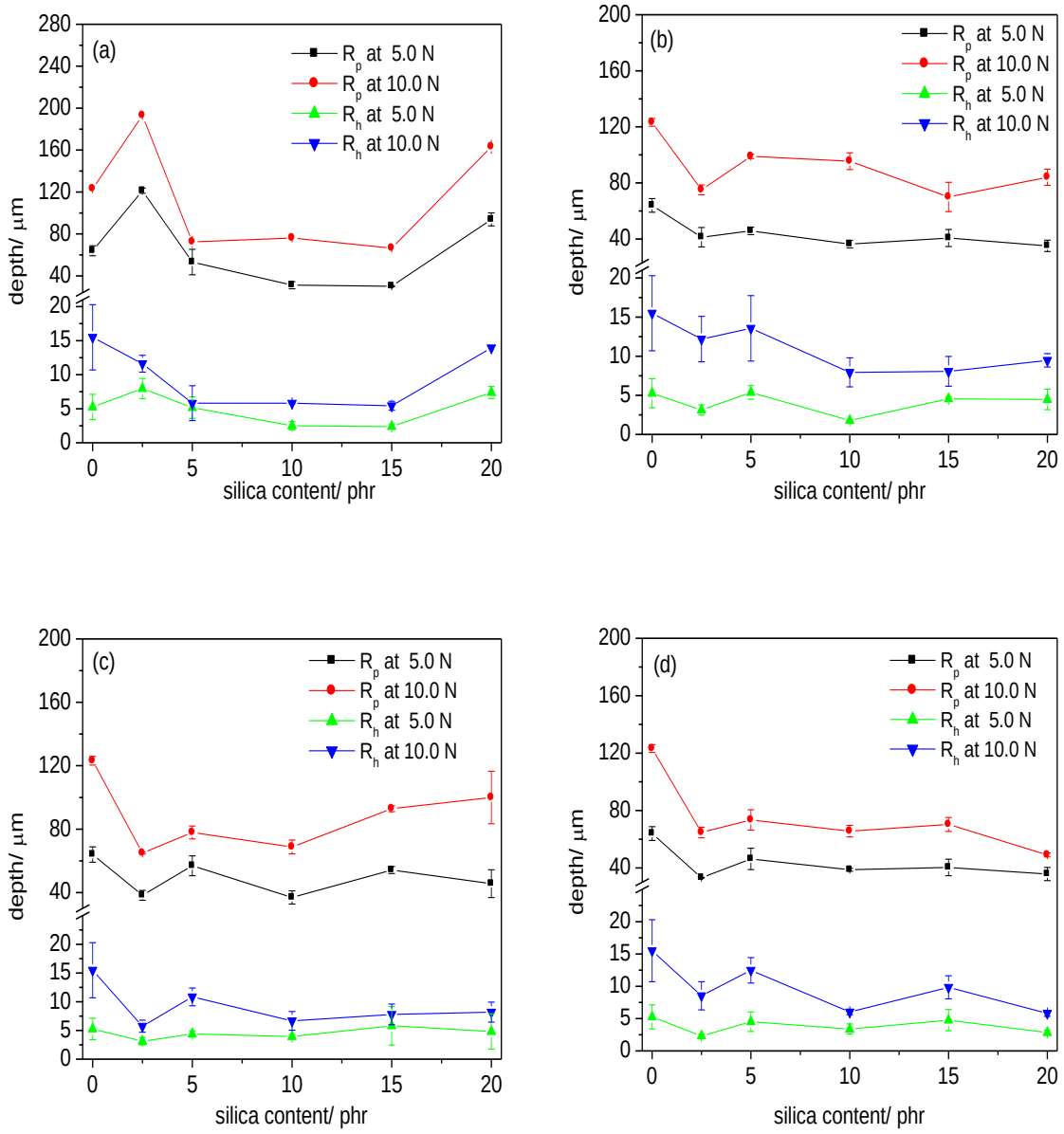

Figure 2.13. Penetration depth R_p and residual depth R_h as a function of silica content at applied forces of 5.0 N and 10.0 N.

2.5.5 Scratch Resistance Testing

In the present study, the effects of silica content and the chemical surface treatment of silica surface on the scratch resistance of epoxy were determined by the scratch testing machine. The obtained results are shown in Figure 2.13.

Figures 2.13(a) to (d) show the penetration depth R_p and residual depth R_h as a function of silica content for epoxy composites filled with neat silica, silica-GPS, silica-MAMS and silica-MPS, respectively. All diagrams show that, apart from deeper depths obtained from applying a higher load, there is no difference in the results obtained at the load of 10.0 N from those of 5.0 N. In Figure 2.13 (a), both R_p and R_h for epoxy + neat silica composites show a similar tendency. When a small amount of silica (2.5 phr) is added, the depths increase. A further addition of neat silica suppresses the penetration of a diamond tip by producing somewhat larger bumps on the route of the travelling diamond or by the hard phase of silica itself. The scratch resistance is improved. However, the R_p increases again after adding neat silica up to 20.0 phr. The increasing depth at high concentration is attributed to the brittle nature of silica clusters. These clusters form due to the agglomeration of silica at a high content and behave as glasses which are naturally easy to be scratched by a diamond.

Compared with pure epoxy, the R_p and R_h values for all the epoxy + surface-treated silica systems (see Figures 2.13 (b) to 2.13 (d)) are lower than that of pure epoxy. The R_h, the final depth which determine the scratch resistance of materials, decreases when surface-treated silica is added, and then levels off at a certain silica content. The optimum silica content which provides the highest scratch resistance (the lowest R_h) is found at 2.5 phr for silica-MAMS and 10 phr for silica-GPS and silica-MPS.

It is interesting that, even though the silica clusters are observed at a high silica load for other epoxy + silica systems, only the epoxy with neat silica shows an increase in depth when silica content is 20 phr. This may be because silica with the silane coupling agent on the surface formed clusters with a lower rigidity.

Figure 2.14 shows percent elastic recovery as a function of silica content. Percent elastic recovery (% ER) is a useful indicator in evaluating the elastic/plastic behavior of materials. The more the recovery of the penetration depth R_p is, the higher the elastic behavior. This parameter is calculated as follows:

$$\%ER = \left[1 - \frac{R_h}{R_p}\right] \times 100 \tag{2.4}$$

In Figure 2.14, silica does not significantly affect the elastic behavior of epoxy resin—the elastic recovery of the composites changes within ±5 %, compared to the pure epoxy resin. At a 10.0 N load, however, the epoxy composites filled with neat silica exhibit the highest percent recovery. This means that the composites filled with neat silica behave more elastically than the epoxy composites filled with surface-treated silica even though the latter exhibits the lowest R_h (highest scratch resistance).

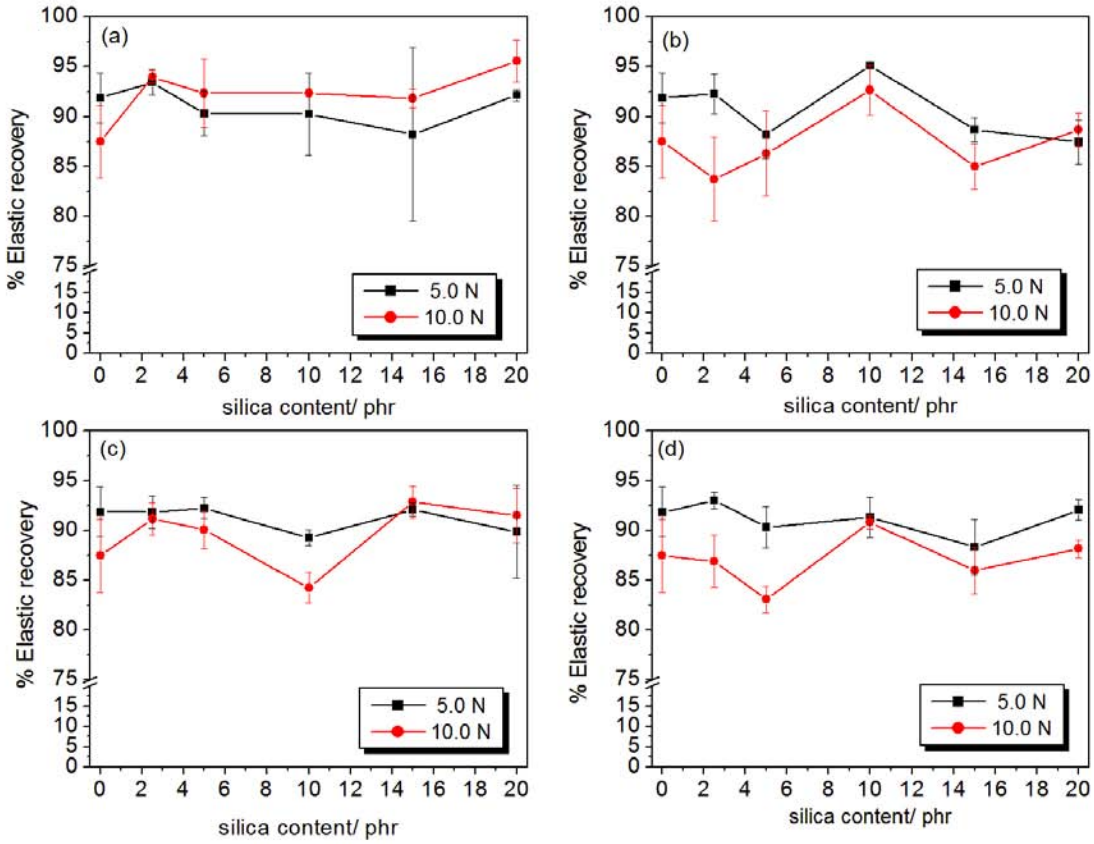

Figure 2.14. Percent elastic recovery as a function of silica content for (a) epoxy + neat silica, (b) epoxy + silica-GPS, (c) epoxy + silica-MAMS and (d) epoxy + silica-MPS.

2.5.6 Friction and Wear

The tribological data present in this section were obtained using a pin-on-disc type of tribometer at an average contact pressure (p) of 70 MPa and sliding velocity (v) of 4.19 mm/s (see APPENDIX A). Note that the pv condition used here (2.92 MPa × m/s) is high relative to similar studies, which are about 1.725 MPa × m/s [61], 1.5 MPa × m/s [36] or below [27, 29, 62, 63]. The different wear and friction behaviors were expected for observation.

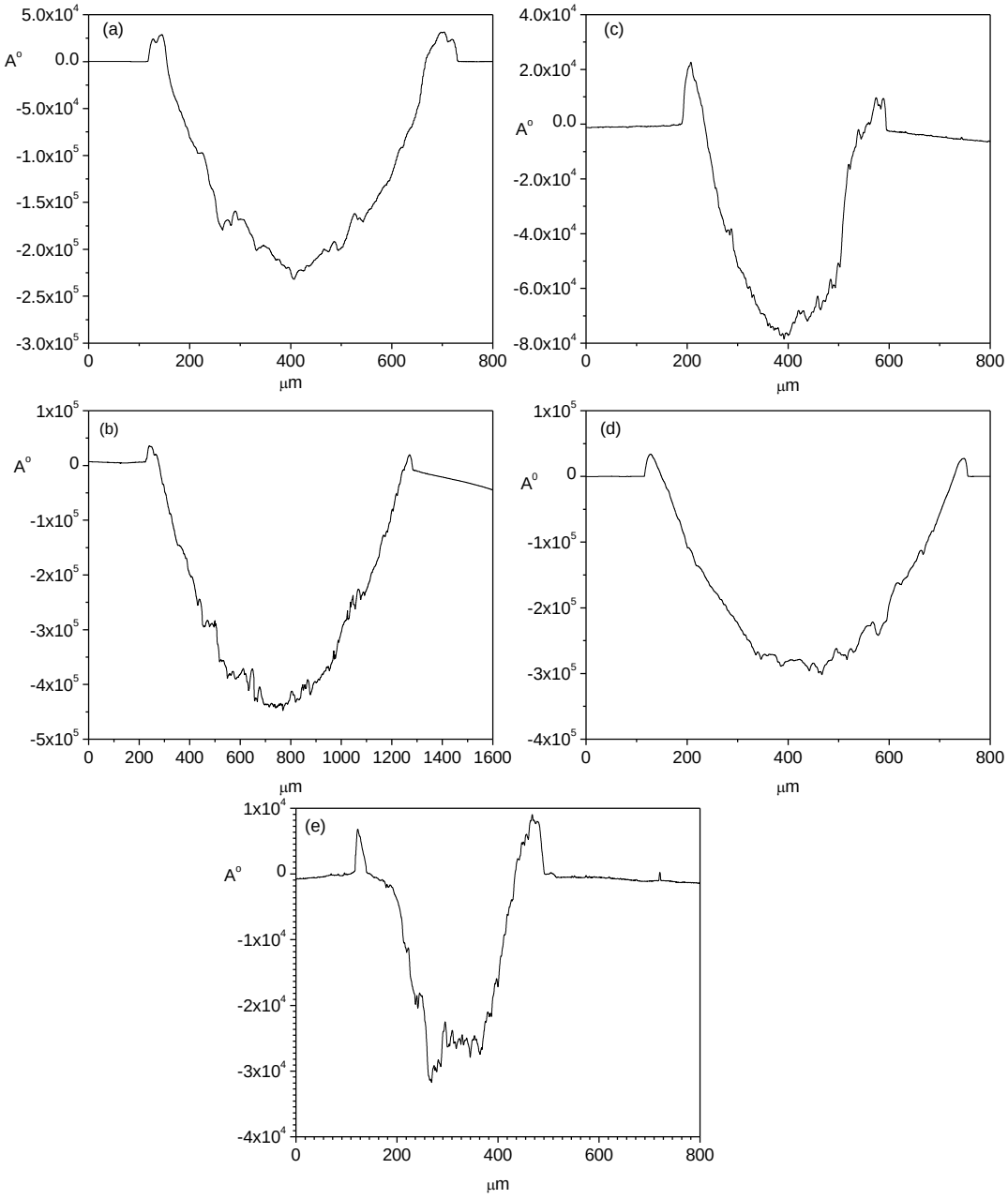

Figure 2.15. Profilometer cross section of wear traces for (a) pure epoxy, (b) epoxy + neat silica, (c) epoxy + silica-GPS, (d) epoxy + silica-MAMS and (e) epoxy + silica-MPS after sliding against Si_3N_3. Silica content: 20.0 phr; sliding speed: 200 rpm; normal load: 5.0 N; revolution: 10,000 turns.

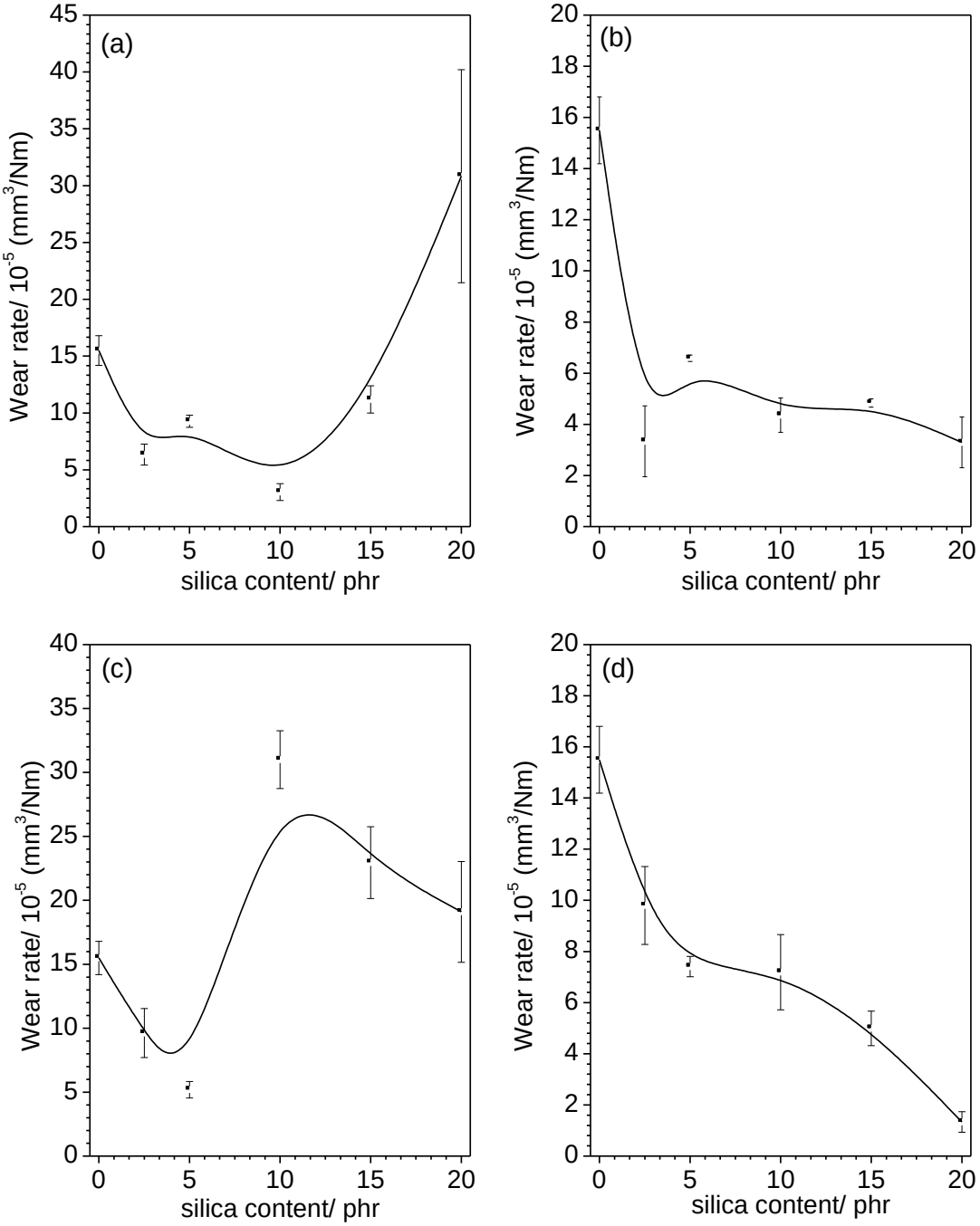

Figure 2.16. Wear rate of the epoxy composites filled with (a) neat silica, (b) silica-GPS, (c) silica-MAMS, (d) silica-MPS. Sliding speed: 200 rpm; normal load: 5.0 N; revolution: 10,000 turns.

To determine wear volume, the profiles of the epoxy surface after sliding against a Si_3N_4 ball for 100000 turns were investigated. Figure 2.15 shows the typical examples of cross-section profiles for the different epoxy systems acquired in the center of each wear track. On all samples, wear traces left by the removed material can be observed and quantified. In the cross-section profile, peaks and small grooves are observed. These peaks and grooves imply a cracking process that occurs inside the wear track [22]. Ridges along the side of the wear trace are also observed. This ridge formation, known as plouging process, occurs as a result of the deformation of materials [41]. The cross-section area obtained then is multiplied by the wear trace length in order to estimate the wear volume V_m as shown here,

$$V_m = 2\pi R_m A_m \tag{2.5}$$

where R_m and A_m correspond to the radius of the wear track and to the average cross-section area of the wear track, respectively. To facilitate comparison of the wear resistance of the hybrid, the wear rate K (mm^3 /N m) was determined by the following equation

$$K = \frac{V_m}{Wvt} \tag{2.6}$$

or

$$K = \frac{V_m}{Wx} \tag{2.7}$$

where W is the normal load, V_m is the volume of wear, ν is the sliding velocity, t is the test duration and x is the sliding distance. Plots of wear rate K, defined by Equation (2.7) as a function of silica content for epoxy composites filled with neat silica, silica-GPS, silica-MAMS and silica-MPS are shown in Figure 2.16 (a), (b), (c) and (d), respectively.

For epoxy + neat silica (see Figure 2.16 (a)), the addition of silica less than 10 phr significantly reduces the wear rate of unfilled epoxy. However, adding a larger amount causes wear to increase again. It is found that wear rate is even higher than that of pure epoxy when 20.0 phr of neat silica is added. One of the possible reasons for the increasing wear rate, for epoxy composites filled with non active-surface silica at higher silica loading, is the increasing brittle nature of materials. Accumulation of these hard particles can also increase wear due to third body abrasive wear.

In contrast, the wear rate of the epoxy filled silica-GPS (see Figure 2.16 (b)) decreases as silica content is increased. A similar tendency is also observed in the case of epoxy + silica-MPS (see Figure 2.16 (d)), but the reduction in wear rate of epoxy + silica-MPS at 20.0 phr is much lower than that for epoxy + silica-GPS. In fact, the value of wear rate of epoxy + silica-MPS is almost one order of magnitude lower than that of the pure epoxy. The increasing interfacial interactions between the inorganic and organic phases through a chemical bonding contribute to the improvement in wear resistance at high silica loading of the epoxy + silica-GPS and epoxy + silica-MPS systems. It is shown in Figure 2.16 (c) that at high silica content (20.0 phr), the silica-MPS provides the most effectiveness in reducing wear rate among any other surface-modified silica. Zhang et al. [31] demonstrated that the enhanced wear resistance of epoxy composites filled with nanosilica grafted polyacrylamide (PAAM) was due to the improvement of the interfacial interaction between the particles and the matrix.

It is interesting that unexpected results are observed. The effect of silica content on the wear rate of the epoxy + silica-MAMS differs from that observed in the epoxy + silica-GPS and epoxy + silica-MPS systems. As discussed earlier, silica-MAMS can

perform chemical interactions with amines and cause the reduction in cross-link density. High interfacial adhesion between an inorganic and organic phase is expected as well for the epoxy + silica-MAMS systems. Thus, the higher the silica content that is in the systems, the lower the wear rate should be. It is found in Figure 2.16 (c) that wear rate of epoxy + silica-MAMS decreases only when the addition of silica is less than 5.0 phr. A further rise in silica loading leads obviously to a deterioration of the wear rate. A change in the wear mechanism should be involved, which may be ascribed to the large amount of hard particles leading to increased third body abrasive wear.

Durand et al. [64] were the first to propose a wear mechanism of epoxy resins. The mechanisms include the formation of surface and subsurface cracks, the development from cracks to waves and the production of debris. For epoxy composites, the particles hinder cracking and thus increase wear resistance when compared to pure epoxy [24]. In the present studies, a similar wear mechanism is observed. Figures 2.17 (a) and (b) show the optical image and Raman mapping across the wear track of the pure epoxy resin after passing 3.0 N load of a Si_3N_4 ball at 10,000 revolutions. There is no change in the chemical structure found in the worn surface relative to a fresh one. Only a change in the Raman intensity is observed. The crack propagated perpendicularly to the sliding direction and the surface fatigue-delamination generated under repeated loading during sliding are observed. The strong dependence of the fatigue wear on the load is demonstrated in Figure 2.17 (c). When a higher load (10.0 N) is applied, a substantial increase in wear is observed. A larger track and more surface delamination appear on the surface. It should be noted that, for such a high pv condition (3.68 MPa × m/s), the heat of friction is considerable. Another wear mechanism, namely thermal

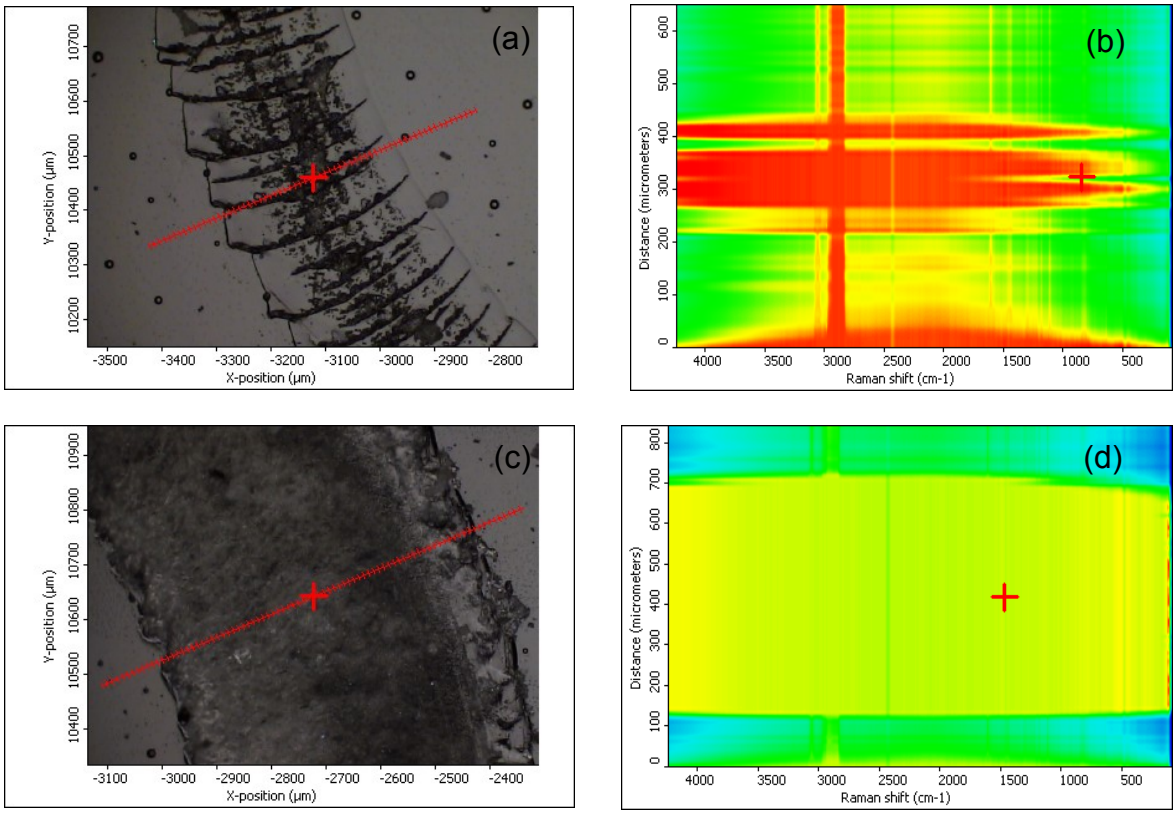

Figure 2.17. Optical image (100x) and Raman mapping of worn surface for pure epoxy. Condition of sliding wear tests: (a, b) normal load of 3.0 N; sliding speed of 200 rpm; revolution of 10,000 turns (c, d) normal load of 10.0 N; speed of 200 rpm; revolution of 10,000 turns.

softening, is incorporated and causes the severe worn surface at this load (10.0 N).

For more information about the characteristics of the wear traces among the systems, the worn surface of the pure epoxy and composites filled with treated and untreated silica particles were examined with SEM at identical magnifications.

Figure 2.18 demonstrates a comparison of worn surfaces of the pure epoxy and epoxy composites filled with untreated silica and surface-treated silica. In Figure 2.18 (a), the scale-like damage pattern, generated under repeated loading during sliding, leaves traces on the worn surface, indicating the surface fatigue-delamination types of wear. This process causes subsurface plastic deformation and may have contributed to

the nucleation of surface and subsurface crack [41]. Magnified microstructures of the worn surface (Figures 2.18 (b, c)) show that there are, like those found in the optical micrographs, cracks across the wear tracks and large material waves, which occur due to the brittle nature of the epoxy. For the silica-reinforced composites, material waves [24, 64] along the sliding direction are observed. The size of the material waves found in the composites varies, depending on the types of silane modified silica, but all of them are smaller than that of the pure epoxy system.

For the epoxy + neat silica composites, the scale-like damage of the worn surface is found to be less severe than that observed in pure epoxy resin. In a more magnified microstructure, the crack formation is rarely observed because there are particles to arrest the cracks (see Figure 2.18 (f)). Similar phenomena are observed in epoxy composites filled with surface-treated silica, except for in the epoxy + silica-GPS systems. The appearances of worn surfaces of epoxy + silica-GPS are different. The magnified microstructure of epoxy + silica-GPS shows a smoother surface (see Figure 2.18 (h)) than any others. Some small holes due to debris pulled out and minute material waves are present (see figure 2.18 (i)), indicating the effectiveness of crack arresting due to the presence of silica-GPS particles.

For the epoxy + silica-MPS composites, besides the smallest width of wear track (see Figure 2.18 (m)), a distribution of the damage produced on the worn surface is found to be a continuous mode instead of a discontinuous mode as found in others. These results imply that the uneven stress concentration built up inside epoxy may have been somehow homogenized in the composites of silica-MPS, which is certainly

beneficial for reducing the amount of material loss [32]. This is why the wear rate of epoxy + silica-MPS is remarkably lower than that of pure epoxy resin (see Figure 2.16).

For the epoxy + silica-MAMS composites, worn surface shows the largest width of wear track due to the weakening of material after adding silica-MAMS. It is found in Figure 2.18 (l) that there is no major difference from other epoxy + surface-treated silica. Only some holes due to debris pulled out are found, but no evidence of cracks is observed. Thus, cracking, the wave formation and production of debris are also parts of the wear process for the epoxy composites filled with silica-MAMS. However, it should be noted that the variation of wear rate with silica content for the epoxy + silica-MAMS differs from that for other epoxy composites filled with surface-treated silica.

Based on the mechanisms discussed above, a correlation between mechanical properties and wear behavior should exist. Zhang et al. [32] reported that the wear rate of poly(ether ether ketone) composites showed a slight dependence on the material composites, modulus, density and impact resistance, opposite to the flexural strength and toughness, which were not so influential. However, no such a link is found here between the wear rate and the tensile properties of all the epoxy + silica systems. For example, the epoxy + silica-GPS at high silica content (20 phr) exhibits a lower wear rate and lower Young's Modulus as well as a lower strain at break than pure epoxy, while the epoxy + silica-MPS at high silica content (20 phr) exhibits a lower wear rate and lower strain at break but a higher modulus than the pure epoxy. Thus, the mechanical properties cannot account alone for observed differences in wear behavior. It is usually found for polymers that the combination of high tensile strength and strain to failure enhances the wear resistance. According to the Ratner-Lancaster correlation,

wear of polymer was inversely proportional to the product of fracture stress and fracture strain [65]. Again, such a correlation cannot be found in the present sets of results. Similar results have been also found by others [22, 66, 67]. The improvement in wear resistance is reported despite a measured deterioration in flexural strength. Thus, a conclusion can be drawn that the improvement in mechanical properties may not always be a requirement for tribological optimization, especially when multiple wear modes are active.

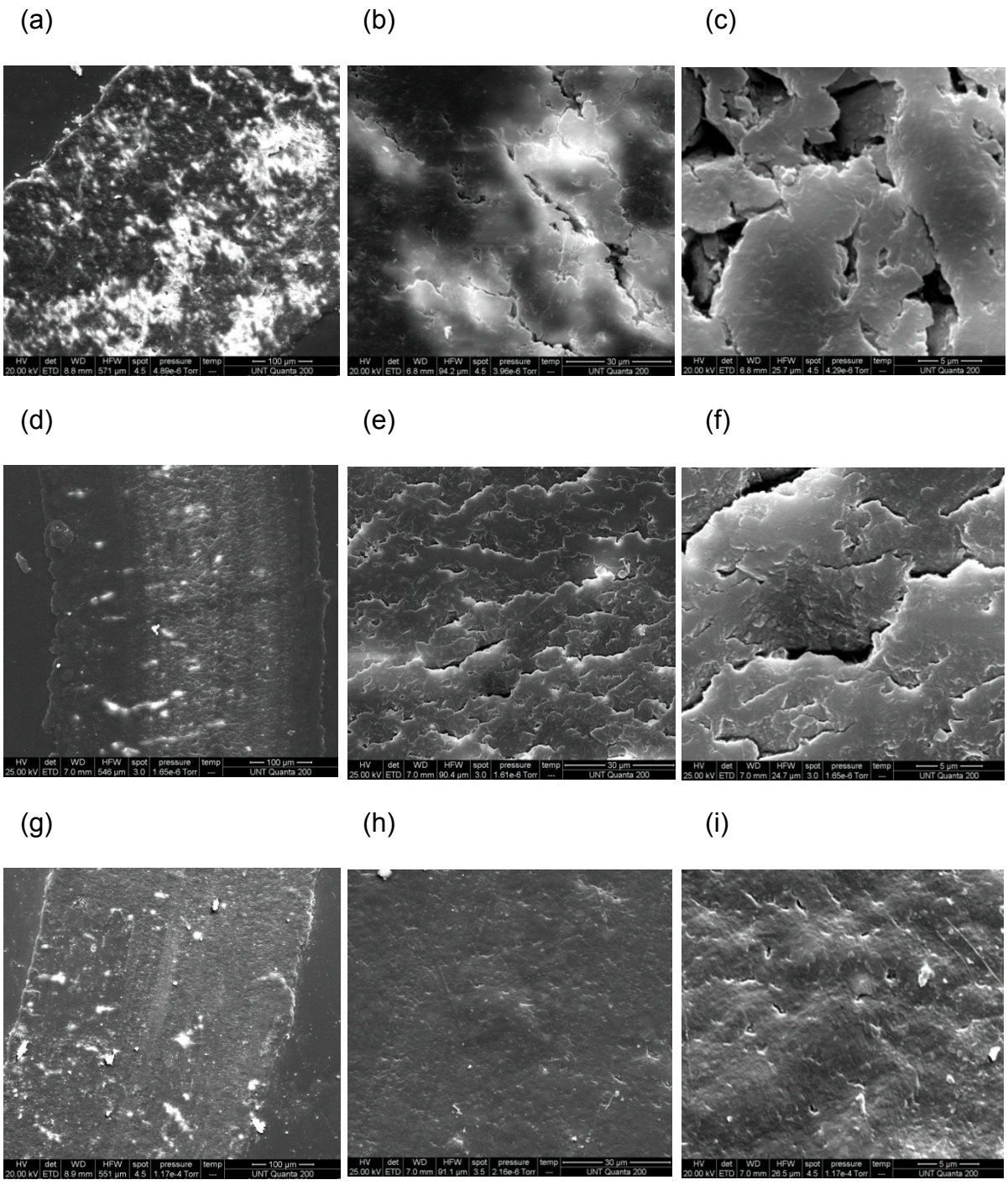

Figure 2.18. The SEM micrographs of the worn surface for (a, b, c) pure epoxy, (d, e, f) epoxy + neat silica and (g, h, i) epoxy + silica-GPS. Silica content: 15.0 phr. Condition of sliding wear tests: normal load of 5.0 N; sliding speed of 200 rpm revolution of 10,000 turns. Magnification: 260x for (a, d, g), 1600x for (b, e, h) and 5800x for (c, f, i).

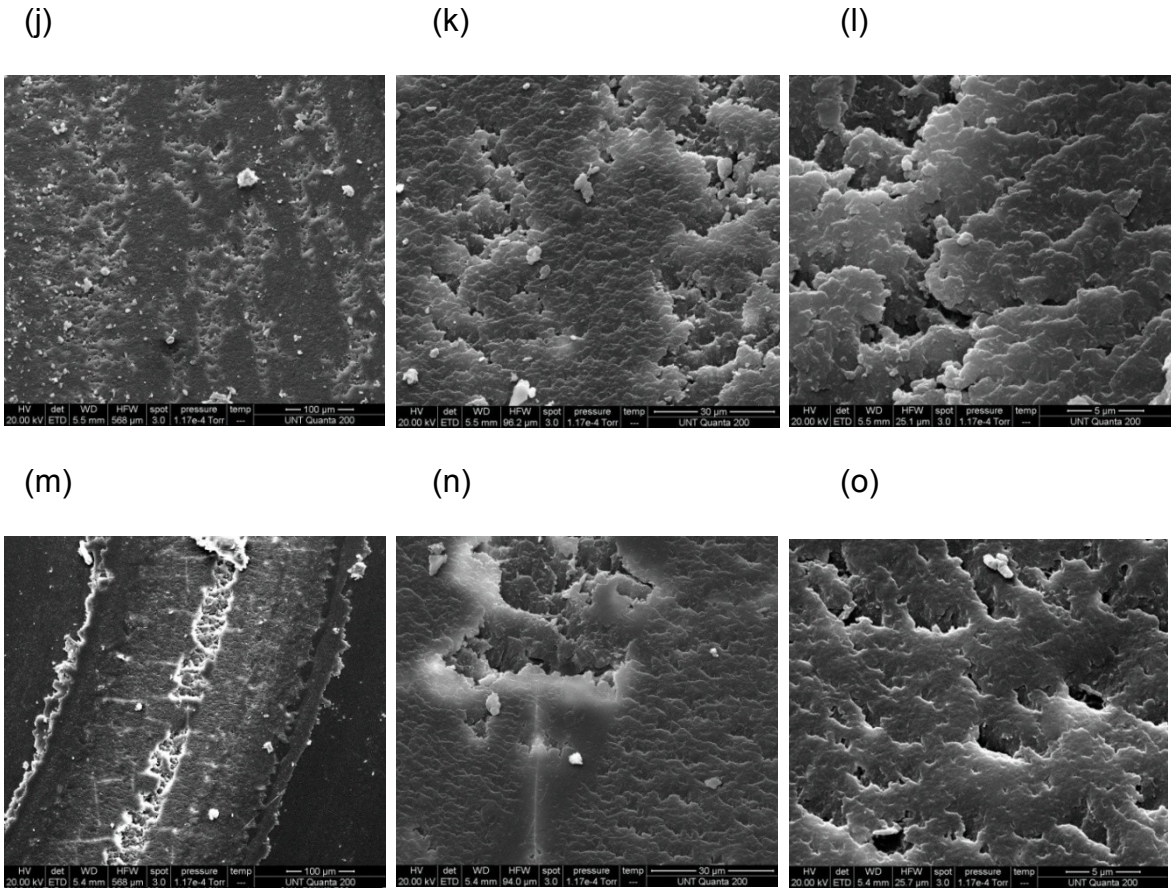

Figure 2.18. The SEM micrographs of the worn surface for (j, k, l), epoxy + silica-MAMS (m, n, o) and epoxy + silica-MPS. Silica content: 15.0 phr. Condition of sliding wear tests: normal load of 5.0 N; sliding speed of 200 rpm revolution of 10,000 turns. Magnification: 260x for (j, m), 1600x for (k, n) and 5800x for (l,o).

The evolution of the friction coefficient of the pure epoxy and epoxy composites filled with silica particles sliding against a Si_3N_4 ball are presented in Figures 2.19 (a) to 2.19 (d). It is found in Figure 2.19 that the improvement in steady state friction coefficient of all the epoxy + silica composites relative to the pure epoxy resin is not significant. Some systems even produce a greater friction coefficient than the pure epoxy. For almost all the epoxy systems, the evolution of friction coefficient exhibits a short run-in period, together with the peak due to the lumpy transfer film before attaining a steady

state. Wang and Li [68] explained that the initial formation of ridges contributed to the run-in period found in polymers. During this period, these ridges were progressively worn away until sufficient debris covered the surface leading to stable lowered-friction coefficient. Bhushan [41] explained in his book that transfer film of the plastic onto the mating surface usually occurred in many polymers sliding against hard mating surface. The decrease in friction coefficient at the steady state occurs, due to the development of a thinner transfer film as sliding progresses. It is found in Figure 2.19 that friction coefficient in the steady region gradually increases with time. This implies that the softening mechanism due to frictional heat takes place. Further discussion about frictional heat is provided later.

To facilitate the comparison, average values of the steady state friction coefficient, plotted against silica contents, are shown in Figure 2.20.

In Figure 2.20 (a), the friction coefficient of the epoxy composites filled with neat silica decreases as neat silica is added up to 5.0 phr. Further addition of neat silica leads to an increase in the friction coefficient relative to the pure epoxy. A similar tendency is found in the epoxy + silica-MAMS systems, but the optimum silica content causing the reduction in friction coefficient is at 2.5 phr.

In Figures 2.20 (b) and (d), the addition of either silica-GPS or silica-MPS in the epoxy causes the reduction in friction coefficient. Values of friction coefficient decrease as silica content increases up to 15.0 phr. Then, when filler content is raised to 20.0 phr, both systems exhibit an increase in the friction coefficient; however, their values are still lower than that of the pure epoxy.

It is generally known that polymers have low thermal conductivity, thus resulting in a high sliding interfacial temperature at a lower pv condition than that of metals. The temperature at sliding interface affects changes in modes of wear and friction. If the temperature at sliding interface is higher than T_g, the thermal softening and the associated increase in the real contact area cause the friction coefficient to rise. If the sliding interfacial temperature is higher than T_m, the friction coefficient goes down due to lubrication by a molten film of polymers [42]. In this study, melting/re-melting of sliding surface should not be found due to the nature of thermosetting materials. Only the thermal softening and thermal decomposition are expected for such a high pv condition. Nevertheless, no evidence of these mechanisms is detected from the SEM micrograph. Only the adhesion, abrasion and fatigue, as types of wear mechanisms, are observed on the worn surface of studied epoxy systems. To explain more about this phenomenon, the determination of the sliding interfacial temperature is necessary. The average transient surface temperature for circular contacts due to the friction in the high speed case (see APPENDIX C) was developed by Archard [69]. The formula is presented as [70]:

$$T_{fa} = 0.308 \frac{\mu W |U_A - U_B|}{Ka} \left(\frac{\chi}{Ua}\right)^{0.5} \quad (2.8)$$

where T_{fa} is the average flash temperature (^oC), μ is friction coefficient, W is the normal load (N), U_A and U_B are the surface velocities of solid A and solid B, respectively (m/s), a is the radius of the contact circle (m), χ is the thermal diffusivity (m^2/s) and K is the thermal conductivity (W/mK). The tentative flash temperature for the pure epoxy resin is approximately 114^oC (see APPENDIX C). The T_g determined from the peak of tan δ for the pure epoxy resin is 118^oC, while one determined from the peak of loss modulus is

106^{o}C. The flash temperature is in the range of the T_g of the studied epoxy resin. The resin just below the surface is probably beyond the T_g and consequently becomes rubbery. The thermal softening should be able to take place, accordingly. Defined as the Peclet number, the capability of heat transfer to a stationary body varies with speed ranges. The Peclet number for the present system is 31.6. Thus the system is modeled by a fast moving heat source (see APPENDIX B for more details). This implies that there is insufficient time for the temperature distribution of contact to be established in the stationary body and the depth at which heat penetrated into the stationary body is very small compared to the contact dimension [70]. Due to a higher thermal conductivity of Si_3N_4, the heat generated mostly transfers to the Si_3N_4 ball. It should be noted that the flash temperature of the epoxy composites filled with silica is lower than that of pure epoxy resins. Their thermal conductivities are between the range of 0.418 to 0.836 W/mK [71], more than two times higher than that of pure epoxy. These altogether may be reasons why the thermal softening was not observed from the worn surface of the studied epoxy + silica systems.

Another aspect for the tribological improvement is the transfer film formation. The transfer films are expected to act as a protective spacer between the surfaces. Thus, an enhanced ability to form thin homogeneous and tenacious transfer films on the counterpart is one of the keys for the improvement in wear resistance. The stabilization of transfer films is typically attributed to tribo-chemical reactions, which increase the adhesion of the film to the counterpart [72-75]. Their formation and behavior seem to depend on external conditions of temperature and sliding speed [76]. It is suggested

that the cohesive strength of the transfer film was increased because of the capability of particles to blend well with the wear debris [33, 67].

To examine the effect of transfer films on the tribological properties, the Si_3N_3 ball after sliding against epoxy samples was investigated with the optical microscope at identical magnification. Only the epoxy composites filled with silica at high content demonstrated different behaviors. Increasing friction coefficient is found in the epoxy + neat silica and epoxy + silica-MAMS systems, while decreasing friction coefficient is found in the epoxy + silica-GPS and epoxy + silica-MPS systems. Thus, the pure epoxy and epoxy composites filled with the different types of silica at 15.0 phr are chosen for this study.

Figure 2.21 shows the optical micrograph of transfer film formed on the surface of Si_3N_4 counterface after sliding against various epoxy systems. The intermittent, thick and lumpy transfer film is observed in the Si_3N_4 conterface after sliding against the pure epoxy (Figure 2.21 (a)). This is unexpected unless the pv condition is high. Epoxy is not known for forming a transfer film due to cross-linked structure. Larsen et al. [36] suggested that the smooth counterface combined with the thermal degradation of epoxy due to the frictional heat during sliding caused the film formation in epoxy. In this study, the thermal softening, due to the frictional heat generated at the contact surface during sliding, probably enhances the plastic deformation and thus the adhesion of the resin to the counterpart.

For epoxy + neat silica (Figure 2.21 (b)), the dark transfer film together with streaks of black lines due to abrasiveness of neat silica particles is observed. This blackening transfer film from the thermal decomposition is believed to develop because the

frictional heat preferably transfers to the ball. This transfer film looks homogenous but uneven; some parts are thicker than others. According to adhesive model of friction,

$$F_f = \tau A_r \tag{2.9}$$

By combining Equation (2.9) and the Amonton's law of friction, one obtains

$$\mu = \frac{F_f}{W} = \frac{\tau A_r}{W} = \frac{\tau}{p} \tag{2.10}$$

Then the interfacial shear stress can be determined by

$$\tau = \mu p \tag{2.11}$$

where μ is friction coefficient, F_f is friction force, τ is interfacial shear stress, A_r is a real contact area, W is normal force and p is average contact pressure. Interfacial shear stress of epoxy + silica composites shows in Table 2.5.

Table 2.5. Interfacial shear stress of epoxy + silica composites.

Silica content / phr	Interfacial shear stress / MPa			
	Epoxy + neat silica	Epoxy + silica-GPS	Epoxy + silica-MAMS	Epoxy + silica-MPS
0	38.0	38.0	38.0	38.0
2.5	35.4	36.0	36.5	35.8
5.0	33.6	35.3	37.4	36.3
10.0	36.8	35.0	39.1	35.0
15.0	40.0	35.2	39.5	33.2
20.0	39.7	38.1	40.4	36.9

In Table 2.5, epoxy composites with neat silica at high contents (15.0 and 20.0 phr) do not provide a significant change in the interfacial shear stress, compared to the pure epoxy resin. Thus, increasing real contact area causes friction coefficient of the epoxy composites with neat silica at high content to increase (see Equation 2.10). On the other hand, the third body adhesive wear of the accumulated silica plays a key role for increasing wear rate.

For epoxy + silica-GPS (Figure 2.21 (c)), only a small trace of transfer film is observed. This result implies that only loose debris is produced, or this debris adheres preferably to the epoxy component rather than to the Si_3N_4 counterpart. The author suggests the latter reason due to the obtained SEM micrograph (Figure 2.18 (h)) together with results shown in Figure 2.16 (b) and in Figure 2.20 (b). The debris, which smears on the wear track, acts as a protective layer; thus, a low wear rate is observed. In addition, a low friction coefficient is due to a low interfacial shear stress of the worn surface on which debris smears (see Table 2.5).

As discussed previously, the cross-link density and T_g of the epoxy decreases when silica-MAMS and silica-MPS are added. Thus, compared to the pure epoxy, a higher amount of film transferred to the counterface is expected.

For epoxy + silica-MAMS (Figure 2.21 (d)), the transfer film is observed on the surface of the Si_3N_4 ball. The film contains some area where it is thin and other area where it is thick and lumpy. Traces of transfer film, which are peeled off from the Si_3N_4 surface during sliding, are observed. Thus, it can be inferred from this result, together with the size of wear track from SEM image in Figure (2.18 (j)), that epoxy + silica-MAMS is easy to abrade. The possible explanation is the weakening of material due to the low cross-link density. However, only loose debris, but not homogeneous and tenacious transfer films, is formed on the counterpart. Thus, the addition of silica-MAMS causes the deterioration in the wear resistance and friction coefficient of epoxy. It was found by Hak Gu Lee et al. [27] that loose debris not only increased the friction coefficient, but also induced the fluctuation in friction coefficient.

For epoxy + silica-MPS (Figure 2.21 (e)), in contrast, the homogeneous dark transfer film is observed. The blackening film from thermal decomposition is due to the frictional heat preferably transferred to the ball. This observed transfer film is uniform and well-adhered across the contact area, and there are no lumpy parts of the film observed. The thermal decomposition of the epoxy + silica composites containing sulfur atoms probably causes the formation of the film with low shear stress (see Table 2.5) and consequently causes a low friction coefficient. The complete transfer film covering the contact acts as the protective spacer between surfaces, which explains the decrease in wear rate found in the epoxy + silica-MPS systems.

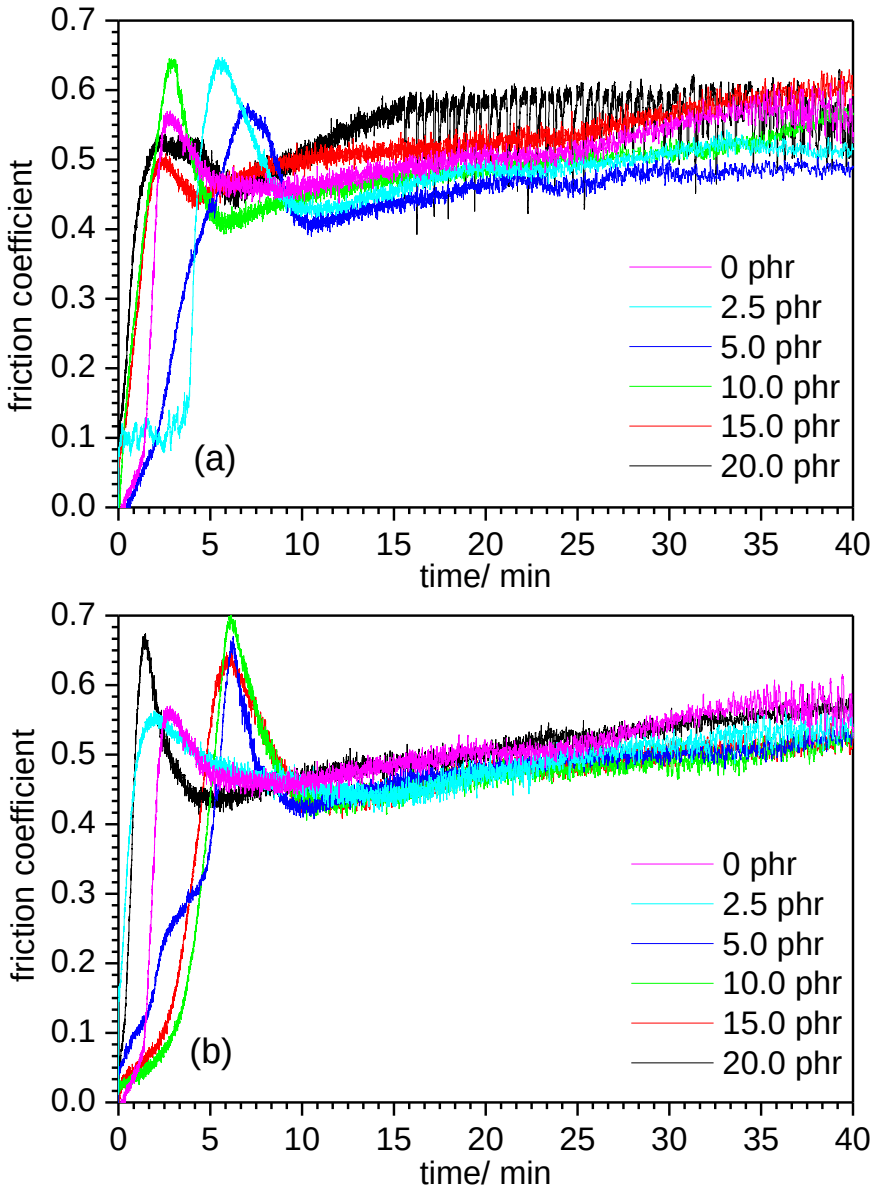

Figure 2.19. Evolution with time of the friction coefficient under a normal load of 5.0 N and sliding speed of 200 rpm against Si_3N_4 ball for (a) epoxy + neat silica and (b) epoxy + silica-GPS.

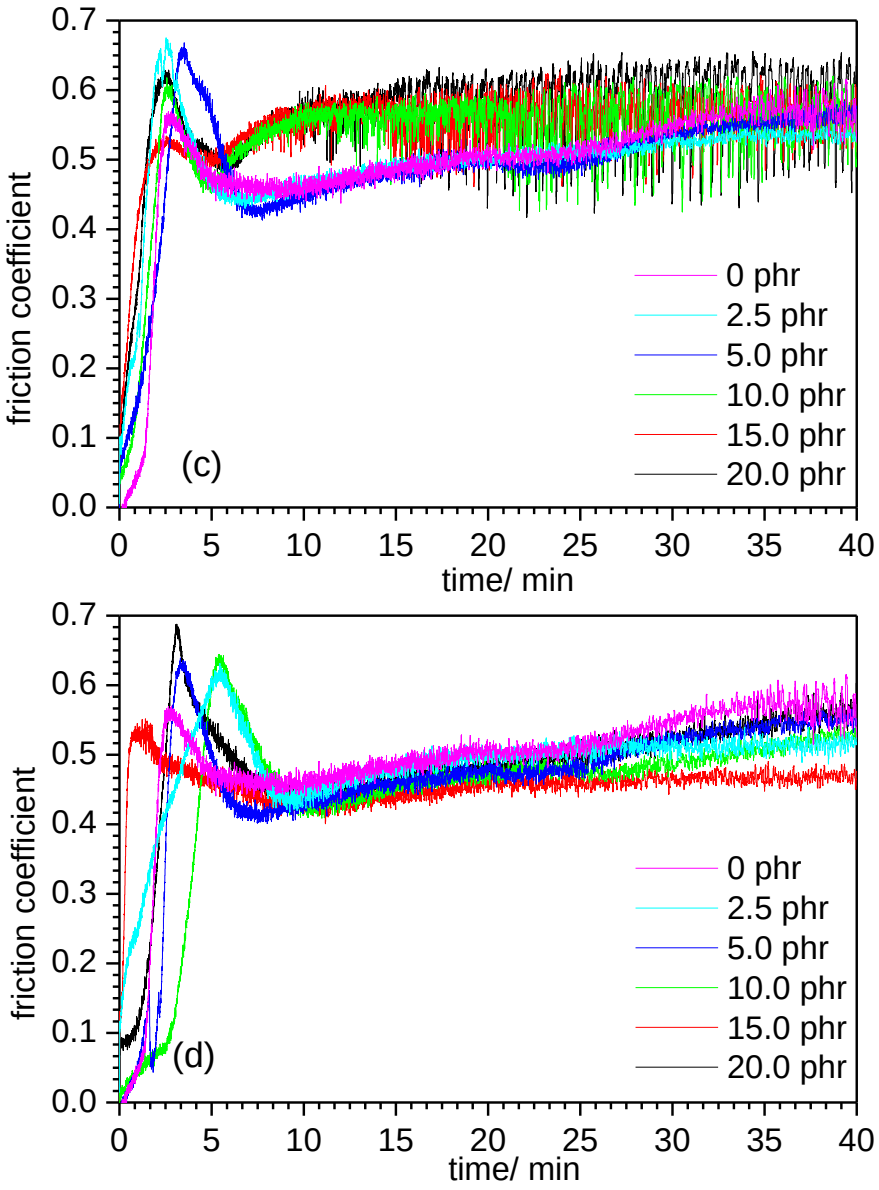

Figure 2.19. Evolution with time of the friction coefficient under a normal load of 5.0 N and sliding speed of 200 rpm against Si_3N_4 ball for (c) epoxy + silica-MAMS and (d) epoxy + silica-MPS.

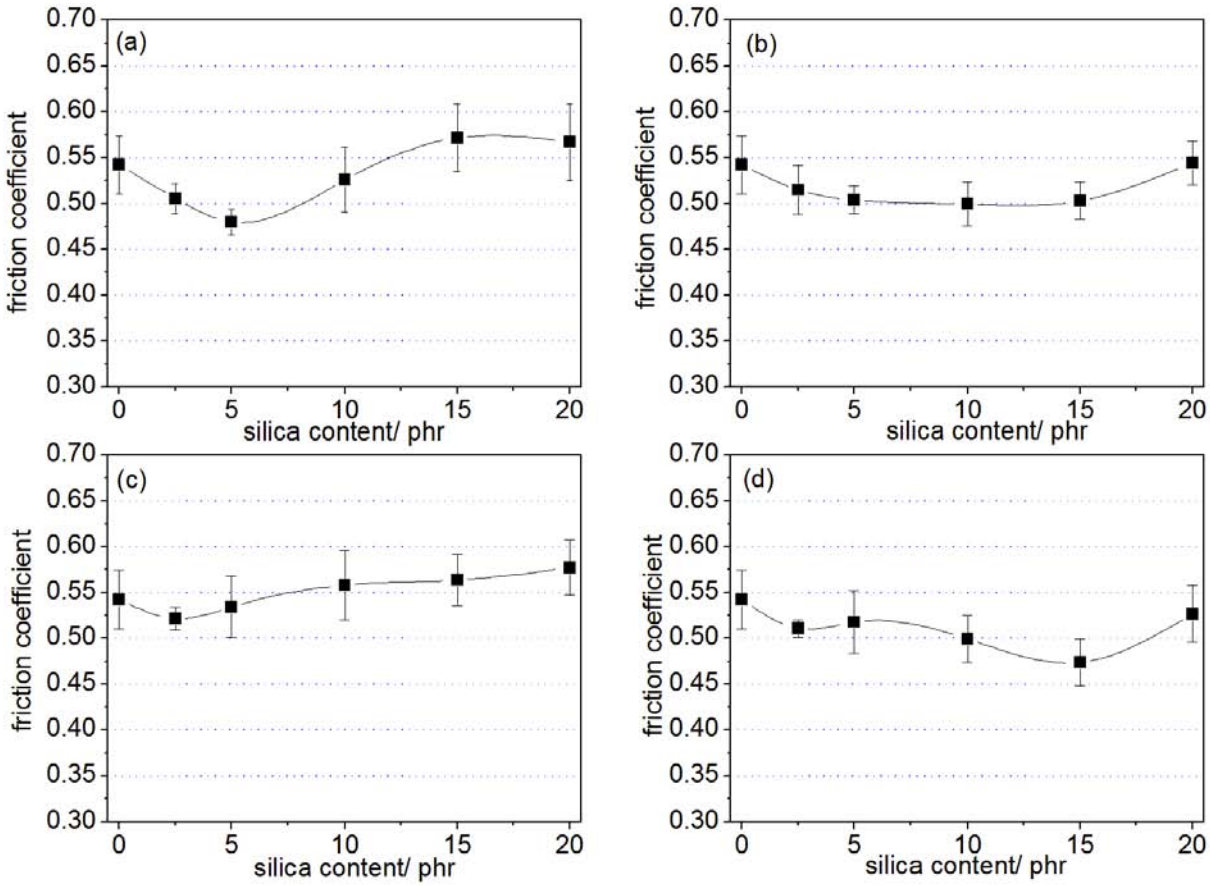

Figure 2.20. Steady state friction coefficient of (a) epoxy + neat silica, (b) epoxy + silica-GPS, (c) epoxy + silica-MAMS and (d) epoxy + silica-MPS systems. Normal load: 5.0 N; sliding speed: 200 rpm; revolution: 10,000 turns.

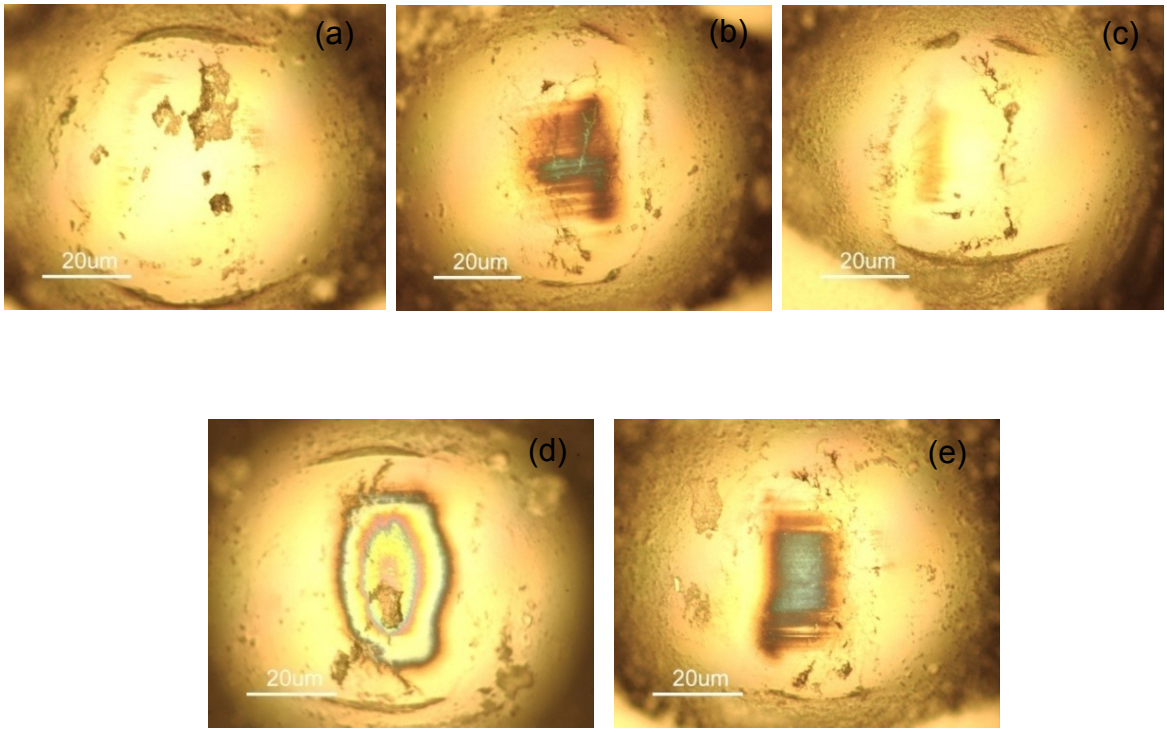

Figure 2.21. Optical image (100x) of transfer film formed on the surface of Si_3N_4 counterface after sliding against (a) pure epoxy, (b) epoxy + neat silica, (c) epoxy + silica-GPS, (d) epoxy + silica-MAMS and (e) epoxy + silica-MPS. Normal load: 5.0 N; sliding speed: 200 rpm; revolution: 10,000 turns.

2.6 References

[1] Frisch HL, Mark JE. Chem Mater 1996;8:1735-1738.

[2] Park J, Jana S. Macromolecules 2003;36:8391-8397.

[3] Chawla KK. Composite materials, New York: Springer-Verlag, 1998.

[4] Reck E, Seymour S. Macromol Symp 2002;187:707-718.

[5] Borup B, Edelmann R, Mehnert R. Eur Coat J 2003;6:21.

[6] Zhou S, Wu L, Sun J, Shen W. Prog Org Coat 2002;45:33-42.

[7] McAdams LV, Gannon JA. Epoxy resin. In: Mark HF, editor. Encyclopedia of polymer science and engineering, vol. 6. New York: Wiley, 1985.

[8] Richerson DW. Modern ceramic engineering: properties, processing and uses in design, 2nd ed. New York: Marcel Dekker, 1992.

[9] Stöber W, Fink A, Bohn E. J Colloid Interface Sci 1968;26:62-69.

[10] Eller RK. The Chemistry of silica, New York: Wiley, 1979.

[11] Prosposito P, Casalboni M. Optical properties of functionalized sol-gel-derived hybrid materials, 1st ed. Stevenson Ranch: American Scientific Publishers, 2003.

[12] Rahman IA, Vejayakumaran P, Siput CS, Ismail J, Bakar MA, Adnan R, Chee CK. Ceram Internat 2006;32:691-699.

[13] Novak BM. Adv Mater 1993;5(6):422-433.

[14] Jensen RE, Palmese GR, McKnight SH. Int J Adhesion & Adhesives 2006;26:103-115.

[15] Lin CH, Feng CC, Hwang TY. Eur Polym J 2007;43:725-742.

[16] Davis SR, Brough AR, Atkinson A. J Non-Cryst Solids 2003;315:197-205.

[17] Ochi M, Takahashi R, Terauchi A. Polymer 2001;42:5151-5158.

[18] Wang H, Zhong W, Du Q, Yang Y, Okamoto H, Inoue S. Polym Bull 2003;51:63-68.

[19] Lui YL, Hsu CY, Wei WL, Jeng RJ. Polymer 2003;44:5159-5167.

[20] Lui YL, Wei WL, Hsu KY, Ho WH. Thermochim Acta 2004;412:139-147.

[21] Rapoport L, Nepomnyashchy O, Verdyan A, Popovitz-Biro R, Volovik Y, Ittah B, Tenne R. Adv Eng Mater 2004;6(1-2):44-48.

[22] Jiguet S, Judelewicz M, Mischler S, Hofmann H, Bertsch H, Renaud P. Surf Coat Technol 2006;201:2289-2295.

[23] Visconti IC, Langella A, Durante M. Appl Comp Mater 2001;8:179-189.

[24] Xing XS, Li RKY. Wear 2004;256:21-26.

[25] Rabinowicz E. Friction and wear of materials, 2nd ed. New York: Wiley, 1995.

[26] Chan N, Sharma MK. Wear 2008;264:69-74.

[27] Lee HG, Kim SS, Lee DG. Compos Struct 2006;74:136-144.

[28] Thorp JM. Tribol Internat 1982;15:59-68.

[29] Shi G, Zhang MQ, Rong MZ, Wetzel B, Friedrich K. Wear 2004;256:1072-1081.

[30] Zhang H, Zhang Z, Friedrich K, Eger C. Acta Mater 2006;54:1833-1842.

[31] Zhang MQ, Rong MZ, Yu SL, Wetzel B, Friedrich K. Wear 2002;253:1086-1093.

[32] Zhang Z, Breidt C, Chang L, Friedrich K. Tribol Internat 2004;37:271-277.

[33] Sawyer GW, Freudenberg KD, Bhimaraj P, Schadler LS. Wear 2003;254:573-580.

[34] Xu YM, Mellor BG. Wear 2001;251:1522-1531.

[35] Friedrich K. Wear of reinforced rolymers by different abrasive counterparts. In: Friedrich K, editor. Friction and wear of polymer composites-composite Materials series 1, Amsterdam: Elsevier, 1986. pp 233-287.

[36] Larsen T, Andersen TL, Thorning B, Horsewell A, Vigild ME. Wear 2007;doi: 10.1016/j.wear.2007.10.003.

[37] Stuart B, George WO, McIntyre PE. Modern infrared spectroscopy, Chichester, England: Wiley 1998.

[38] Wendlandt WW, Gallagher PK. Instrumentation. In: Turi EA, editor. Thermal characterization of polymeric materials, New York: Academic Press, 1981. pp 9-34.

[39] Menard KP. Dynamic mechanical analysis: a practical introduction, CRC Press LLC, 1999.

[40] Wong M, lim GT, Moyse A, Reddy JN, Sue H-J. Wear 2004;256:1214-1227.

[41] Bhushan B. Introduction to tribology, New York: Wiley, 2002.

[42] Steijn RP. Friction and wear. In: Brostow W, Corneliussen RD, editors, Failure of plastics, New York: Hanser, 1986. pp 356-392.

[43] Pearce EM, Khanna YP, Raucher D. Thermal analysis in polymer flammability. In: Turi EA, editor. Thermal characterization of polymeric materials, New York: Academic Press, 1981. pp 793-844.

[44] Becker O, Varley RJ, Simon GP. Eur Polym J 2004;40:187.

[45] Hsiue GH, Lui YL, Liao HH. J Polym Sci Polym Chem 2001;39:986-996.

[46] Hussain F, Chen J, Hojjati M. Mater Sci Eng 2007;A 445-446:467-476.

[47] Kormann X, Thomann R, Mulhaupt R, Finter J, Berglund LA. Polym Eng Sci 2002;42:1815-1826.

[48] Messermith PB, Giannelis EP. Chem Mater 1994;6:1719.

[49] Xu WB, Bao SP, He PS. J Appl Polym Sci 2002;84:842-849.

[50] Feng W, Ait-Kadi A, Riedl B. Polym Eng Sci 2002;42:1827-1836.

[51] Pham JQ, Mitchell CA, Bahr JL, Tour JM. J Polym Sci Polym Phys 2003;41:3339.

[52] Ash BJ, Schadler LS, Siegel RW. Mater Lett 2002;55:83-87.

[53] Becker O, Varley R, Simon G. Polymer 2002;43:4365-4373.

[54] Kormann X, Lindberg H, Berglund LA. Polymer 2001;42:4493-4499.

[55] Ahmad Z, Sarwar MI, Wang S, Mark JE. Polymer 1997;38:4523.

[56] Al-Sagheer F, Ali AAM, Muslim S, Ahmad Z. Sci Technol Adv Mater 2006;7:111-118.

[57] Hu Q, Marand E. Polymer 1999;40:4833-4843.

[58] Harsch M, Karger-Kocsis J, Holst M. Eur Polym J 2007;43:1168-1178.

[59] Fox TG, Loshaek S. J Polym Sci 1955;15:371-390.

[60] Pascault JP, Sautereau H, Verdu J, Williams RJJ. Thermosetting polymers, New York: Marcel Dekker, 2002.

[61] Romanes MC, D'Souza NK, Coutinho D, K.J. BJ, Scharf TW. Wear 2007;doi: 10.1016/j.wear.2007.08.022.

[62] Lee HG, Hwang HY, Lee DG. Wear 2006;261:453-459.

[63] Wetzel B, Haupert F, Zhang MQ. Compos Sci Technol 2003;63:2055-2067.

[64] Durand JM, Vardavoulias M, Jeandin M. Wear 1995;181-183:833-839.

[65] Hutchings IM. Tribology: friction and wear of engineering materials, Edward Arnold, 1992.

[66] Bahadur S, Sunkara C. Wear 2005;258:1411-1421.

[67] Schwarts CJ, Bahadur S. Wear 2000;237:261-273.

[68] Wang YQ, Li J. Mater Sci Eng A 1999;266:155-160.

[69] Archard JF. Wear 1958;2:438-455.

[70] Stachowiak G, Batchelor AW. Engineering tribology, 3 ed. New York: Elsevier Butterworth Heinemann, 2005.

[71] Engineering fundamental. http://www.efunda.com/materials/materials_home/materials.cfm (1/12/2008),

[72] Bhimaraj P, Burris DL, Action J, Sawyer WG, Toney CG, Siegel RW, Schadler LS. Wear 2005;258:1437-1443.

[73] Garcai M, De Rooij M, Winnubst L, van Zyl WE, Verweij H. J Appl Polym Sci 2004;92:1855-1862.

[74] Shao X, Liu W, Xue Q. J Appl Polym Sci 2004;92:906–914.

[75] Wang Q, Xue Q, H. Liu H, Schen W, Xu J. Wear 1996;198:216-219.

[76] Kar MK, Bahadur S. Wear 1978;46:189-202.

CHAPTER 3

MODIFICATION OF EPOXY RESIN WITH FLUORO-EPOXY OLIGOMER

3.1 Introduction

One of the interesting methods used to improve the tribological performance of epoxy resins is chemical modification with fluorine functional groups. The use of the fluorinated compounds is very attractive due to their characteristics. A carbon-fluorine bond is one of the strongest organic covalent bonds; the bond energy of C-F is 485 $kJmol^{-1}$[1]. Due to the presence of fluorine atoms [2-4], compounds develop these outstanding properties: chemical and thermal stability, weathering resistance, low dielectric constant [5], low surface tension, low friction coefficient, hydrophobicity and oleophobicity. Thus the introduction of fluorine atoms into the systems may combine those properties of fluorinated compounds and the advantages of epoxy resins.

A number of new fluorinated epoxy monomers and oligomers have been synthesized. There have been reports comparing commercial epoxies and their curing networks with lower surface tension, lower dielectric constant and better mechanical properties. Park et al. synthesized new fluorine-containing epoxy resins by incorporating a phenyl-trifluoromethyl (-Ph-CF_3) group both into the main chain [5] and into the side chain [3] of epoxy resins. Montefusco et al. [6] synthesized the new difunctional fluoro-epoxide monomers, starting by allylation of the fluorinated diols and following by epoxidation reaction. The monomers obtained showed a higher reactivity with respect to hexanedioldiglycidyl ether (HDGE) when used in UV curing. This behavior was attributed to the lower nucleophilicity of glycidyl oxygen in the fluorinated monomers. The surface properties of the cured film were found to be highly

hydrophobic even in those blended with HDGE. The air surface, the surface exposed to air, of the blend systems was found to have a similar hydrophobicity as the pure fluoro-epoxy cured films. This high hydrophobicity implied the selective enrichment of the fluorinated segments at the air surface. As shown in photocured systems of 1,4-cyclohexanedimethanol-diglycidyl ether studied by Sangermano et al. [7], there was a selective migration of fluorine atoms to the air surface of UV cured films. Only a small amount of two commercially available epoxy-fluorinated monomers, 3-(perfluorooctyl)-1,2-propenoxide and 3-(1H, 1H, 9H-hexadecafluorononyloxyl)-1,2 propenoxide, was used as modifying additives. They found that the surface properties of the UV cured films filled with fluorinated additives at the air surface became highly hydrophobic, while at the mold surface they were unchanged. On the other hand, changes in their bulk properties and kinetics of photopolymerization of the systems with fluorinated additives were not observed due to the low amount of the additives.

Bilyeu [8] used a fluorinated aromatic amine mixed with a standard aliphatic amine as a curing agent for a commercial diglycidylether of bisphenol-A (DGEBA) epoxy. The resulting cured networks were determined to have lower wear than the unmodified epoxy resins.

Van de Grampel et al.[4] proposed other choices of modifications. In their study, the curing agents, instead of epoxy monomers, were modified. Partially fluorinated diamine monomers were prepared by the reaction of perfluoroalkyl epoxide with a known excess of diamine. The fluorinated epoxy films obtained were stable, and the surface modification was permanent in nature.

An explanation for the improvement in surface properties is the segregation of fluorinated species at the epoxy surface. This is advantageous in the case of self-stratifying coatings [9-19]. Only a small quantity of fluorinated species, which are needed to produce the surface with low interfacial energy, migrates to the surface of the bulk to form a coating [4, 20].

Blending is an alternative method. Uses of nonreactive fluoropolymers as the epoxy modifiers that blend with a commercial epoxy have been proposed in the literatures [4, 20-23]. Kasemura et al. [24] blended the fluorine-containing block copolymers, consisting of methylacrylate, glycidyl methylacrylate and 3, 3, 4, 4, 5, 5, 6, 6, 7, 7, 8, 8, 9, 9, 10, 10, 10-heptadecafluorodecyl acrylate with an epoxy resin. They reported the improvement of water repellency of the fluorinated modified epoxies. The fluorocarbon segments with low surface energy oriented toward the exterior surface of the blend to give rise to a fluorinated surface.

Brostow et al. [20, 23] used fluorinated poly(aryl ether ketone) as the epoxy modifier for diglycidyl ether of bisphenol-A epoxy system. The modified epoxies were cured at two different temperatures, 24^{o}C and 70^{o}C. They found a significant lowering in friction coefficient at 10% addition of fluorinated poly(aryl ether ketone) for the systems cured at 24^{o}C, while for those cured at 70^{o}C the friction coefficient increased. The SEM micrograph showed the segregation of fluorinated species formed at 10% addition for those epoxies cured at 24^{o}C, but there was no evidence of a phase inversion or a higher fluorine concentration found close to the surface for those cured at 70^{o}C. These results show us that the segregation of fluorinated species at the surface plays an important role in the reduction of friction coefficient.

Besides the above, fluorination of the polymer surface by an implantation is another option, as the process can give rise to a highly hydrophobic surface. Du Toit et al. [25] reported that direct fluorination with fluorine gas resulted in a marked decrease in the total surface tension of high-density polyethylene. To improve the water repellency of polymer surface, highly fluorinated compounds, such as CF_4, C_2F_6 and SF_6 [26-29] have been used as plasma gases in the implantation of fluorine functionalities on the polymer surface. The potential methods for reducing friction coefficient, decreasing moisture absorption and lowering surface energy by fluorination have performed not only with chemical methods, but also with physical methods. One of the methods was done by Han et al. [30]. They enhanced the surface hydrophobicity of epoxy resins, using a simple physical method. Epoxy resins were fluorinated with poly(tetrafluoroethylene) PTFE molecules by curing epoxy resins against PTFE mold. They found that the PTFE molecules anchored firmly on the epoxy surface, which caused the stable fluorination on the surface. The fluorinated epoxy resin surfaces were as highly hydrophobic as the pristine PTFE surface.

Thus it is worthwhile to pursue the modification of epoxy resin by incorporating some fluoro-functional groups into the system. In this study, the new fluoro-functionalized epoxy oligomer was synthesized and blended with the commercial DGEBA epoxy resin. The effects of fluoro-functionalized epoxy oligomer content on the thermal and mechanical properties as well as the tribological properties were investigated.

3.2 Experimental

3.2.1 Materials

Diglycidyl ether of bisphenol A (DGEBA) and aliphatic polyamines (Hardener 1) from

the System Three were used as a commercial epoxy resin and a curing agent, respectively. An epoxide equivalent weight of the commercial epoxy resin is 210 g eq^{-1}. The amine hydrogen equivalent weight of the curing agent is 93 g eq^{-1}. Those chemicals were used as received. Epichlorohydrin and m- trifluoromethyl aniline were purchased from Aldrich. All chemicals were used without further purification. Diglycidyl of trifluoromethyl aniline (DGTFA) epoxy oligomer was synthesized according to the procedure reported below.

3.2.2 Synthesis of Diglycidyl of Trifluoromethyl Aniline (DGTFA) Epoxy Oligomer

Trifluoromethyl aniline (20.0 g) and trace of water were charged in the four-neck round-bottom flask equipped with a mechanical stirrer, reflux condenser, dropping funnel, and thermometer controller. The mixture was heated to 60-65^{o}C, and ephichlorohydrin (57.4 g) was added dropwise over 1.5 hours at the same temperature with agitation. After a 3-hour holding period, the temperature was lowered to 50-55^{o}C and 50% aqueous NaOH solution was introduced dropwise during 1 hour. The mixture was heated again to 60-65^{o}C and held further for 30 minutes. The mixture was then cooled to room temperature and neutralized with 50% acetic acid, and allowed to separate into layers. The organic phase was separated and treated with warm water (about 60^{o}C) until the salt was completely removed; the organic phase then was dried over sodium sulfate. The obtained product was purified under vacuum oven at temperature of 70-90^{o}C and pressure of 100-150 mmHg.

3.2.3 Determination of Epoxy Equivalent Weight

The epoxy content of resins is frequently expressed as epoxide equivalent weigh (EEW). Epoxy functionalities were determined according to the pyridine/HCl method.

The principle of the method is hydrochlorination reaction of epoxy, which forms the corresponding chlorohydrins. The residual HCl was then determined by titration with basic solution. In this respect, the hydrochlorination reagent, a 0.2 N solution of HCl in pyridine, was prepared by pipetting 17 ml of concentrated hydrochloric acid into 1 liter of pyridine and mixing thoroughly. Then 25 ml of the pyridine hydrochlorination reagent were pipetted into a 250 ml round bottle flask, equipped with a standard taper joint. A known amount of sample was added and dissolved by heating the mixture at about 40^{o}C. After dissolution was complete, the mixture was refluxed for 20 minutes. The flask and contents were cooled. Then 6 ml of distilled water together with 0.2 ml of phenolphthalein indicator solution was added. The titration was made with standard 0.1 M ethanolic potassium hydroxide solution to a definite pink color.

3.2.4 Preparation of DGEBA + DGTFA Epoxy Resin

DGTFA were blended with DGEBA at various ratios from 0 phr to 20.0 phr. The products obtained were then mixed with stoichiometric amount of polyamine curing agent. The mixtures were poured into the silicone-opened molds and cured at 25^{o}C for 24 hours in a conventional oven under N_2 atmosphere. The cured epoxies were taken off the molds. All samples were kept at least a week before testing.

3.2.5 Determination of Gel Content

The gel content or insoluble fraction, produced by cross-link, was determined by measuring the weight loss after extracting with chloroform at room temperature for 24 hours, according to the standard method ASTM D 2765-95 with test method C. The percent extraction was calculated as follows:

$$\% \text{ Extraction} = [(W_o - W_d)/W_o]*100$$

where W_o is original polymer weight and W_d is weight of dried gel

3.2.6 Fourier Transform Infrared Spectroscopy (FTIR) [31]

FTIR measurement was performed with IR spectroscopy from Perkin Elmer. To prepare a liquid film, small amounts of viscous liquid sample were dropped on a KBr infrared plate, which was then mounted to a cell holder. A test was run under N_2 gas atmosphere.

3.2.7 Thermogravimetric Analysis (TGA) [32]

Thermal stability of samples was determined using Pyris 1 TGA from Perkin Elmer. Cured samples were performed at a heating rate of 40^{o}C/min from 30 to 700^{c}C in N_2 atmosphere, then from 700 to 1000^{o}C in air.

3.2.8 Dynamic Mechanical Analysis (DMA) [33]

Dynamic mechanical analysis, DMA, was performed using DMA 7e Perkin Elmer with the three point bending configuration. The temperature dependence of the storage modulus $E^{/}$, loss modulus $E^{//}$, and the loss factor tan δ of each cured sample were determined with the temperature scan mode of operation at constant frequency of 1 Hz and a scan rate of 5.0^{o}C/min. The sample size used was about 6.0 × 2.0 × 20 mm.

3.2.9 Mechanical Properties of DGEBA + DGTFA Epoxy

Three point bending experiments were conducted on DMA 7e from Perkin Elmer with stress strain scan mode of operation. The force applied was from 0 N up to the load of permanent deflection with rate of 100 mN/min. All tests were performed at 25.0^{o}C. The sample size was about 6.0 × 1.5 × 20.0 mm.

3.2.10 Pin on Disc Tribometer

A pin-on-disk type of tribometer, Nanovea from Micro Photonics, was used to

determine friction coefficient and wear rate of fluorinated modified epoxy + epoxy systems. The pin used was silicon nitride (Si_3N_4) ball with a diameter of 3.2 mm. A test pin was loaded perpendicularly against a rotating disk by applying a dead end load. The test pin was mounted in a lever arm via a sample holder. The lever arm was kept in a fixed position by a load cell which measured the frictional force. The load applied to the level arm during the test was 5.0 N which is equivalent to the initial Hertzian contact radius of 226 μm, maximum and mean contact pressures of 47 MPa and 31 MPa, respectively (see APPENDIX A). The rotation speed of the disc was 200 rpm and the radius of wear track was 2.0 mm. The equivalent sliding speed was 4.19 mm/s. The test was performed for 5,000 revolutions under ambient conditions (at temperature of 22^{o}C and % RH of 35-45%). The friction coefficient (μ) was obtained by using Amonton's first law of friction i.e. $\mu = F_f/W_N$ [34, 35], and was reported as an averaged value based on data points in the steady state regime.

Before testing, the ball surface was cleaned using Kimwipes® soaked in isopropanol.

3.2.11 Profilometer

Cross-section areas of wear track remaining after each pin-on-disc friction test were determined with a Veeco Dektak 150 Profilometer. A stylus with tip radius of 12.5 μm was used. The force applied to sample was 2 mg, and scan rate was 26.7μm/sec. The basic principle of this technique is that instrument amplifies and records a vertical motion of a stylus displaced at a constant speed by the surface to be measured [34]. As the stylus moves, it rides over the sample surface detecting surface deviations.

All samples were cleaned by high pressure air to eliminate all debris before each test. At least 5 scans were run for each sample, and the average value of area was

used to calculate the wear rate.

3.2.12 Scanning Electron Microscope (SEM) and Optical Microscope

The scanning electron microscope (FEI Quanta E-SEM) was used to observe the worn surface of samples. All samples were gold coated before observing the worn surface. After sliding against each sample surface, the silicon nitride ball was investigated for traces of the transfer film using the optical microscope, Nikon Eclipse ME600.

3.3 Results and Discussion

3.3.1 Characterization of Fluoro-Epoxy Oligomer

A yellowish viscous liquid was obtained from the reaction of epichlorohydrin (white powder) with trifluoromethyl aniline (yellow liquid) in a strong basic condition. The synthesized diglycidyl of trifluoromethyl aniline, named DGTFA epoxy oligomer, was characterized for the functional groups by FTIR. Figure 3.1 shows an infrared spectrum of the synthesized product. The characteristic absorption bands at 853, 1233 and 1259cm^{-1} show the glycidyl of epoxide. The characteristic absorption band of the CF_3 appears at 1322 cm^{-1}. The characteristic absorption bands at 1614, 1500 and 1165 cm^{-1} are attributed to the aromatic ring. The overtone band pattern in the region from 1700 to 2000 is attributed to 1,3-substituted benzene. The characteristic absorption bands at 2956 and 2917 cm^{-1} are attributed to C-H stretching from CH_2 and CH, respectively. The absorption band of the OH appears at 3339 cm^{-1}.

Thus, from characteristic peaks discussed above, the synthesized product was roughly proved to be DGTFA. The chemical reaction of epichlorohydrin (EP) with m-trifluoromethyl aniline and the product obtained are shown in scheme 3.1. The epoxy

content of the product determined in terms of epoxy equivalent weigh (EEW) is 2003. The product was then blended with DGEBA epoxy resin and cured stoichiometrically with polyamines. However, due to a high EEW of the synthesized DGTFA, the DGEBA + DGTFA blends at only the concentration range from 2.5 to 20.0 phr of DGTFA was prepared and studied.

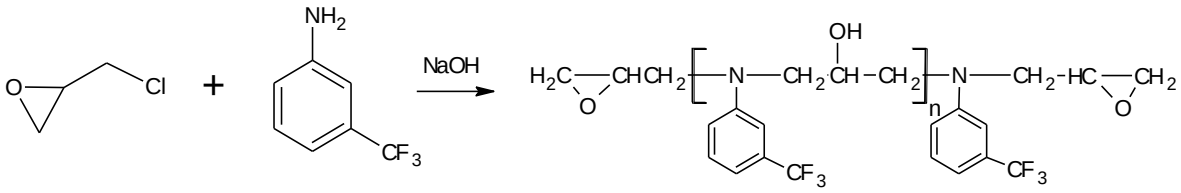

EP m-trifluoromethyl aniline DGTFA

Scheme 3.1. Chemical reaction of epichlorohydrin (EP) with trifluoromethyl aniline.

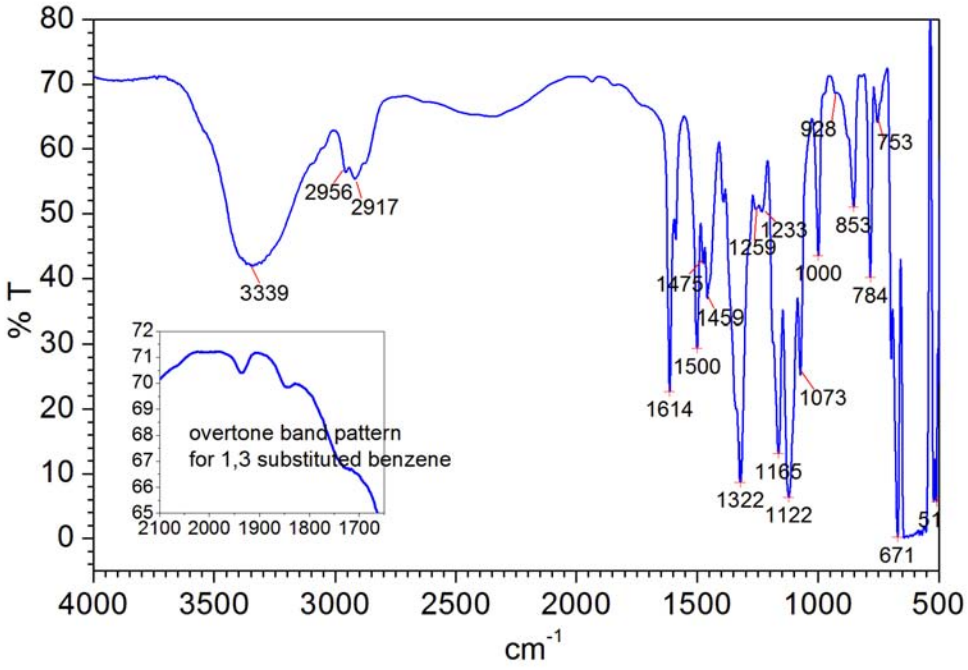

Figure 3.1. FT-IR spectrum of DGTFA.

3.3.2 Thermogravimetric Analysis

Thermal degradation behavior of cured DGEBA epoxy blended with various amounts of DGTFA were studied with TGA. Thermograms are shown in Figure 3.2. Two distinct weight losses are observed due to gas switching at a temperature of 700°C. The first stage of weight loss refers to thermal decomposition of epoxy resins in inert N_2 atmosphere at 200 to 400°C. The latter stage refers to the oxidation of the residuals after switching from N_2 gas to air at 700°C. It is shown that the weight loss is shifted to a lower temperature by adding DGTFA into the DGEBA epoxy resin. The thermal stability parameters, including the initial decomposition temperature (IDT) and the temperature of maximum rate of degradation (T_{max}) of the cured DGEBA epoxy and the blends, are determined. The results are listed in Table 3.1.

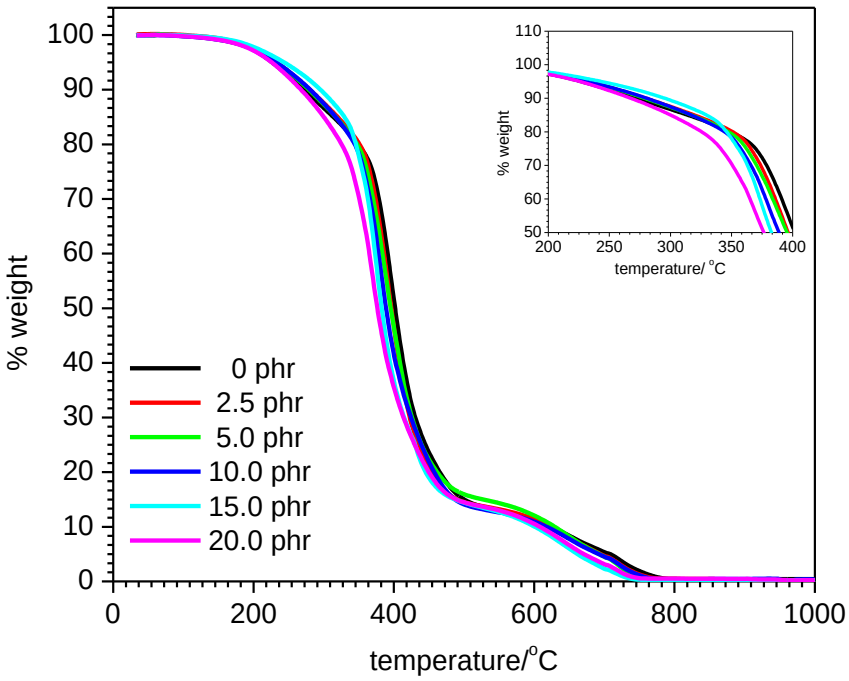

Figure 3.2. TGA thermograms of the cured DGEBA + DGTFA epoxy resins.

Table 3.1. TGA data of the cured DGEBA + DGTFA epoxy resins.

DGTFA content/phr	IDT / ^{o}C	T_{max} /^{o}C
0	372.9	396.5
2.5	364.8	391.0
5.0	360.5	389.3
10.0	357.1	381.9
15.0	350.6	372.5
20.0	344.2	368.5

From Table 3.1, both IDT and T_{max} of the cured epoxy resin decrease when 2.5 phr of DGTFA is added. These values continue to decrease as the amount of DGTFA increases. It can be inferred from the results that DGTFA causes the reduction in thermal stability of DGEBA epoxy resin. The reason for the decrease in thermal stability is that DGTFA contains tertiary amine (R_3N) functional groups in the molecular backbone. This group can function as a catalyst [36-38] but is less thermally stable than the nitrogen-free multifunctional epoxy resin [38].

3.3.3 Dynamic Mechanical Analysis

Figure 3.3 shows the temperature dependence of storage modulus $E^{/}$, loss modulus $E^{//}$ and tan δ for the cured DGEBA blended with DGTFA samples. The glass transition temperature and the $E^{/}$ at three different temperatures are shown in Table 3.2. Unlike those obtained from DGEBA epoxy curing with cycloaliphatic amine (see chapter 2), the peak of loss modulus $E^{//}$ is not sharp and symmetrical (Figure 3.3 (a)). It is difficult to define the glass transition temperature T_g using the peak of loss modulus. Thus, the values of glass transition temperature T_g reported in this chapter are recorded as the temperature at maximum value of the tan δ curve.

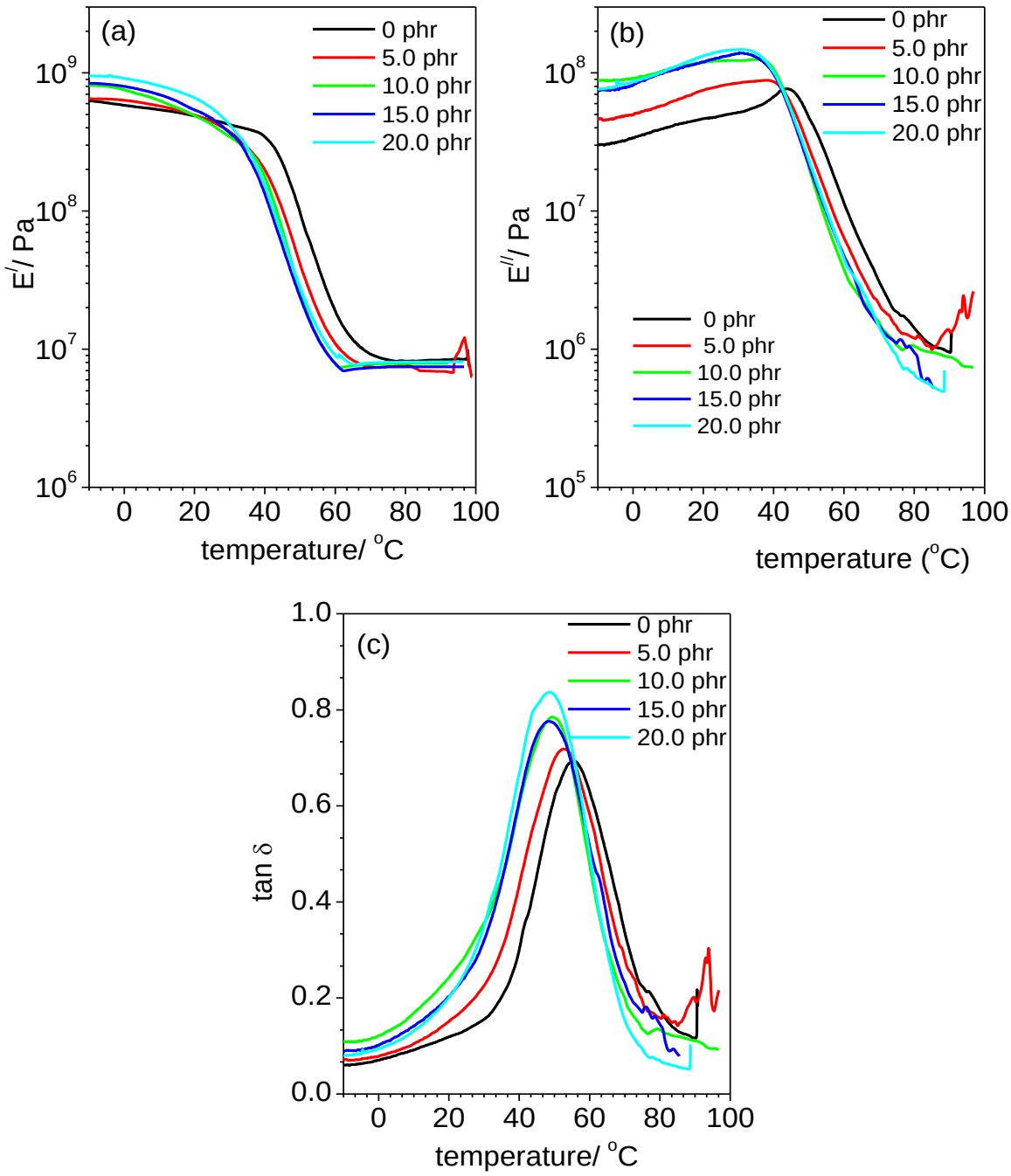

Figure 3.3. (a) Storage modulus, (b) loss modulus and (c) tan δ of DGEBA + DGTFA epoxies curing with polyamine.

Table 3.2. DMA data of DGEBA + DGTFA epoxies curing with polyamine.

	$E^{/}$ at			
DGTFA /phr	0°C	25°C	80°C	T_g /°C
0	5.54×10^8	4.59×10^8	8.19×10^6	55.7
5	6.34×10^8	4.47×10^8	7.45×10^6	52.6
10	7.47×10^8	4.23×10^8	7.92×10^6	49.3
15	7.89×10^8	4.72×10^8	7.57×10^6	48.1
20	9.31×10^8	5.56×10^8	8.06×10^6	48.6

Figure 3.3 (b) shows the storage modulus $E^{/}$ of DGEBA + DGTFA epoxies curing with polyamines. In the following manner: the $E^{/}$ values at 0°C, which represent the storage modulus at glassy state, increase as the amount of DGTFA increases, then the antiplasticization effect manifests itself. Plasticization, whose main manifestation is the decrease of the glass transition temperature, is generally accompanied by an increase of the glassy modulus in the temperature interval between T_β and T_α [39]. The effect is known as antiplaticization. This phenomenon is common for amines-crosslinked epoxies, and it is usually a consequence of both internal (a change of network structure) and external (incorporation of miscible additives) modification of structure or composition [39].

In Figure 3.3 (c), a single relaxation process is observed at the temperature range of -20°C to 100°C. This relaxation peak is associated with the glass transition temperature, namely the α peak, because changes in the storage modulus gap are more than one decade. Only singlet tan δ peak is found for all compositions; however, their width likely increases with increasing amounts of DGTFA. This indicates the increasing degree of inhomogeneity of the spatial distribution of cross-link density. The superposition of the peaks possibly occurs and causes a single tan δ peak due to good

solubility of DGTFA oligomers in the epoxy matrix. The T_g depletion of the epoxy, due to the plasticizing effect, is observed instead. As seen in Figure 3.3 and Table 3.2, T_g of the epoxy is reduced about 3 ^oC when 5.0 phr of DGTFA is introduced to the system. The value of T_g keeps decreasing as the amount of DGTFA increases up to 15.0 phr and levels off. According to the Fox and Loshaek equation [40] (see Equation (2.1), chapter 2), it is possible to link the decrease in T_g to the reduction in the degree of cross-links. Another parameter which is used to indicate the cross-link density is the plateau modulus at given temperature above T_g [33]. The inverse of storage modulus at rubbery plateau relates to cross-link density. However, it is shown in Table 3.2 that plateau storage modulus at 80^oC shows only a slight decrease in the value when DGTFA oligomer is added. No further significant reduction in the plateau modulus as a function of DGTFA content is found. To confirm the inference that cross-link density is reduced by adding DGTFA, percent extraction of the uncross-linked portion was determined. This value can be used to indicate percent gel or cross-link density of thermosets. The higher the percent extraction, the lower the cross-link density is. In Figure 3.4, the percent extraction increases about 3.5 % when 5.0 phr of DGTFA is added. Only a small increase in value of percent extraction is observed with increasing amounts of DGTFA. Nevertheless, this result supports the idea that the addition of DGTFA causes the reduction in cross-link density. Cross-link density decreases as the amount of DGTFA increases.

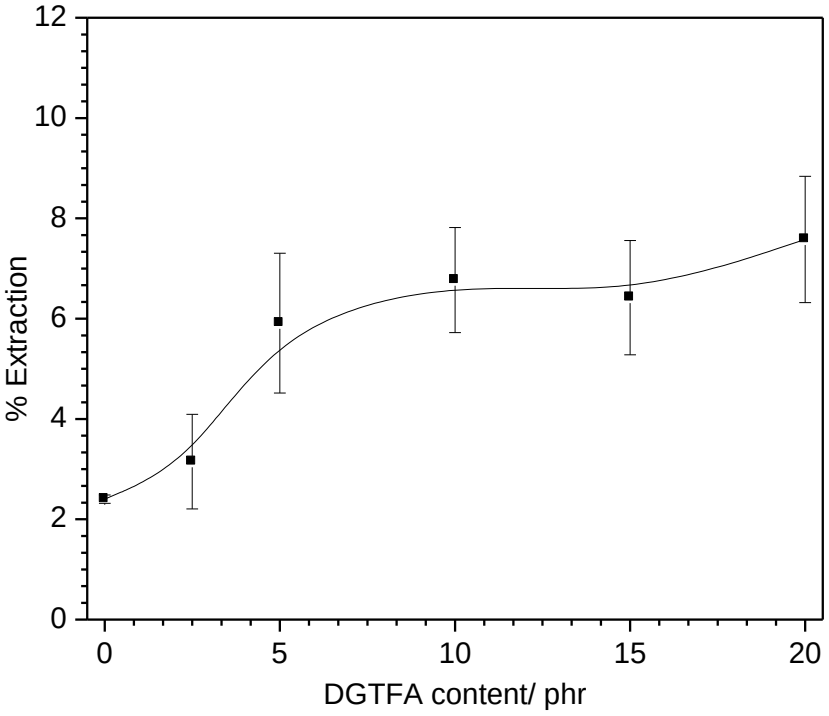

Figure 3.4. Percent extraction as a function of DGTFA content.

3.3.4 Mechanical Testing of the DGEBA + DGTFA Epoxy Resins

Figure 3.5 shows stress-strain curves from which the flexural modulus and ultimate strength of DGEBA + DGTFA epoxy resins are determined. Table 3.3 lists the flexural modulus, percent strain at a permanent deflection point and the flexural strength. The flexural strength is determined from the stress of material at a permanent deflection point. It is found that the flexural modulus decreased when DGTFA is added up to 15.0 phr, and it likely levels off at 20.0 phr of DGTFA content. This result implies that the flexural stiffness of the epoxy is decreased by adding DGTFA. A similar tendency is observed for the storage modulus at 25.0^{o}C obtained from the DMA testing, but only until the DGTFA content is added up to 10.0 phr. The value then increases with

increasing DGTFA content, and it is even higher than that of the pure epoxy when the addition of DGTFA is larger than 15.0 phr. This implies that the antiplasticization effect still plays a role at this temperature for the DMA testing. The difference in the changes in the modulus as a function of DGTFA content for two different methods can possibly be explained by the difference in the strain rate to which the material are exposed. The storage modulus E' is obtained by applying dynamic force at constant frequency whereas the flexural modulus from the transient experiment is obtained by applying static force at constant stress rate. DMA experiments are run at a very low strain to stay within the linear viscoelastic region, whereas the static experiments are not necessary.

In Table 3.3, percent strain at a deflection point increases as the amount of DGTFA increases. A lower cross-link density is one possible explanation. The flexural strength increases as the amount of DGTFA increases. This is interesting, and it could be advantageous for this material. The toughness normally determined from the area under the stress-strain curve is defined roughly as the product of the flexural strength (σ_f) and strain at a deflection point (ε_d). This product provides an indicative value of work done for deflecting. In Table 3.3, the toughness of the epoxy resin is improved by adding DGTFA to the epoxy resin.

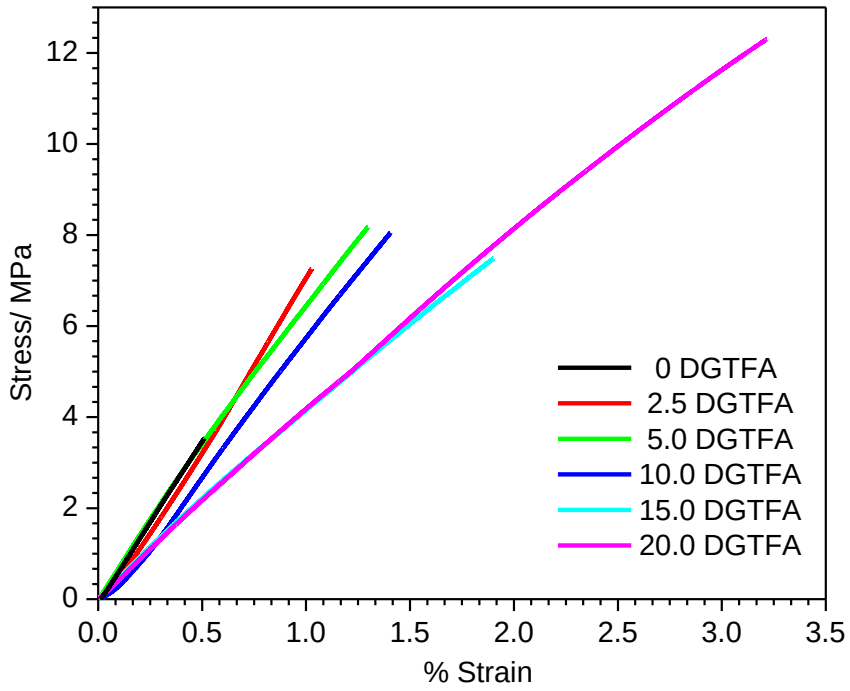

Figure 3.5. Flexural stress vs percent flexural strain for DGEBA + DGTFA epoxy resins measured at 25.0°C.

Table 3.3. Data from flexural testing of DGEBA + DGTFA epoxys resin at 25°C.

DGTFA content/ phr	Flexural modulus / Pa	Flexural Strength (σ_f) / MPa	Strain at deflection point (ε_d) / %	Product of Flexural Strength and strain at deflection point ($\sigma_f \times \varepsilon_d$) / 10^{-2} MPa
0	7.21×10^8	3.52	0.52	1.83
2.5	7.23×10^8	7.26	1.03	7.48
5.0	7.16×10^8	8.18	1.30	10.63
10.0	6.27×10^8	8.00	1.39	11.12
15.0	4.03×10^8	7.50	1.90	14.25
20.0	4.11×10^8	> 12.30	> 3.22	> 39.60

3.3.5 Friction and Wear

Figure 3.6 shows the evolutions of the friction coefficient of DGEBA + DGTFA epoxies sliding against a silicon nitride (Si_3N_4) ball. In the case of pure DGEBA epoxy resin curing with polyamines, friction coefficient remains at an initial value before increasing and attaining steady state. The increase in friction coefficient after a run-in period may be associated with ploughing process because of roughening and trapped wear particles. Unlike pure epoxy, the epoxy blended with 2.5 and 5.0 phr of DGTFA exhibit steady state values soon after the onset of rubbing. On the other hand, the epoxy blended with 15.0 phr of DGTFA exhibits the run-in period. The higher the amount of DGTFA that is added, the longer this period is. The run-in phenomenon for polymer is related to the initial formation of ridges [41]. These ridges are progressively worn away until the sufficient amount of wear debris covers the surface leading to the stable lower friction coefficient. Then friction coefficient slowly increases to the high value and levels off at a steady state. Due to the smooth surface of the blend at high DGTFA content, the increase in friction coefficient after the run-in period is associated with an adhesive component of friction. The smoothing of the surface, due to the sliding of the ball leading to a larger area of contact, contributes to the increasing friction coefficient in this regime. Note that surface roughness can be quantified using average roughness parameters [34]. These parameters usually refer to variations in the height of surface relative to a reference plane. In this study, the center-line average (R_a) and the root mean square average (R_q) (see APPENDIX D) are determined by scanning line profiles with the profilometer. The values are shown in Table 3.4. The R_a and R_q decrease as the amount of DGTFA increases, indicating that surface roughness of

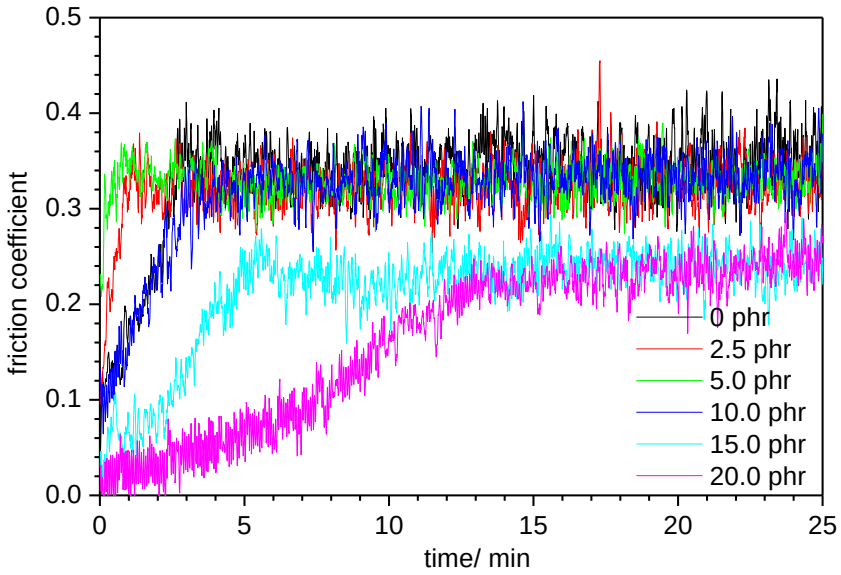

Figure 3.6. Evolution of the friction coefficient with time for DGTFA epoxy resins blending with various amounts of DGTFA.

Table 3.4. Surface roughness of DGEBA + DGTFA epoxy resins.

DGTFA content / phr	R_a / A^o	R_q /A^o
0	5186.7	7961.1
2.5	5875.2	8141.1
5.0	3356.5	4673.6
10.0	1464.3	1670.4
15.0	1002.9	1432.0
20.0	1386.4	1639.6

epoxy resin somehow decreases as the amount of DGTFA increases.

To facilitate the comparison, the average values of the friction coefficient at a steady state are plotted as a function of DGTFA content. It is shown in Figure 3.7 that all blends exhibit a lower friction coefficient than the pure DGEBA epoxy. Friction coefficient decreases slightly when the small amount (2.5 phr) of DGTFA is added, and it seems to remain constant if only 5.0 and 10.0 phr of DGTFA are used. After adding

high enough amounts of DGTFA (15.0 phr), friction coefficient reduces significantly and levels off at DGTFA content of 20.0 phr.

The worn surfaces of DGEBA epoxy resin and its blends after sliding against a silicon nitride ball are analyzed with the profilometer to quantify wear damage. Figure 3.8 shows the cross section of wear traces on the surface of DGEBA epoxy and its blends. Ridges are observed in all the worn surface of DGEBA epoxy and its blends. These ridges are formed along the sides of wear traces due to the plouging process [34], grooves and peaks left by the material peeling off and the cracking process [42].

The wear volume was calculated by multiplying the cross-sectional area obtained from profilometer by the wear trace length (see Equation 2.5, chapter 2). The wear rate was then determined according to Equation (2.7), chapter 2.

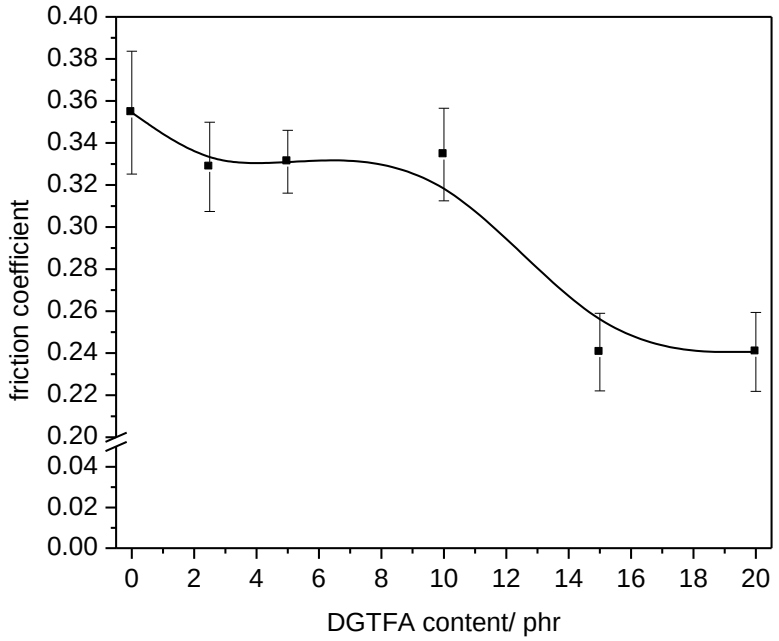

Figure 3.7. Steady state friction coefficient of DGEBA + DGTFA epoxy resins as a function of DGTFA content.

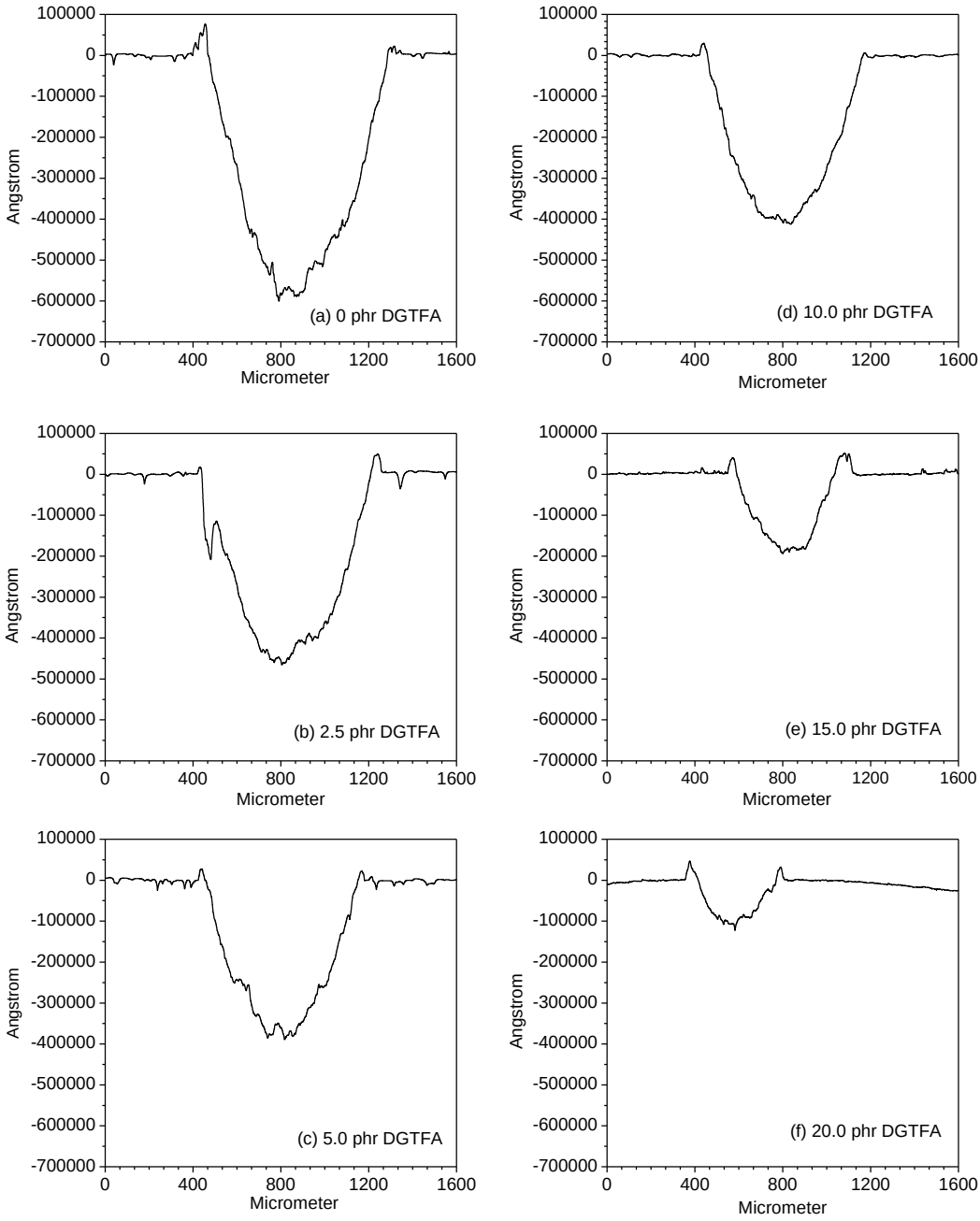

Figure 3.8. Profilometer cross section of wear traces for (a) pure DGEBA epoxy resin, DGEBA epoxy resin blending with (b) 2.5 phr of DGTFA, (c) 5.0 phr of DGTFA, (d) 10.0 phr of DGTFA, (e) 15.0 phr of DGTFA and (f) 20.0 phr of DGTFA after sliding against Si_3N_3. Sliding speed: 200 rpm; normal load: 5.0 N; revolution: 5,000 turns.

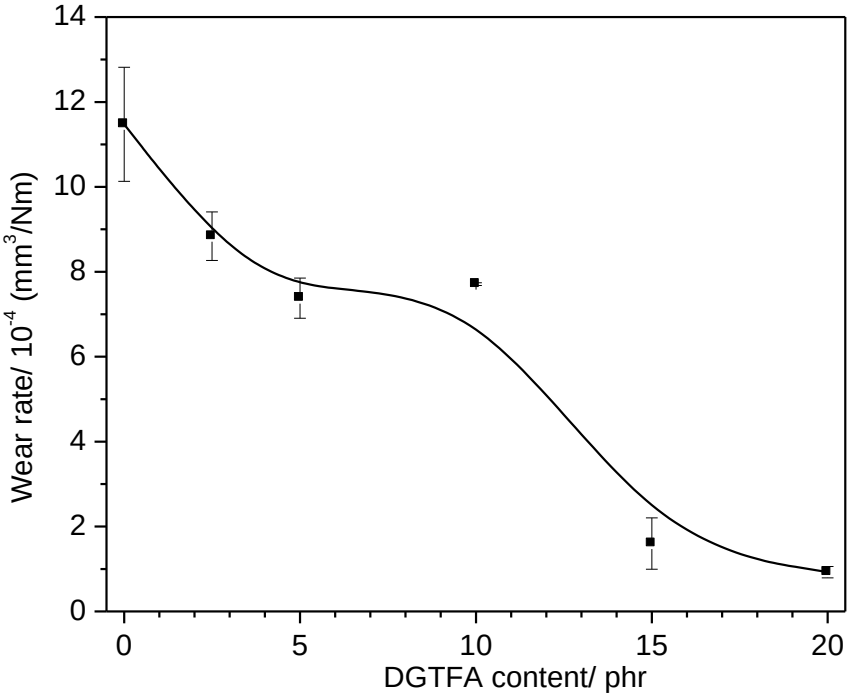

Figure 3.9. Wear rate of DGEBA + DGTFA epoxy resins as a function of DGTFA content.

The wear rate of DGEBA + DGTFA epoxy resins as a function of DGTFA content is demonstrated in Figure 3.9. Low wear rate represents high wear resistance of materials. Interestingly, the dependence of wear rate on the DGTFA content is found to be similar to that observed in friction coefficient. Wear rate decreases when 2.5 phr of DGTFA is added, and its value seems to remain constant if only 5.0 and 10.0 phr are used. Then with rising DGTFA content, the wear rate exhibits a significant decrease at 15.0 phr, and it levels off again at 20.0 phr. Thus, the incorporation of DGTFA into the system, at least for the range of this study, could improve both wear resistance and friction coefficient of the epoxy resin. A possible reason for the improvement is that the friction of adhesion is reduced [34]. According to the adhesive model of friction, the interfacial shear stress can be estimated (see Equation (2.11)), and the values are

tabulated in Table 3.5. The epoxy blended with DGTFA, at high content (15.0 and 20.0 phr), shows a lower interfacial shear stress, compared to the pure epoxy resin. This result is expected. The incorporation of fluorine functional groups into the systems leads to lower surface energy of epoxy [3, 4, 6, 23, 24, 30]. The fluorine modified epoxy-containing debris is smeared over the surface, thereby decreasing the interfacial shear stress, which lowers friction coefficient and results in a more gentle wear mechanism.

Table 3.5. Interfacial shear stress of DGEBA + DGTFA epoxy resins

DGTFA content / phr	Interfacial shear stress / MPa
0	11.0
2.5	10.2
5.0	10.3
10.0	10.4
15.0	7.5
20.0	7.5

Due to the brittle nature of epoxy, the wear mechanism of epoxy involves the formation of surface and subsurface cracks, the development from cracks to waves, the surface fatigue-delamination and the production of debris [43]. It should be noted that the pv condition used in the present study (1.31 MPa × m/s) is similar to other studies [44, 45] which surface heating does not affect the wear rate and wear mechanism. However, the determination of a sliding interfacial temperature is still necessary. The average flash temperature [46] is estimated using again Equation (2.8). When friction coefficient of 0.35 is reached, the tentative value of flash temperature for pure epoxy is about 40^{o}C (see APPENDIX C). In the case of the blends, their friction coefficients are lower, ranging from 0.33 to 0.24, depending on the amount DGTFA in the epoxy. Thus, the average flash temperature reduces and varies from 38^{o}C to 29^{o}C for low amount of

DGTFA to higher amount of DGTFA in epoxy resin. These values are below the range of T_g for all the present studied epoxy systems. The Peclet number, defining the heat transfer effect for this study, is 47.3 (see APPENDIX B) which refers to the fast moving heat source. As discussed in chapter 2, when one surface moves faster relative to the other, there is insufficient time to the temperature distribution of the contact to be established in the stationary body and the depth for which heat penetrates into the stationary body is very small compared to the contact dimension [47]. Thus, thermal softening due to the frictional heat is not expected.

To further explain the mechanism, the worn surfaces of the epoxy resin and its blends were investigated with SEM. Only the epoxy resin blended with 5.0 phr and 20.0 phr of DGTFA were chosen to represent each step of the change found in Figures 3.7 and 3.9. Figure 3.10 demonstrates a comparison of worn surface of the pure epoxy resin and its blends. The scale-like damage generated under repeated loading is observed, indicating the occurrence of surface fatigue-delamination process. The magnified microstructures of the worn surface (Figures 3.10 (b, c)) show wear platelets together with chunks of debris loosely smeared on the worn surface. These platelets occurs as a result of the generation and propagation of surface and subsurface cracks [34]. The small sized platelets and debris found on the worn surface refer to the brittle nature of the epoxy resin. When DGTFA is added (see Figures 3.10 (e, f)), bigger sized platelets with more homogeneity are observed. Moreover, platelets seem to adhere more tightly to the worn surface than those found in the pure DGEBA epoxy resin. A further increase in DGTFA content to 20.0 phr (see Figures 3.10 (h, i)) results in more continuous and tenacious platelets which become a protective layer of the material

underneath. No sign of small sized platelets or debris is found on the worn surface. These results imply that the toughness increases when DGTFA is introduced to the epoxy system; more work is needed to create the same amount of wear. Thus, the higher amount of DGTFA that is in the system, the lower the wear rate is. Moreover, the protective layer formed at high DGTFA content is believed to contribute to the significant reduction in wear rate found in DGEBA blended with 20.0 phr of DGTFA.

From the mechanism proposed above, a correlation between the mechanical properties and wear resistance seems to exist. According to Ratner-Lancaster [48], wear of polymer is reciprocally proportional to the product of the fracture stress and fracture strain, which indicates the value of work done for tensile rupture or toughness of materials. In the present study, the product of flexural strength and % strain at a deflection point, which is used to indicate the toughness of materials, is found to correlate with the reduction in wear rate as well. The plot of wear rate as a function of a product of the flexural strength and % strain at a deflection point of DGEBA + DGTFA epoxy resins is shown in Figure 3.11.

It is well known that the phenomenon of material transfer during sliding is important because material transfer is the beginning of film development [49]. The transfer film affects both the friction and wear behavior of materials. It has been believed that the formation of transfer film is associated with the frictional heat generated at contact surface during sliding, which enhances the plastic deformation and thus the adhesion of the resin to the counterpart. However, the effect of frictional heat is not expected in the present study according the discussion above.

To investigate transfer film, silicon nitride balls, after sliding against epoxy samples, were examined using the optical microscope. The results are shown in Figure 3.12.

For pure DGEBA epoxy resin (see Figure 3.12 (a)), no transfer film is observed; only loose debris is formed with no tendency to adhere to the silicon nitride counterface. This result is expected due to the cross-linked structure of epoxy. However, the addition of DGTFA into the system leads to the formation of a transfer film on the Si_3N_4 counterpart. One possible reason is that the decrease in cross-link density due to the addition of DGTFA enhances the deformation. The increase in percent strain as increasing DGTFA content (see section 3.3.4) is the evidence for this rationale. The enhancement of the deformation of the epoxy whose T_g is low leads to more adhesion of the resin to the counterpart. The blends with a higher amount of the DGTFA show more transfer film on the Si_3N_4 counterpart. The continuous and tenacious transfer film is formed when 20.0 phr of DGTFA is incorporated to the DGEBA epoxy resin (see Figure 3.12 (c)).

Thus, the increase in toughness of bulk materials together with the formation of transfer film, which serves as a stress reducer [49], contributes to the reduction of friction coefficient and wear rate for this system.

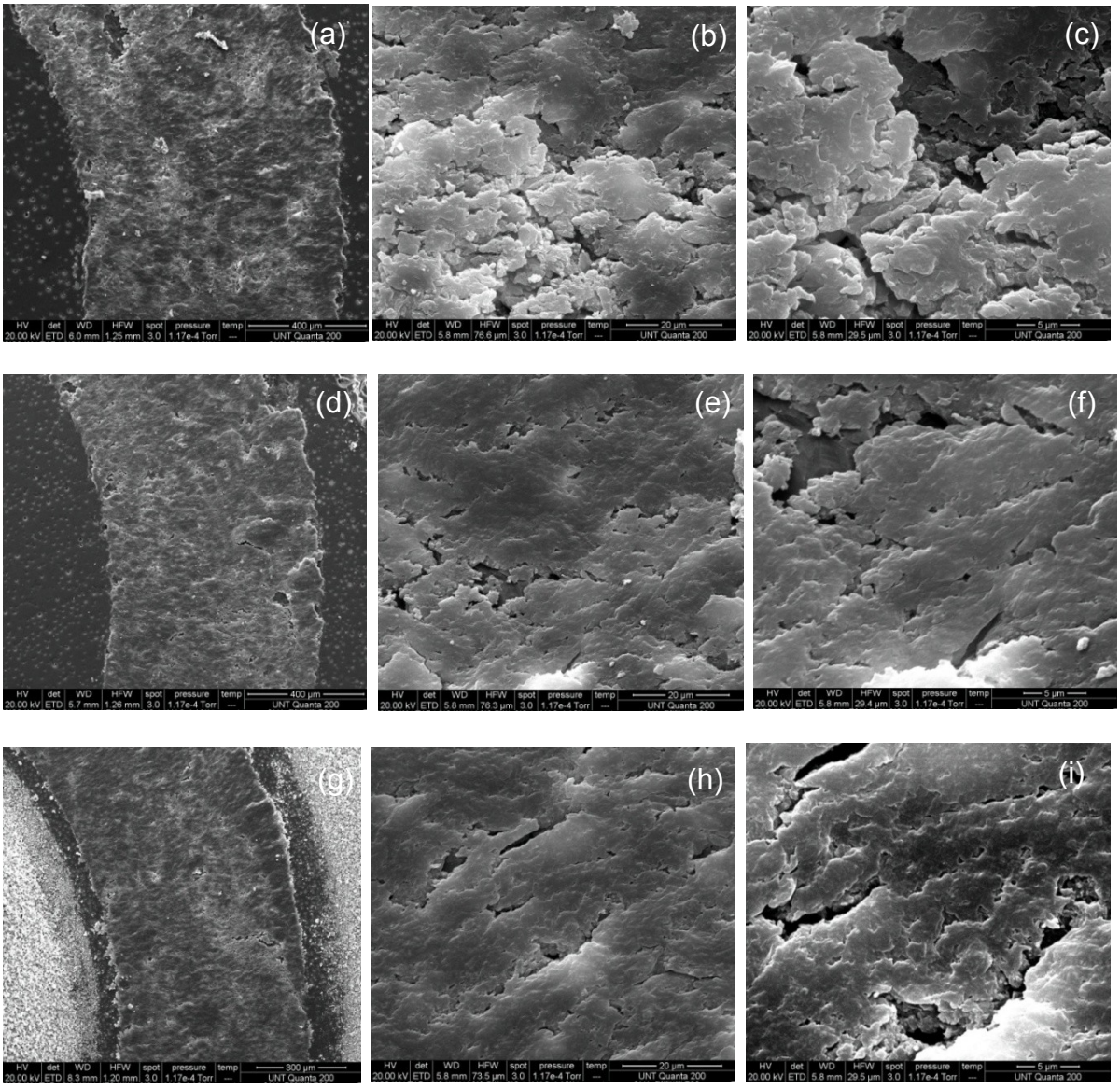

Figure 3.10. The SEM micrographs of the worn surface for (a, b, c) pure DGEBA epoxy resin, (d, e, f) DGEBA epoxy blended with 5.0 phr of DGTFA and (g, h, i) DGEBA epoxy blended with 20.0 phr of DGTFA. Condition of sliding wear tests: normal load of 5.0 N; sliding speed of 200 rpm revolution of 5,000 turns. Magnification: 120 x for (a, d,g), 2000x for (b, e, h) and 5000x for (c, f, i).

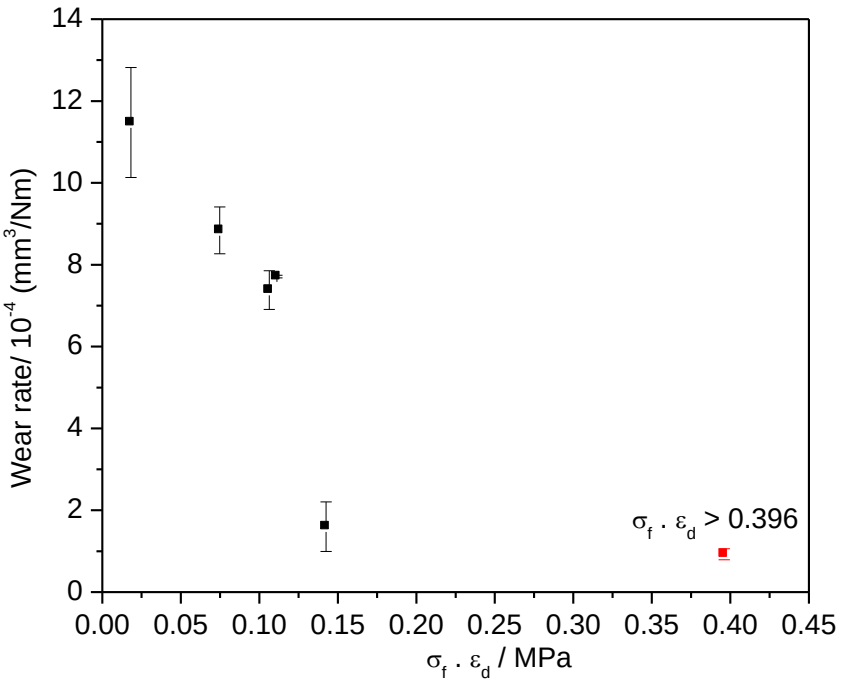

Figure 3.11. Wear rate as a function of the product of flexural strength and strain at deflection point for DGEBA + DGTFA epoxy resins.

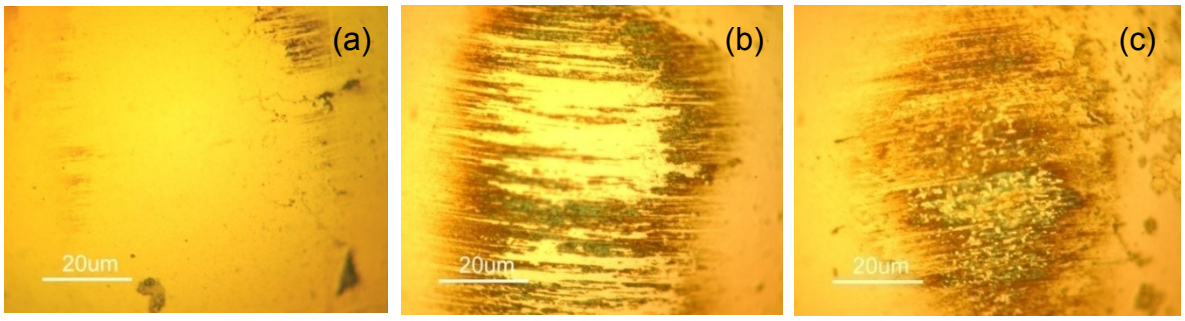

Figure 3.12. Optical image (200x) of transfer film formed on the surface of Si_3N_4 counterface after sliding against (a) pure DGEBA epoxy and DGEBA epoxy blended with (b) 5.0 phr of DGTFA and (c) 20.0 phr of DGTFA. Normal load: 5.0 N; sliding speed: 200 rpm; revolution: 5000 turns.

3.4 References

[1] Cottrell TL. The strengths of chemical bonds, 2nd ed. Butterworth, London: 1958.

[2] McCloskey CB, Yip CM, Santerre JP. Macromolecules 2002;35(3):924-933.

[3] Park S-J, Jin F-L, Shin J-S. Mater Sci Eng A 2005;390(1-2):240-245.

[4] van de Grampel RD, Ming W, van Gennip WJH, van der Velden F, Laven J, Niemantsverdriet JW, van der Linde R. Polymer 2005;46(23):10531-10537.

[5] Lee JR, Jin FL, Park SJ, Park JM. Surf Coat Technol 2004;180-181:650-654.

[6] Montefusco F, Bongiovanni R, Sangermano M, Priola A, Harden A, Rehnberg N. Polymer 2004;45(14):4663-4668.

[7] Sangermano M, Bongiovanni R, Malucelli G, Priola A, Pollicino A, Recca A. J Appl Polym Sci 2003;89(6):1524-1529.

[8] Bilyeu B. Characterization of cure kinetics and physical properties of a high performcance, glass fiber-reinforced epoxy prepreg and a novel fluorine-modified, amine-cured commerial epoxy. Dissertation, University of North Texas, Denton, 2003.

[9] Chapman TM, Marra KG. Macromolecules 1995;28(6):2081-2085.

[10] Iyengar DR, Perutz SM, Dai CA, Ober CK, Kramer EJ. Macromolecules 1996;29(4):1229-1234.

[11] Ming W, Tian M, van de Grampel RD, Melis F, Jia X, Loos J, van der Linde R. Macromolecules 2002;35(18):6920-6929.

[12] Thomas RR, Anton DR, Graham WF, Darmon MJ, Sauer BB, Stika KM, Swartzfager DG. Macromolecules 1997;30(10):2883-2890.

[13] Thomas RR, Anton DR, Graham WF, Darmon MJ, Stika KM. Macromolecules 1998;31(14):4595-4604.

[14] van de Grampel RD, Ming W, Gildenpfennig A, vanGennip WJH, Laven J, Niemantsverdriet JW, Brongersma HH, deWith G, vanderLinde R. Langmuir 2004;20(15):6344-6351.

[15] Wang J, Mao G, Ober CK, Kramer EJ. Macromolecules 1997;30(7):1906-1914.

[16] Yoon SC, Ratner BD. Macromolecules 1986;19(4):1068-1079.

[17] Yoon SC, Ratner BD. Macromolecules 1988;21(8):2401-2404.

[18] Yoon SC, Ratner BD, Ivan B, Kennedy JP. Macromolecules 1994;27(6):1548-1554.

[19] Yoon SC, Sung YK, Ratner BD. Macromolecules 1990;23(20):4351-4356.

[20] Brostow W, Cassidy PE, Hagg HE, Jaklewicz M, Montemartini PE. Polymer 2001;42(19):7971-7977.

[21] Brostow W, Bujard B, Cassidy PE, Hagg HE, Montemartini PE. Mater Res Innov 2002;6:7-12.

[22] Brostow W, Bujard B, Cassidy PE, Venumbaka S. Int J Polym Mater 2004;53:1045-1060.

[23] Brostow W, Cassidy PE, Macossay J, Pietkiewicz D, Venumbaka S. Polym Internat 2003;52:1498-1505.

[24] Kasemura T, Oshibe, Y., Uozumi, H., Kawai, S., Yamada, Y., Ohmura, H., Yamamoto,T. J Appl Polym Sci 1993;47(12):2207-2216.

[25] du Toit FJ, Sanderson RD, Engelbrecht WJ, Wagener JB. J Fluor Chem 1995;74(1):43-48.

[26] Anand M, Cohen RE, Badour RF. Polymer 1981;22:361-371.

[27] Inagaki N, Tasaka S, Mori K. J Appl Polym Sci 1991;43(3):581-588.

[28] Strobel M, Corn S, Lyons CS, Korba GA. J Polym Sci Polym Chem Ed 1985;23(4):1125-1135.

[29] Strobel M, Thomas PA, Lyons CS. J Polym Sci Polym Chem 1987;25(12):3343-3348.

[30] Han HS, Tan KL, Kang ET. J Appl Polym Sci 2000;76(3):296-304.

[31] Stuart B, George WO, McIntyre PE. Modern infrared spectroscopy, Chichester, England: Wiley 1998.

[32] Wendlandt WW, Gallagher PK. Instrumentation. In: Turi EA, editor. Thermal characterization of polymeric materials, New York: Academic Press, 1981. pp 9-34.

[33] Menard KP. Dynamic mechanical analysis: a practical introduction, New York: CRC Press, 1999.

[34] Bhushan B. Introduction to tribology, New York: Wiley, 2002.

[35] Steijn RP. Friction and wear. In: Brostow W, Corneliussen RD, editors, Failure of plastics, New York: Hanser, 1986. pp 356-392.

[36] Marsella JA, Starner WE. J Polym Sci Polym Chem 2000;38:921-930.

[37] Matynai T, Gawdzik B. J Appl Polym Sci 1997;65(8):1525-1531.

[38] McAdams LV, Gannon JA. Epoxy resin. In: Mark HF, editor. Encyclopedia of polymer science and engineering, vol. 6. New York: Wiley, 1985.

[39] Pascault JP, Sautereau H, Verdu J, Williams RJJ. Thermosetting polymers, New York: Marcel Dekker, 2002.

[40] Fox TG, Loshaek S. J Polym Sci 1955;15:371-390.

[41] Wang YQ, Li J. Mater Sci Eng A 1999;266:155-160.

[42] Jiguet S, Judelewicz M, Mischler S, Hofmann H, Bertsch H, Renaud P. Surf Coat Technol 2006;201:2289-2295.

[43] Durand JM, Vardavoulias M, Jeandin M. Wear 1995;181-183:833-839.

[44] Larsen T, Andersen TL, Thorning B, Horsewell A, Vigild ME. Wear 2007;doi: 10.1016/j.wear.2007.10.003.

[45] Romanes MC, D'Souza NK, Coutinho D, K.J. BJ, Scharf TW. Wear 2007;doi: 10.1016/j.wear.2007.08.022.

[46] Archard JF. Wear 1958;2:438-455.

[47] Stachowiak G, Batchelor AW. Engineering tribology, 3 ed. New York: Elsevier Butterworth Heinemann, 2005.

[48] Hutchings IM. Tribology: friction and wear of engineering materials, Edward Arnold, 1992.

[49] Bahadur S. Wear 2000;245:92-99.

CHAPTER 4

CURING KINETICS OF EPOXY-AMINE SYSTEMS

4.1 Introduction

Curing kinetics of epoxy resin with amines has been extensively investigated over the past four decades. Their physical, mechanical and electrical properties depend to a large extent on the degree of cure. On the other hand, their processability depends on the rate and extent of reaction under process conditions. The knowledge of mechanism and curing kinetics is not only important for a better understanding of the structure-property relations, but it is also fundamental in optimizing process conditions and product qualities.

4.2 Cure Mechanisms of Epoxy-Amine Systems

During a cure reaction, the epoxy resin is converted into a three-dimensional network. There are three probable reactions occurring in the reaction as shown in Scheme 4.1.

1. The addition of primary amine to the epoxide ring

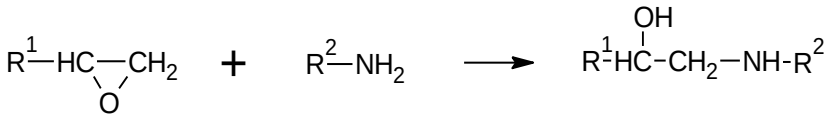

epoxide primary amine

2. The addition of secondary amine to the epoxide ring

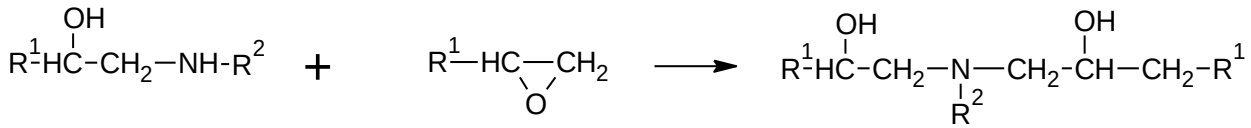

secondary amine tertiary amine

3. The etherification of hydroxyl group to the epoxide ring

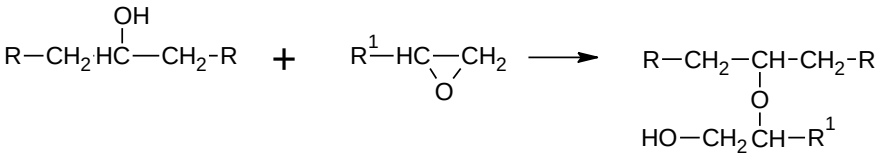

where R, R^1, R^2 represent any alkyl group.

Scheme 4.1. The chemical reactions occurring in epoxy-amine system.

However, only the combination of epoxides and amines is considered major reactions. Shechter et al. [1] studied the cure mechanisms of epoxy-amine systems. They found that a hydroxyl group only served as a catalyst for the reactions and was not a serious contender in competition with amines. The reaction rates of primary and secondary hydrogens with epoxide occur almost simultaneously, and only one overall reaction can be detected—this has been manifested by a single DSC peak. However, the ratio of reaction rates of secondary amine-epoxy reactions to primary amine-epoxy reactions have been 0.5 for most systems. Liu et al. [2] used near-infrared (NIR) spectroscopy to investigate in situ the kinetics of epoxy-aromatic diamine resins. They found that reactivity of primary and secondary amines depended upon the steric hindrance of the epoxy and/or the combination of the electron-donating/withdrawing effects and the deconjugation effects from substituent groups.

4.3 Kinetic Equations

All kinetic studies begin with a basic rate equation [3] which links the rate of reaction or rate of conversion to the concentrations or pressures of reactants and constant parameters: typically rate coefficients and a partial reaction order. For cure kinetics, one can express the rate of conversion, $d\alpha/dt$ at constant temperature as a conversion-

dependent function as:

$$\frac{d\alpha}{dt} = kf(\alpha) \tag{4.1}$$

Constitutive modeling equations for the cure kinetics of thermosetting materials generally fall under two general categories: nth-order and autocatalyzed model. As shown previously, there are several chemical reactions occurring during cure. The chosen kinetic model should represent an entire reaction. This is true if these chemical reactions occur simultaneously [4]. Thermosets follow nth-order kinetics; the rate of conversion is proportional to the concentration of reactants that have not reacted at time *t*. Thus conversion-dependent function can be expressed as:

$$f(\alpha) = (1-\alpha)^n \tag{4.2}$$

where α is degree of conversion or one can call as the fractional concentration of reactants consumed after time *t*, and n is a reaction order. The maximum rate of reaction is the beginning of the reaction or at *t* = 0. On the other hand, the cure reaction that follows the autocatalyzed model is characterized by a maximum reaction rate at about 30-40% of the reaction. The simple conversion-dependent function for autocatalyzed model is:

$$f(\alpha) = \alpha^n(1-\alpha)^m \tag{4.3}$$

where m is another reaction order. According to this model, the rate is zero or very small at initial reaction and attains a maximum value at some intermediate conversion as mentioned before. However, the initial rate of autocatalyzed reaction may not be necessarily zero. It is possible that reactants can be converted into products via alternative paths.

Horie et al. [5] studied the reaction between phenyl glycidyl ether and n- butyl amine in the presence of n-butyl alcohol. They found that the uncatalyzed reaction behaved according to the third order autocatalytic kinetics, but the psuedo-second-order (nth-order) kinetics were observed in the reaction catalyzed with high concentrated n-butyl alcohol. They proposed that there was an external catalyst or impurity initially present in the system, and reaction products having hydroxyl groups acted as true catalysts and were not consumed in any side reactions.

A generalized model describing the autocatalytic reaction is shown as:

$$\frac{d\alpha}{dt} = (k_1 + k_2\alpha^m)(1-\alpha)^n \tag{4.4}$$

where k_1 and k_2 are the externally catalyzed rate constant and the autocatalyzed rate constant, respectively. Both m and n are the kinetic exponents of the reaction, and $m+n$ is the overall reaction order. Both kinetic constants, k_1 and k_2 depend on temperature according to Arrhenius law. Such a model has been successfully applied to describe the initial stage of cure of epoxy/diamine systems. Kamal and his coworkers [6-8] showed that the model was valid only for the initial stage of cure but not for the later stage of cure where the reaction mechanism was diffusion controlled. Prime [4] pointed out that curing was not necessarily limited to one chemical reaction, and the kinetics might be those of an overall process when the reactions occurred simultaneously. Two or more consecutive reactions were possible.

Lee et al. [9] proposed the model for more complex reactions. The model was separated into two elemental parts. One was represented by the nth order type of reaction and the other was by the autocatalyzed type of reaction, shown as:

$$\frac{d\alpha}{dt} = k_a(1-\alpha)^l + k_b\alpha^m(1-\alpha)^n \quad (4.5)$$

where k_a and k_b are the non-catalyzed and autocatalyzed rate constant, respectively, and l, m, n are the respective reaction orders.

4.4 Determination of Cure Kinetics

Various experimental techniques have been developed for cure reactions of thermosets. These techniques include chromatography, infrared spectroscopy, nuclear magnetic resonance, dielectric spectroscopy, raman spectroscopy, calorimetry, chemical analysis and dynamic mechanical measurement, etc. Generally differential scanning calorimetry (DSC) has been mostly used for the estimation of kinetic parameters. This calorimetric technique gives a quantitative measurement on the heat of reaction and permits the determination of the glass transition T_g of materials. Thus, in this work the DSC technique was used to investigate the kinetics of the epoxy system. However, it should be noted that the complementary nature of several techniques, including IR spectroscopy, chromatography, and rheological measurements, can provide such information. By DSC, two basic approaches are used to determine the curing kinetics—the isothermal approach, where a single curve temperature is used at a given cure cycle, and the dynamic approach, where the rate of heat is kept constant for a given cure cycle.

4.4.1 Cure Kinetics from Dynamic tests

There are a number of different methods to calculate kinetic parameters from a dynamic experiment which is also called a non-isothermal heating method. Essentially, these methods can be categorized into 2 main groups. One is analysis from a single heating rate experiment; another is analysis from a multiple heating rate experiment.

A. Analysis from a single heating rate experiment.

This method is very convenient because it involves analysis of a single exotherm, but it lacks consistent accuracy. For most reactions, this method gives an overestimate of the activation energy and preexponential factor. However, in practice, it gives accurate kinetic parameters for some reactions, especially for the first order reaction.

Borchardth and Daniels [4] were the first to describe the application of dynamic DTA and DSC to the study of reaction kinetics. They assumed that the heat, evolved in a small time interval, was directly proportional to the number of moles reacting during that time. They also assumed that no enthalpic events other than the chemical reactions of cure contributed to the heat flow. Thus, the reaction rate or rate of conversion, $d\alpha/dt$ is:

$$\frac{d\alpha}{dt} = \frac{dH}{dt} \cdot \frac{1}{\Delta H_{\text{tot}}} \tag{4.6}$$

where ΔH_{rxn} is the total heat liberated when a completely uncured resin is taken to complete cure. dH/dt or heat flow represents the rate of heat generated during curing reaction.

The conversion-dependent function as proposed by Borchardth and Daniels is

$$f(\alpha) = (1-\alpha)^n \tag{4.7}$$

Thus the rate of conversion can be described as

$$\frac{d\alpha}{dt} = k(1-\alpha)^n \tag{4.8}$$

where k is the rate constant. The temperature dependence of the rate constant can be expressed through an Arrhenius equation as

$$k = Aexp(-E_a/RT) \tag{4.9}$$

where E_a is an activation energy, R is gas constant, T is the absolute temperature and A is the preexponential factor. By combining Equation (4.8) and (4.9), one obtains

$$\frac{d\alpha}{dt} = Aexp\left(-\frac{E_a}{RT}\right) \cdot (1-\alpha)^n \tag{4.10}$$

Due to linear dependence of the temperature with time, one can describe (4.10) as

$$\beta \frac{d\alpha}{dT} = Aexp\left(-\frac{E_a}{RT}\right) \cdot (1-\alpha)^n \tag{4.11}$$

or, in the logarithmic form:

$$ln\left[\beta\left(\frac{d\alpha}{dT}\right)\right] = lnA - \frac{E_a}{RT} + nln(1-\alpha) \tag{4.12}$$

where the value of α can be obtained from the area under the DSC curve as

$$\alpha = \frac{\Delta H_T}{\Delta H_{tot}} \tag{4.13}$$

where ΔH_T is given by the fractional peak area, ΔH_{tot} is given by the total peak area obtained from an average of the values at different heating rates and $\beta = dT/dt$ is the scanning rate.

Zvetkov [10] studied the reaction kinetics of diglycidyl ether of bisphenol A (DGEBA) with *m*-phenylene diamine using various kinds of nonisothermal reaction kinetics. He performed a mechanistic-like four stage kinetic analysis consisting of isoconversional or apparent kinetic methods, analysis at the peak maximum of DSC curves, integral and differential single curve methods and modeling of the reaction and comparison of the model with the experiment. He showed that with isoconversional method, side reactions manifested itself at a high degree of conversion, whereas a single DSC curve kinetics exhibited non-typical false kinetic compensation effects above 5 $Kmin^{-1}$. He attributed this to an incomplete curing at the end of the scanning experiments.

B. Analysis from multiple heating scan experiment.

This method provides the kinetic parameters with accuracy. It is valuable as a precursor to isothermal studies and is often the only means to analyze the curing kinetics of system with multiple exotherms, solvent effects or an unreliable baseline [4].

A basic concept of the analysis is that the peak exotherm temperature T_p varies in a predictable manner with heating rate β. According to the Kissinger method, the activation energy can be obtained from the maximum reaction rate where the exothermal peak appears under a constant heating rate.

$$E_a = -R\left[\frac{d\left(\ln\left(\frac{\beta}{T_p^2}\right)\right)}{d\left(\frac{1}{T_p}\right)}\right] \tag{4.14}$$

Thus, the activation energy E_a can be obtained from the slope of the plot of $ln\,(\beta/T_p^2)$ as a function of $1/T_p$ without a specific assumption of the conversion-dependent function.

Ozawa [11] developed an alternative method to determine the activation energy from T_p. The equation shows as following:

$$E_a = -\frac{R}{1.052}\left(\frac{dln\beta}{d\left(\frac{1}{T_p}\right)}\right) \tag{4.15}$$

Thus, E_a can be obtained from the slope of the plot of $ln\,\beta$ as a function of $1/T_p$.

Another method for determining E_a was first developed by Fava [12], named as an isoconversional method. With this method, the degree of conversion can be predicted without the knowledge of the conversion-dependent function $f(\alpha)$, which is a distinct advantage over the single scan rate method. This method is based on the assumption

that the reaction rate at a constant conversion depends only on the temperature. Based on this concept, [13-18] the equation for determining the activation energy shows as:

$$E_\alpha = -R\left[\frac{d(ln(\beta)_\alpha}{d\left(\frac{1}{T}\right)_\alpha}\right] \quad (4.16)$$

where E_α is the activation energy at a given conversion degree and T is the temperature of a selected degree of conversion at each heating rate.

It is assumed that a single reaction occurs during the curing process given the complexity of the reaction, so values obtained from both Kissinger and Ozawa's methods are an overall value representing all complex reactions that occur during curing.

4.4.2 Cure Kinetics from Isothermal Tests

Two different techniques have been used for isothermal experiments. One is that an uncured sample is cured isothermally in a calorimeter at desired curing temperatures for a certain period of time. This method allows monitoring of the conversion and the rate of conversion simultaneously over the entire course of reaction. The heat of cure at time *t,* ΔH_t, can be measured directly from the partial area under the isothermal curve. The degree of conversion at time *t,* α_t can be defined as

$$\alpha_t = \Delta H_t / \Delta H_{tot} \quad (4.17)$$

The rate of reaction is given analogously as explained by Equation (4.6) in dynamic methods.

Fava [12] studied the curing kinetics of an epoxy-anhydride system by means of both isothermal and dynamic methods. He was the first to demonstrate the deficiencies of this isothermal method in which rate of reaction and conversion were monitored

continuously in DSC. The isothermal DSC technique he used involved insertion of the sample at ambient temperature, programming as rapidly as possible to the measurement temperature, and operating isothermally, following the DSC output as a function of time. He found that the ΔH_{rxn} from the isothermal was not constant; it varied systematically with temperature. At low curing temperature, the rate of reaction was too low to detect due to the limitation in the sensitivity of the calorimeter; the incomplete cure contributed to low values of ΔH_{rxn}. At high temperature, the rate of reaction was so fast that the heat absorbed as the sample equilibrated at the cure temperature partially cancelled out the exotherm; the ΔH_{rxn} was low. For autocatalytic reactions, the extent of reaction up to the exotherm peak, where the rate of reaction is the highest, is constant and independent of temperature for a given thermosetting system. Sourour and Kamal [8] were the first to find this phenomenon. They studied the curing reactions of DGEBA with m-phenylene diamine (m-PDA), using a differential scanning calorimeter (DSC) and rheological data under isothermal condition. The isothermal DSC technique they used involved pre-heating the DSC to the temperature of interest, starting the time base scan, and loading the sample into the cell as rapidly as possible. They found that the time for materials to gel under isothermal conditions and the peak isothermal reaction rate $(d\alpha/dt)_{max}$ can be used as kinetic parameters to determine an overall activation energy.

Miller and Oebser [19] used isothermal DSC techniques described by Fava [12] and Sourour and Kamal [8] to determine cure time and activation energies of one-container epoxy resin systems. No significant differences were observed between results obtained by both methods for cure times in the order of 10-20 minutes.

The other technique is that several samples are cured isothermally, either in the oven or the calorimeter, for various times until no additional curing can be detected. Samples are then scanned in the calorimeter to determine the residual heat of reaction at that particular time t, $\Delta H_{resid,\,t}$. The degree of conversion at time t can be defined as:

$$\frac{\Delta H_{tot} - \Delta H_{resid\,,t}}{\Delta H_{\mathrm{tot}}} = \Delta H_t. \qquad (4.18)$$

Like the single scan rate method, the isothermal method requires an accurate value of ΔH_{tot}. It is recommended [4] that ΔH_{tot} be determined from scanning experiments, preferably but not necessary more than one scanning rate between 2 to 20^{o}C/min. However, except for the multiple heating rate method, the isothermal is considerably accurate and informative in characterizing the curing kinetics.

4.5 Effects of Additives and Fillers on Curing Kinetics

Kinetic parameters on the curing system are usually studied on systems containing mostly the resin and hardener. However for industrial applications which require high performance materials, all resins are modified with various additives and fillers to improve the processibility, mechanical, tribological, thermal and electrical properties.

Additives and fillers can act as an accelerator, retarder or even inhibitor with regard to the reaction system. Prime [4] reported that inorganic additives and fillers affected the cure kinetics of thermosets. They could change the network structure and affect the curing kinetics of epoxy resins. The presence of reactive groups at the surface of fillers has been believed to affect the cure reaction. The work done by several researchers seems to support the rationale. Dutta and Ryan [20] studied the effect of carbon black and Novakup fillers on the reaction of liquid epoxy systems cured with m-

phenylenediamine. They found that only carbon black, which had chemical complexes on the surface, showed significant effects on the reaction rate of the curing process. Lem and Han [21] found that the activation energy of a commercial unsaturated polyester was reduced significantly from 83 to 37.5 kJ/mol when 50 wt. % of $CaCO_3$ was added. Harsh et al. [22] studied the cure kinetics of a cycloaliphatic epoxy + an anhydride with and without additives. They found that the fillers without surface treatment did not influence the activation energy, while the fillers with surface modification showed an accelerating effect on the cure kinetics. Macan et al. [23] studied the kinetics of epoxy + silica hybrid materials. They reported that the presence of the inorganic phase hindered the complete cross linking of the organic phase and influenced the kinetics of cure. In contrast, Serier et al. [24] investigated kinetics of epoxy reaction with aminosilane in solution, and they found no influence of sol-gel reaction on kinetics of epoxy cure. Besides the inorganic fillers, other additives, such as poly(ether imide) [25, 26], a liquid crystalline monomer [27] and carboxyl-terminated butadiene-co-acrylonitrile, have been studied for the curing kinetics [28]. Results showed that those additives hindered the reaction between epoxy and hardener.

Thus it is worthwhile to pursue the effects of fillers on curing kinetics of epoxy systems. In the present work, curing kinetics for two different epoxy systems was investigated. One was epoxy DGEBA curing with polyamine curing agent, and the effect of concentration of diglycidyl of trifluoromethyl aniline (DGTFA) on curing kinetics has been studied using non-isothermal methods. Another system was epoxy DGEBA curing with cycloaliphatic amine curing agent; the effect of silica content, as well as

types of silica particles has been studied using both isothermal and non-isothermal methods.

4.6 Experimental

4.6.1 Materials

The commercial epoxy used in this study was diglycidyl ether of bisphenol A (DGEBA) from System Three with epoxy equivalent weight of 210. The hardeners used were methylenebiscyclohexanamine, 4, 4' (AMICURE®PACM) from Air Products with hydrogen-amine equivalent weight of 52.5 and polyamines (hardener 1) from System Three with hydrogen-amine equivalent weight of 93. The fluoro-modified epoxy oligomer was diglycidyl of trifluoromethyl aniline (DGTFA) with an epoxy equivalent weight of 2003. The synthesis procedure of this oligomer is described in chapter 3. These three chemicals were used as received without further purification. Neat silica powder and silane modified silica powder were placed in a conventional oven at 80^{o}C overnight before use.

4.6.2 Preparation of Epoxy + Silica Composites

Epoxy + silica composites with 10 part per hundreds (phr) silica powder were prepared. First silica powder, either neat silica or silane modified silica, was mixed with DGEBA. Then a 1:1 stoichiometric amount of AMICURE®PACM was added and mixed thoroughly with the DGEBA + silica mixture at room temperature. The mixtures were either used immediately for DSC measurement; or the mixtures were kept in a liquid N_2 Dewar.

4.6.3 Preparation of the Fluorinated Modified Epoxy

Mixtures of DGTFA and commercial epoxy resin DGEBA were prepared with 2.5,

5.0, 10.0, 15.0, 20.0 phr of DGTFA. First, a certain amount of DGTFA was mixed with DGEBA. Then the stoichiometric amount of polyamine-Hardener 1 was added. In order to prevent precuring, the mixture was then immediately used for DSC measurement.

4.6.4 Instrumentation

A differential scanning calorimeter, Perkin-Elmer Diamond DSC, equipped with a cryogenic liquid N_2 tank was used for the kinetic study of epoxy composites filled with silica, while the Perkin-Elmer Diamond DSC, equipped with a refrigerator, was used for the study of DGEBA + DGTFA blends.

The temperature and heat flow were calibrated with the melting temperature and heat of fusion of indium at each scanning rate being used. Nitrogen gas with the flow rate of 40 ml/min was used as purge gas.

For epoxy + silica hybrid systems, approximately 10-20 mg of each sample was enclosed in the hermetically sealed stainless steel pan and was then used immediately or otherwise was kept in Dewar containing the liquid nitrogen, to avoid the reaction occurring prior to the experiment. To characterize the cure kinetics of these epoxy systems, both isothermal and dynamic DSC tests were performed. A series of isothermal curing tests were carried out on the unreacted samples at 80, 85, 90, 95, 100 and 105 ^{o}C, respectively. All samples were placed in a DSC cell and equilibrated at 20^{o}C for 1 minute. The temperature was then raised to the desired isothermal curing temperature at 200^{o}C/min and kept for 30 minutes. By this time, the reaction was considered complete, and the signal leveled off. The samples were then quenched to 5^{o}C and subsequently scanned from 5 to 250^{o}C at heating rate of 20^{o}C/min to determine the glass transition temperature T_g and the residual heat of reaction, if

presented. The dynamic DSC tests were run at 4 different scanning rates: 5, 10, 15 and 20 C^{o}/min from 0 to 250^{o}C.

Unlike epoxy + silica hybrids, approximately 5-10 mg of each fresh fluorinated modified epoxy blend was enclosed in the aluminum pan and used immediately after preparing. Only the dynamic DSC Method was used to investigate their kinetics. The tests were again run at 4 different scanning rates: 5, 10, 15 and 20 C^{o}/min from 10 to 250^{o}C.

4.7 Results and Discussion

4.7.1 Curing of DGEBA + DGTFA Epoxy with Polyamine

For the blends of the fluorinated modified epoxy DGTFA and commercial epoxy DGEBA curing with polyamine systems, the curing kinetics was studied using only the dynamic scanning methods. The kinetic parameters obtained from multiple scanning rate tests were determined and compared with those from single scanning rate.

Thus, the curing behavior of the pure DGEBA epoxy and the blends with polyamine were followed using DSC dynamic scan at various heating rates. The results at heating rate of 10^{o}C/min are shown in Figure 4.1. Only a single exothermic event is found. There is no doublet peak detected in curing of both pure DGEBA and the blends of DGEBA and DGTFA. This implies the miscibility of DGTFA in the DGEBA + polyamine systems. In addition, the introduction of DGTFA does not change significantly the curing behaviors of the systems. Only slight changes in exothermic peak maxima are observed when DGTFA is added more than 10 phr (see Figure 4.1).

A. Single DSC curve kinetic analysis.

The DSC kinetic analysis of the epoxy/polyamine reactions was performed with

Perkin-Elmer software, Pyris 7. The assumption used for single scan kinetic analysis in Pyris 7 is that at the given time during the DSC scan, t and temperature, T, the rate of reaction is assumed to obey the n-order reaction as proposed by Borchart and Daniels. A multilinear regression procedure is performed with $ln\ (\beta\ (d\alpha/dt))$, -1/$T$ and $ln\ (1\text{-}\alpha)$ as variables to solve for E_a and n in Equation (4.12). Results are shown in Table 4.1. It is found that E_a of a DGEBA + polyamine system is reduced by adding DGTFA; the further addition of DGTFA causes more reduction in E_a. The reaction order n is found to vary within the range of 1.4 to 1.8. This finding is in agreement with others [10, 27, 29-36] that n, for nth order reaction, is less than 2 when the epoxy/amine reactions of model compounds have been studied.

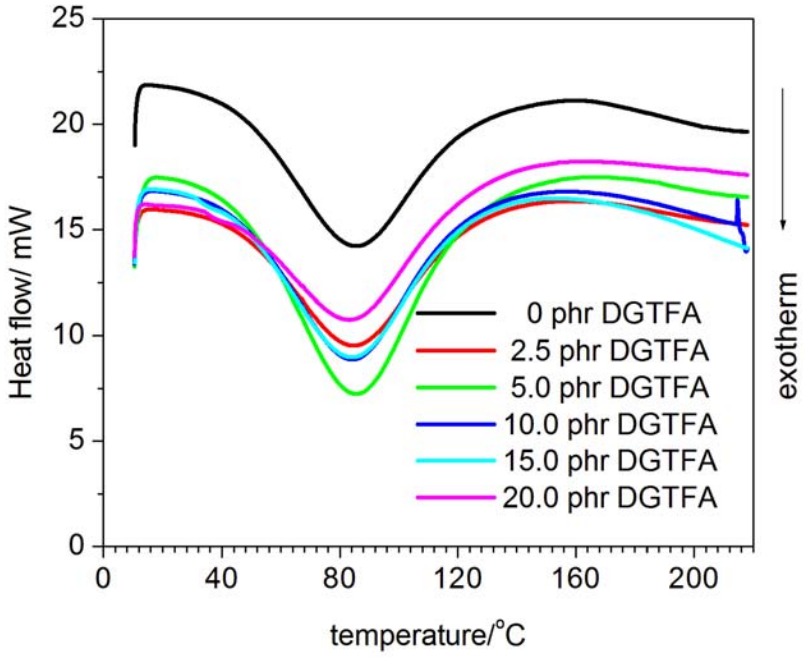

Figure 4.1. Dynamic DSC thermograms at 10.0°C/min for unreacted DGEBA + DGTFA curing with polyamine.

Figure 4.2 shows the influence of different heating rates on the curing behavior. It is observed that as heating rate increases, the peak exothermic temperature, T_p, shifts to higher temperature. This kind of dependency was also observed by others [22, 26, 32, 37-39]. For more details, the values of exothermic peak maxima, T_p, and enthalpy of reaction, ΔH_{rxn}, at different heating rates are tabulated in Table 4.2.

The results in Table 4.2 show that the total heat of reaction of all investigated systems varies from -289 to -191 J/g. The highest heat of reaction possesses the pure DGEBA epoxy systems. The addition of any further DGTFA content results in a reduction of the total heat of reaction. It is also observed from Table 4.2 that ΔH_{rxn} is not constant, with its value decreasing particularly for the high heating rate. The decrease in total reaction enthalpy with increasing heating rates may be attributed to the higher temperature attained in these samples. At higher temperature, unreacted molecules or volatiles could be lost, thus providing a contribution to the total heat flow that is not linked to the curing reaction. In addition, at the fast heat rate, thermal decomposition due to the higher temperature attained in the samples probably interferes with the later stage of cure [4]. As the degraded portion of resin does not eventually contribute to the cure exothermic heat output, ΔH_{rxn} appears to diminish with the increasing heat rate.

B. Multiple scan rate method.

Due to the shift in T_p, the activation energy could be calculated by the Kissinger and Ozawa methods. According to Kissinger's and Ozawa's method, $ln\ (\beta/T_p^2)$ and $ln\ \beta$ were plotted as a function of $1/T_p$, respectively. All plots are shown in Figure 4.3. From Figure 4.3, the linear regression fits well for both Kissinger's and Ozawa's analyzed

methods with R^2 of 0.996 to 0.999, thus confirming the validity of both methods. From the fitted slope, the activation energy and E_a are calculated.

The dependency of E_a obtained from both analyzed methods on the DGTFA content is shown in Table 4.3. It is found that the values of E_a calculated from Kissinger's method are slightly lower than those from Ozawa's method for all blend systems. Such a difference is also noticed by others [22]. However, the changes of E_a as a function of DGTFA content obtained from both methods are in the same trend.

Table 4.1. The E_a and n values of DGEBA blended with various amounts of DGTFA curing with polyamine obtained from Pyris 7 software.

scan rate/	E_a / kJmol $^{-1}$						n					
^{o}C/min	0 phr	2.5 phr	5.0 phr	10.0 phr	15.0 phr	20.0 phr	0 phr	2.5 phr	5.0 phr	10.0 phr	15.0 phr	20.0 phr
5	70.4	65.1	68.5	67.8	66.1	62.3	1.80	1.49	1.67	1.40	1.52	1.47
10	66.5	64.0	66.3	63.7	63.3	60.1	1.66	1.52	1.65	1.46	1.49	1.46
15	65.0	64.1	64.6	60.3	62.7	60.1	1.61	1.64	1.62	1.43	1.52	1.43
20	66.3	63.1	61.7	62.4	62.0	62.0	1.62	1.59	1.57	1.45	1.53	1.45

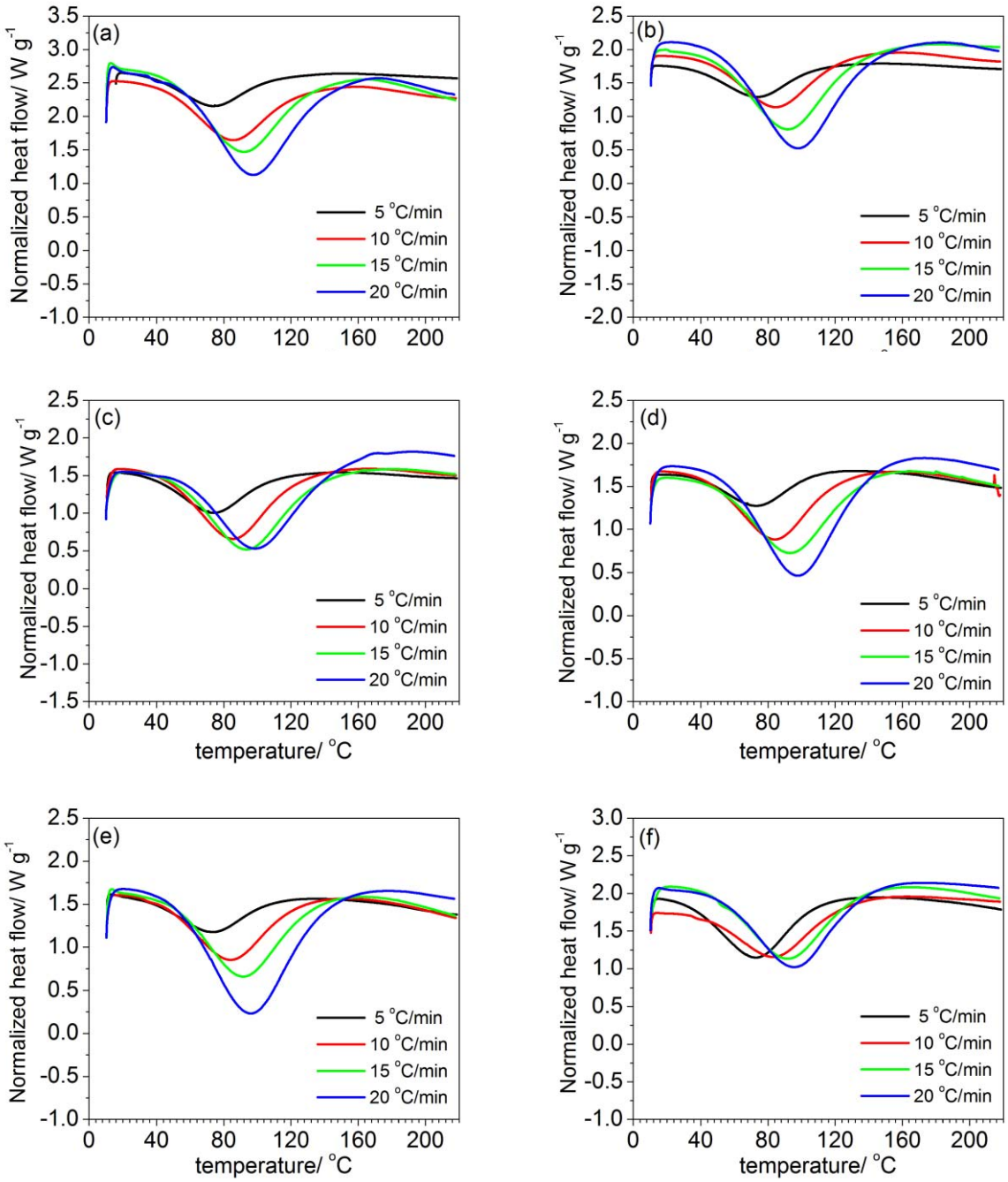

Figure 4.2. Dynamic DSC thermograms at different heating rates for the unreacted (a) pure epoxy DGEBA (b) DGEBA+ 2.5 phr of DGTFA, (c) DGEBA+ 5.0 phr of DGTFA, (d) DGEBA+ 10.0 phr of DGTFA, (e) DGEBA+ 15.0 phr of DGTFA and (f) DGEBA+ 20.0 phr of DGTFA curing with polyamine.

It is shown in Table 4.3 that E_a decreases slightly when DGTFA is added. It decreases of about 5 kJ/mol by adding DGTFA up to 10 phr, but then E_a starts to increase when 15 phr of DGTFA was added.

Theoretically, E_a, the activation energy of reaction, is the amount of energy needed to start the reaction. It may otherwise be denoted as the minimum energy necessary for a specific chemical reaction to occur. From this extent, the introduction of DGTFA to epoxy DGEBA affects the curing mechanism of the epoxy-amine system. Addition of DGTFA causes a decrease in the activation energy, and consequently increases an accelerating effect on the cure reaction. The effect is more pronounced as DGTFA content increases. The possible reason is that the chemical structure of DGTFA contains built-in tertiary amines, R_3N, in the molecular backbone, allowing it to function as a catalyst [40-42]. The tertiary amines [42] are Lewis bases which contain an unshared pair of electrons in an outer orbital and seek a reaction with areas of low electron density. Moreover, the tertiary amines can react with the methylene carbon of the epoxy group to form an intermediate zwitterion ion which can further initiate the curing process.

Table 4.2. Exothermic peak maxima, T_p, and total heat of reaction, ΔH_{rxn}, of DGEBA + DGTFA curing with polyamine.

scan rate / °C min^{-1}	T_p / °C						ΔH_{rxn} / J g^{-1}					
	0 phr	2.5 phr	5.0 phr	10.0 phr	15.0 phr	20.0 phr	0 phr	2.5 phr	5.0 phr	10.0 phr	15.0 phr	20.0 phr
5	73.9	73.9	74.0	73.0	72.8	72.8	-286.0	-273.5	-245.5	-241.5	-238.1	-223.1
10	85.3	84.7	85.7	84.2	83.9	83.5	-263.5	-243.3	-247.2	-236.1	-224.4	-214.9
15	91.5	92.0	93.7	93.3	91.5	91.7	-256.0	-272.8	-227.7	-219.4	-218.7	-204.4
20	97.7	97.7	99.3	98.0	96.7	96.1	-245.6	-271.6	-221.9	-217.8	-217.8	-191.9

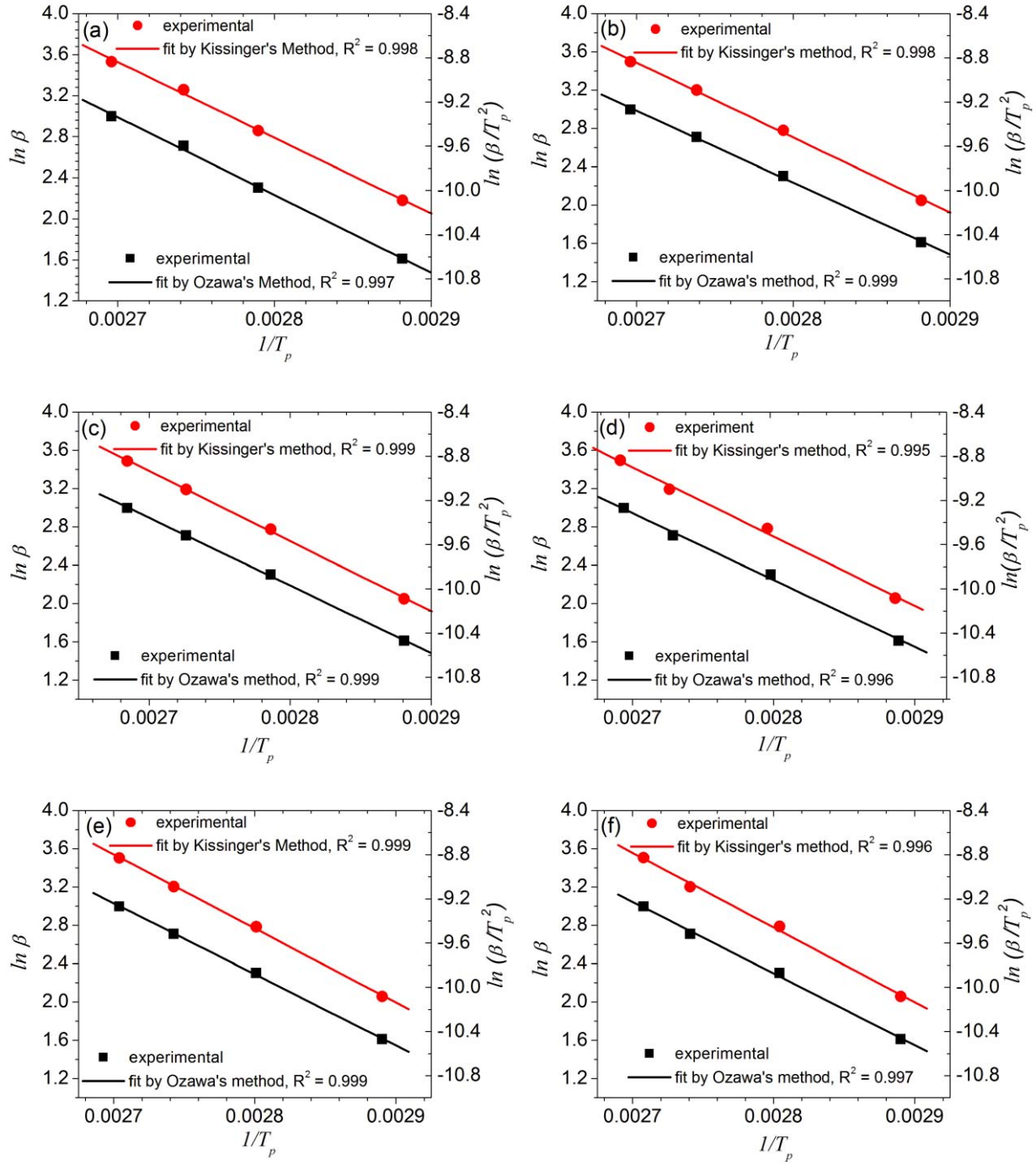

Figure 4.3. Plot of $ln\ (\beta/T_p^2)$ versus $1/T_p$ (Kissinger) and $ln\ \beta$ versus $1/T_p$ (Ozawa) for (a) pure epoxy DGEBA,(b) DGEBA + 2.5 phr of DGTFA, (c) DGEBA+ 5.0 phr DGTFA, (d) DGEBA + 10.0 phr DGTFA, (e) DGEBA + 15.0 phr DGTFA and (f) DGEBA + 20.0 phr DGTFA curing with polyamine.

However, as the amount of DGTFA increases up to 15 phr, the acceleration effect of DGTFA to the overall reaction reduces. The diffusion effect, instead, plays a role. According to chapter 3, the epoxy equivalent weight of DGTFA is 2003, about 9.5 times larger than that of DGEBA. As the rule of thumb, a bigger molecule (DGTFA) diffuses more slowly than a smaller one (DGEBA). Moreover, a larger amount of the high-molecular-weight DGTFA results in a higher viscosity of the system, which causes the movements of reactive groups to diminish. Thus, the explanation for the increase in E_a is that bulky long chains of DGTFA retard the overall reactions between oxirane groups in epoxy resin and N-H groups in amine curing agent.

Table 4.3. Kinetic parameters of DGEBA + DGTFA epoxy curing with polyamine from multiple scanning rate methods.

	E_a / kJ mol^{-1}	
DGETFA/ phr	Ozawa	Kissinger
0	59.86	57.01
2.5	59.3	56.42
5.0	55.79	52.72
10.0	55.16	52.07
15.0	58.56	55.66
20.0	59.09	56.23

C. General remarks.

Interestingly, it is found that the overall activation energy obtained by the multiple scan rate method, for epoxy DGEBA + DGTFA curing with polyamines, is in the range of 55-60 kJ/mol. The values are significantly lower than those obtained by the single heating scan method as shown previously. Moreover, the changes of E_a as a function of DGTFA found using those two methods are not in the same trend. E_a, determined by

the multiple scan rate method, shows the minima at 10 phr of DGETFA while the one obtained using the single scan rate method decreases as DGETFA content increases.

It was pointed out by Vyazovkin [16] that the nature of the models made it impossible to create a method of explicit choices. He explained that a model always gave an inchoate description of the real process because it was created mathematically from an ideal process. Thus, in order to obtain reliable results from the single scan method, one needed the right model for conversion function, $f(\alpha)$, which could explain an entire curing mechanism.

In the dynamic scan, the thermoanalytical curve contains information about the temperature and conversion components in a nonseparated form. However, by substituting the model of the process into the Arrhenius equation, one could isolate the temperature component of the process rate, which is the indispensable condition for estimating E_a. Thus, it is obvious that in this case the correctness of estimating E_a depends on how well the chosen form of $f(\alpha)$ described the conversion component of the process rate. However, by performing a set of non-isothermal experiments for various heating rates, one could correctly separate the contribution of the temperature and conversion components. As discussed previously, the reaction rate at a constant conversion depends only on the temperature; the extent of reaction for epoxy-amine reaction, α, at peak exotherm temperature, T_p, is constant and independent of heating rate [4]. At constant heating rate, the time, at which the same transformation degree is attained in various experiments, is determined by the temperature component alone. This makes it possible to estimate the value of E_a without knowing the curing models.

Thus it can be inferred that E_a values determined from a single heating scan method are less reliable. The discrepancy of E_a obtained from the single and multiple heating scans implies the invalidity of using nth-order kinetic reaction to describe the curing mechanism of this epoxy system. The results of this study are in agreement with those of Catalani and Boniceelli [43] who studied the cure kinetics of diglycidyl ether of bisphenol A (DGEBA) with a modified polyamine by the dynamic method. They determined the kinetic parameters using three different methods of data analysis, namely the Borchardt-Daniels, Kissinger and isoconversional methods. The results obtained from the Borchardt-Daniels method disagreed with those from the Kissinger and isoconversional methods, demonstrating the limitations of the data analysis based on single heating rate measurement.

4.7.2 Kinetics of Epoxy + Silica Composites

Curing kinetics of epoxy composites filled with 10 phr of neat silica and surface-treated silica were investigated both by dynamic scan and isothermal scan methods.

A. Dynamic DSC scan.

The overall cure behavior of the pure epoxy DGEBA curing with clycoaliphatic amines (methylenebiscyclohexanamine, 4, 4') is shown in Figure 5.4 (a). Only a single exothermic peak is observed; the peak temperature T_p increases with ascending heat rate. However, the heat capacity of materials before and after curing is different. The heat capacity after curing increases as a function of temperature, which made it ambiguous to determine the heat of reaction. Thus, determining the curing kinetic by means of a single scan method is meaningless, and only a multiple scan method is

used to determine kinetic parameters. In Figures 4.4 (b) to 4.4 (e), similar results are observed in the curing of epoxy + silica with cycloaliphatic amines.

As discussed before, due to the shift of T_p, the activation energy could be determined by the Kissinger and Ozawa methods. The peak temperatures T_p were then transformed according to Kissinger's and Ozawa's equations (4.14) and (4.15), respectively. Plots of the reciprocal peak temperature $1/T_p$ against the natural logarithm of heating rate $ln\ \beta$ and those of $1/T_p$ against $ln\ \beta/T_p^2$ for the Kissinger and Ozawa methods, respectively are shown in Figure 4.5. The values of activation energy calculated from the fitted slope are shown in Table 4.4.

Table 4.4. Activation energy E_a of pure epoxy resin and epoxy composites filled with different types of silica at the 10 phr.

	E_a / kJ mol^{-1}	
types of silica	Ozawa	Kissinger
neat silica	60.1	57.0
silica-GPS	60.5	57.4
silica-MAMS	62.6	59.6
silica-MPS	54.6	51.2
pure epoxy	59.8	56.6

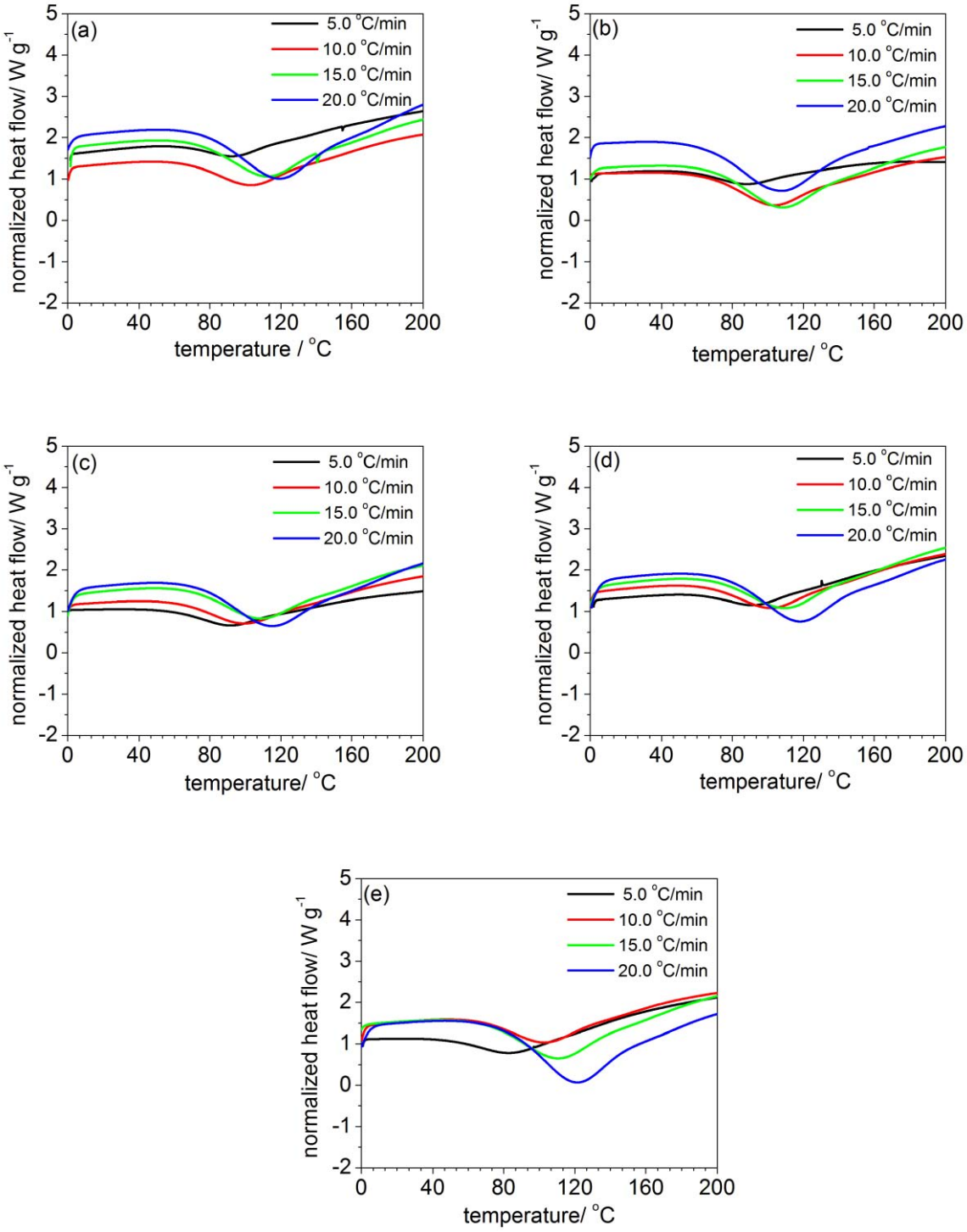

Figure 4.4. Dynamic DSC thermograms at different heating rates for the unreacted (a) pure epoxy (b) epoxy DGEBA + 10.0 phr of neat silica, (c) epoxy DGEBA + 10.0 phr of silica-GPS, (d) epoxy DGEBA + 10.0 phr of silica-MAMS and (e) epoxy DGEBA + 10.0 phr of silica-MPS.

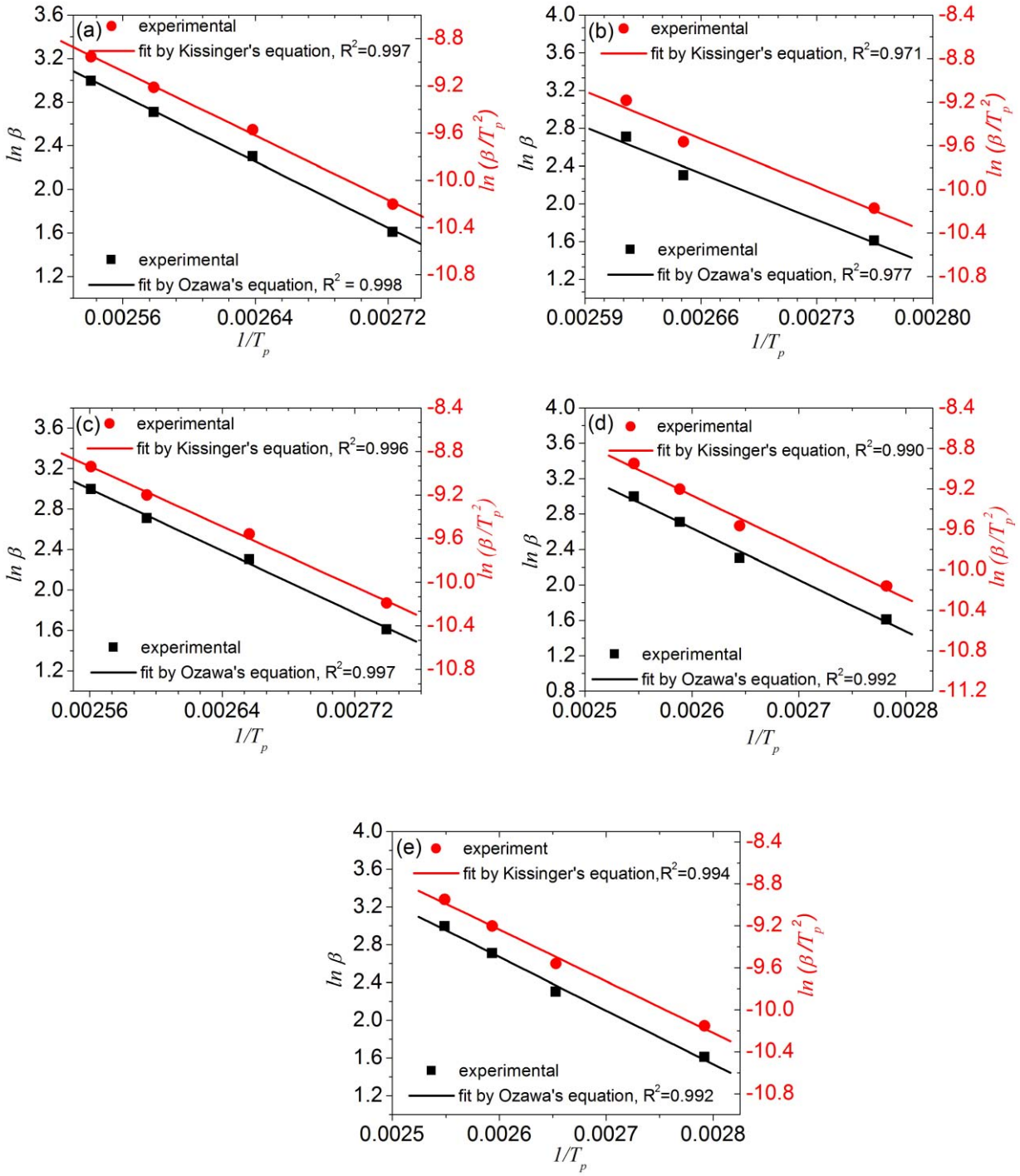

Figure 4.5. Plot of $ln\ (\beta/T_p^2)$ versus $1/T_p$ (Kissinger) and $ln\ \beta$ versus $1/T_p$ (Ozawa) for (a) pure epoxy, (b) epoxy DGEBA + 10.0 phr of neat silica. (c) epoxy DGEBA + 10.0 phr of silica-GPS, (d) epoxy DGEBA + 10.0 phr of silica-MAMS and (e) epoxy DGEBA + 10.0 phr of silica-MPS.

The values of E_a for the pure epoxy system without silica powder are 59.8 and 56.6 kJ/mol according to the Ozawa and Kissinger methods, respectively. Both values are similar, but the E_a determined by Ozawa's equation are slightly higher than that determined by Kissinger's equation. Such a difference is also observed in epoxy DGEBA curing with polyamine systems, discussed in section 4.7.1.

The dependency of E_a on the types of silica powder is shown in Table 4.4. Interestingly, only a slight increase in E_a is observed when either neat silica or silica-GPS is introduced to the epoxy-cycloaliphatic amine system. This means that the untreated silica and silica-GPS do not affect the overall cure kinetics of the epoxy-cycloaliphatic amine system. However, in the case of the curing reaction of epoxy + silica-MAMS and that of epoxy + silica-MPS with cycloaliphatic amines, the change in E_a is observed. E_a of the epoxy + silica-MAMS system increases about 2.8 kJ/mol whereas that of the epoxy + silica-MPS system decreases about 4.2 kJ/mol. This result demonstrates that silica-MPS accelerates the curing reaction of DGEBA epoxy with cycloaliphatic amine whereas silica-MAMS tends to retard the reaction. The possible explanations for these behaviors are provided in section B (isothermal curing).

B. Isothermal curing.

To calculate the total heat of reaction generated to reach full conversion ΔH_{tot}, DSC dynamic scans at different heating rates were performed, and the total area under each thermogram was determined for all systems. The average values of ΔH_{tot} at heating rates from 5 to 15 ^{o}C/min were used to calculate the fraction of conversion α shown in Equation (4.17).

Typical plots of conversion α as a function of time of pure epoxy curing with cycloaliphatic amines at various temperatures are shown in Figure 4.6. The curing reaction is thermally catalyzed: the high conversion is attained earlier at a higher temperature of curing. At the curing temperature T_c of 80°C, the complete maximum conversion reached only to a stage of α = 0.60. The glass transition at complete cure $T_{g\alpha}$ determined from the peak of loss modulus for the cured system is 106.8 (see chapter 2). T_c is much lower than $T_{g\alpha}$, thus cured epoxy is in a glassy state. As known, when the partially reacted thermoset is kept at a constant temperature in a glassy state, two different processes occur: a physical aging and a very slow increase in conversion.

At T_c where vitrification set in ($T_c = T_{g\alpha}$), there is an overall diffusion control that affects the rate of polymerizations because segmental motions are considerably slowed down [44]. Once the vitrification of the epoxy systems has passed, the reaction is dominated by the diffusion effect. If the cure temperature is too low, then the final conversion never reaches the unity [22]. This is well resolved on the conversion versus time traces in Figure 4.6. As the curing temperature increases to 85, 90, 95, 100 and 105°C, the complete maximum conversion rises to 0.70, 0.89, 0.90, 0.92 and 0.99, respectively. This unique relationship between T_g and conversion is striking because one would expect that different network structures result from cure at different temperatures. When different types of silica powders are added, conversion α, as a function of time *t*, changes as shown in Figures 4.7(a) to 4.7(d).

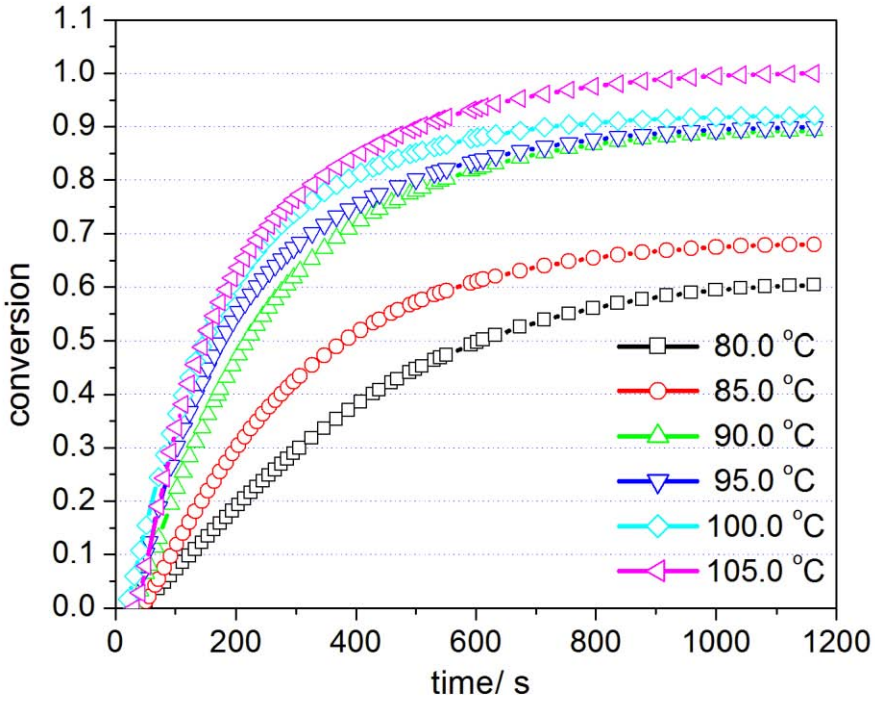

Figure 4.6. Conversion as a function of time for pure epoxy curing with cycloaliphatic amine at different curing temperatures.

For the epoxy composites filled with neat silica, the complete maximum conversion is reduced compared to the pure epoxy. Possibly, the silica molecules interfere with functional groups of reacting monomers. As a consequence, the final network of epoxy resin in the presence of neat silica is not built as homogeneously and tightly as that of the pure epoxy resin [22]. The reduction of a final conversion may be traced to the fact that the silica particles adsorb the reacting monomers at their surfaces, thus affecting the stoichiometry and creating some steric hindrance in respect to the forming network.

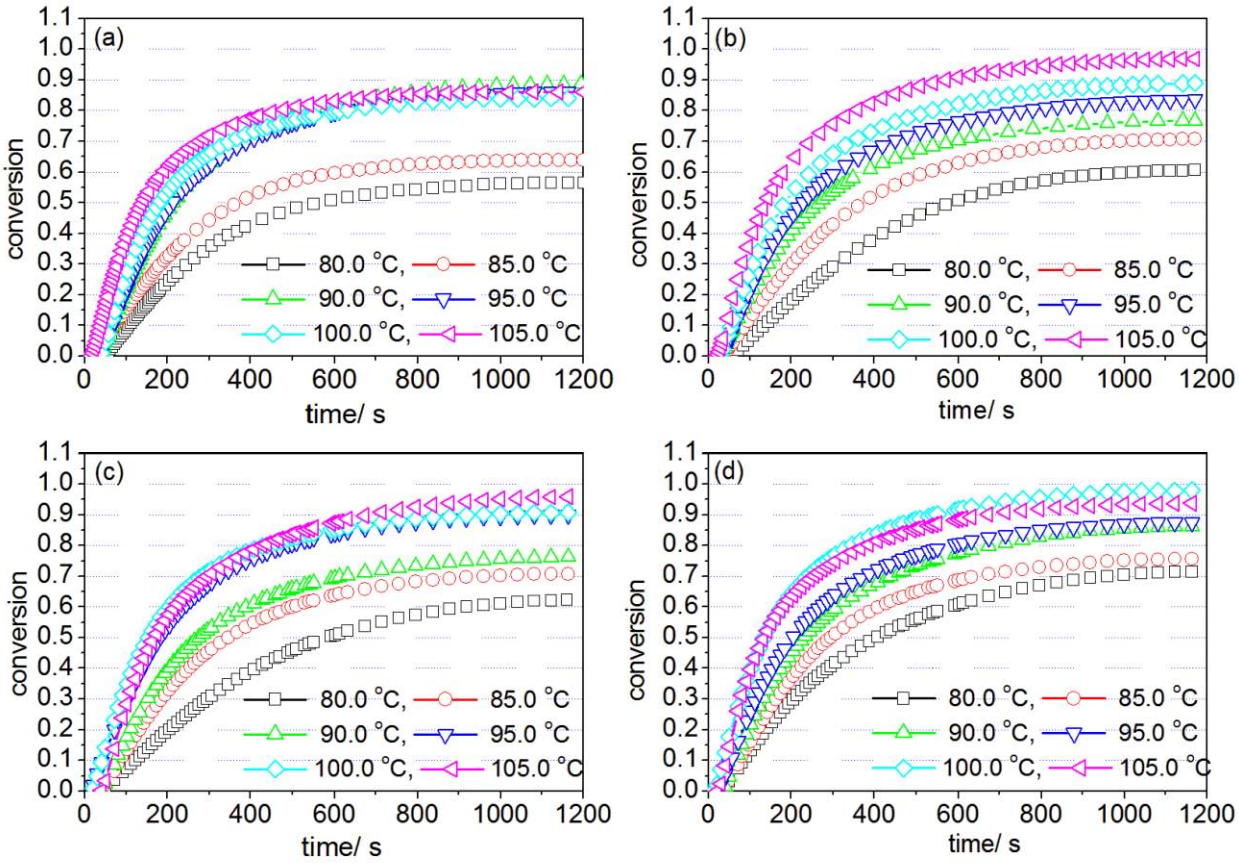

Figure 4.7. Conversion as a function of time for (a) epoxy+neat silica, (b) epoxy+silica-GPS, (c) epoxy+silica-MAMS and (d) epoxy+silica-MPS curing with cycloaliphatic amine at different curing temperatures.

On the other hand, even though fraction of conversions α for the epoxy + surface-treated silica systems are still lower than that of the pure epoxy system, they are slightly higher than that of neat silica. This is because surface-treated silica can be chemically incorporated into the network. Their heat of reactions thereby contributes to the final conversion. The chemical reactions for each surface-treated silica and epoxy-amine system are shown in scheme 4.2.

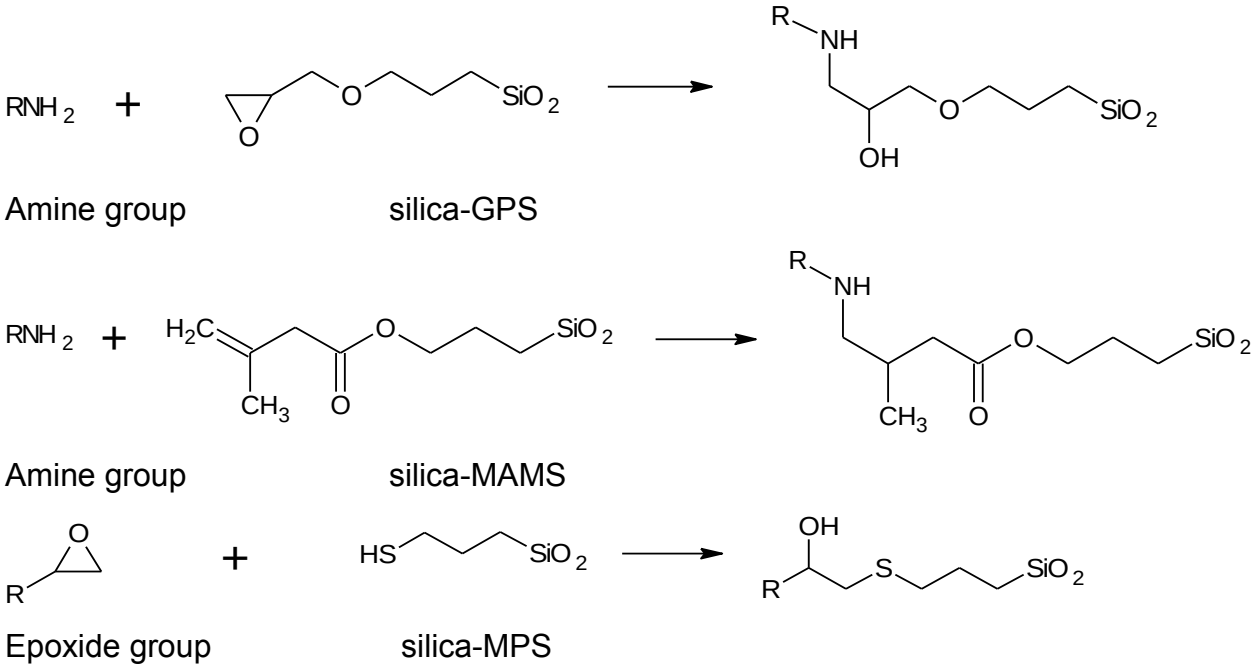

Scheme 4.2. The chemical reactions occurring in each surface- modified silica and epoxy-amine systems.

Figures 4.8 (a) to 4.8(e) show the isothermal rate of curing reaction versus time for curing of the pure epoxy as well as the epoxy + silica systems at 80, 85, 90, 95, 100 and 105^{o}C, respectively. The curves show that the rate of cure increases with increasing curing temperature, and they show a maximum reaction rate at time greater than zero. Thus the nth-order curing kinetics becomes invalid; autocatalytic model is applicable instead. However, the maximum rate is observed at a conversion too low to be a pure autocatalytic reaction because the maximum rate of the autocatalytic reaction usually shows at about 30-40% of reaction [4]. For most of the systems, the maximum peak value of the rate of reaction is higher and shifted to a shorter period of time as the curing temperature increases. The time at maximum rate of reaction, t_p, and the maximum rate of reaction, r_p, at different curing temperatures are shown in Table 4.5.

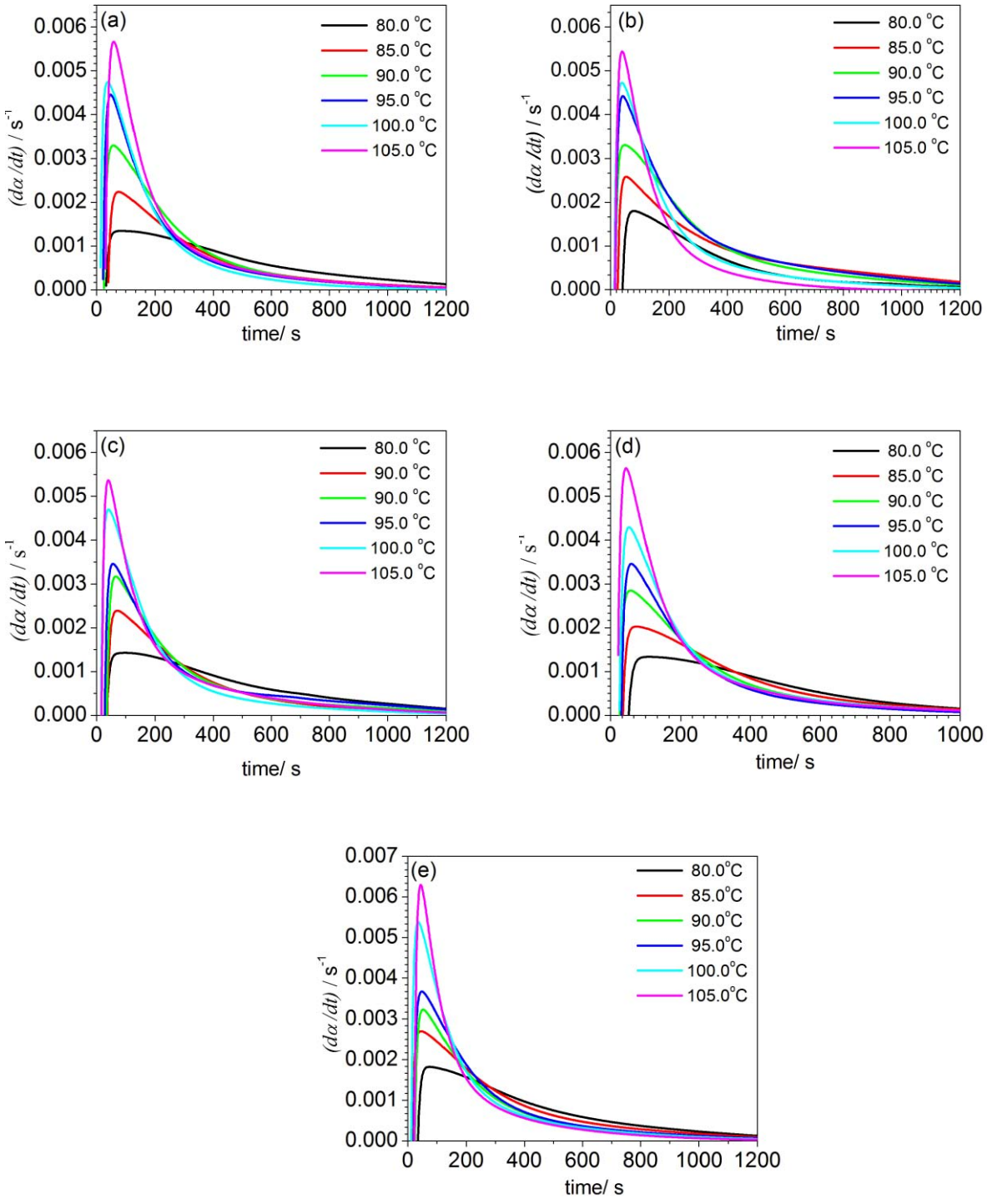

Figure 4.8. Reaction rate as a function of time for (a) pure epoxy, (b) epoxy + neat silica, (c) epoxy + silica-GPS, (d) epoxy + silica-MAMS and (e) epoxy + silica-MPS curing with cycloaliphatic amine.

Table 4.5. Time at maximum rate of reaction t_p and maximum rate of reaction r_p at different curing temperatures.

curing temperature / °C	pure epoxy		epoxy + neat silica		epoxy + silica-GPS		eoxy + silica-MAMS		epoxy + silica-MPS	
	t_p / min	r_p / s^{-1}	t_p / min	r_p / s^{-1}	t_p / min	r_p / s^{-1}	t_p / min	r_p / s^{-1}	t_p / min	r_p / s^{-1}
80.0	1.43	1.33×10^{-3}	1.33	1.79×10^{-3}	1.60	1.44×10^{-3}	1.75	1.33×10^{-3}	1.01	2.19×10^{-3}
85.0	1.26	2.24×10^{-3}	0.87	2.09×10^{-3}	1.18	2.40×10^{-3}	1.03	2.21×10^{-3}	1.02	2.66×10^{-3}
90.0	0.96	3.30×10^{-3}	1.05	3.64×10^{-3}	1.11	3.16×10^{-3}	1.15	2.83×10^{-3}	0.99	3.61×10^{-3}
95.0	0.81	4.44×10^{-3}	1.08	3.80×10^{-3}	0.48	3.67×10^{-3}	0.96	3.48×10^{-3}	0.81	3.69×10^{-3}
100.0	0.64	4.74×10^{-3}	1.03	4.83×10^{-3}	0.68	4.70×10^{-3}	0.88	4.30×10^{-3}	0.60	5.38×10^{-3}
105.0	0.98	5.64×10^{-3}	0.42	6.07×10^{-3}	1.12	5.36×10^{-3}	0.74	5.63×10^{-3}	0.74	6.31×10^{-3}

It is found in Table 4.5 that changes in r_p and t_p, as the introduction of various types of silica into the epoxy systems, are quite complex; the dependency on the types of silica changes as a curing temperature T_c varies. These are because of the dependence of curing mechanisms on the curing temperature T_c. Moreover, side reactions, apart from the reaction between epoxy and cycloaliphatic amines, have occurred (see Scheme 4.2), and their reaction rates are known as the temperature dependence.

Due to the maximum rate of the reaction occurring at time greater than zero, the autocatalytic kinetics, expressed by Kamal as given in Equation (4.4), were selected to represent the experimental isothermal curing behavior of these epoxy systems. To obtain the parameters of Equation (4.4), namely k_1, k_2, m and n, from the experimental data, several methods have been proposed [45-47]. One of them was that the total reaction order was assumed to be 2, $m+n$ = 2, which constrained the range of application of the model. Another was that calculated k_1 first from the intercept of the isothermal thermogram [20], and then determined k_2, m, and n by non-linear least square method. However, in this work, the parameters k_1, k_2, m and n were determined using the Levenberg-Marquardt non-linear regression analysis [48] without any constraints on them. The examples of the plot of reaction rate $d\alpha/dt$ as a function of conversion α, and the fitting curve obtained are shown in Figures 4.9 (a) to 4.9 (e). It is found that the chosen model shows a good fit with the experimental data in the initial stage of reaction. Deviations are observed at the very last step of cure. This is expected since the diffusion effect dominates the reaction at high conversion [6, 7, 22, 28, 32]. The kinetic parameters m, n and $m+n$, obtained for all curing systems as a function of curing

temperature, are shown in Table 4.6. The overall reaction order ($m+n$) are observed to be in the range of 1.7 to 3.0 for all the systems. The parameters m, n and $m+n$ show no temperature dependence. The temperature dependence of the Arrhenius relationship (Equation 4.9) for the rate constants k_1 and k_2, is shown in Figure 4.10. Only the autocatalytic rate constant k_2 shows a good correlation with temperature whereas the correlation for the externally catalyzed rate constant k_1 is found to be poor. However, the overall tendency is the increasing k_1 as a temperature increases. Thus, in order to determine E_{a1}, k_1 from at least 3 different temperatures was arbitrarily chosen and fitted with the Arrhenius equation (Equation 4.9). Activation energies E_{a1} and E_{a2}, calculated from $-R$ × the slope of the plot $\ln k$ as a function of $1/T$, are tabulated in Table 4.7.

It is found in Table 4.7 that, apart from silica-GPS, either neat silica or surface-treated silica causes E_{a1} of the epoxy to decrease. The epoxy resin in the presence of neat silica and silica-MPS show a significant decrease in E_{a1} while the resin in the presence of silica-MAMS shows an increase in E_{a1}, compared to the pure epoxy. According to Horie et al. [5], E_{a1} is the activation energy of the reaction catalyzed by proton donors initially present in the system. Thus, it could be inferred from the results that silica bearing hydroxyl groups(R-OH) and silica bearing mercaptan groups (R-SH) somehow accelerate the reaction between amine and epoxy groups, while silica bearing acrylate ester functional groups on the surface retards the reaction.

As proposed by many researchers and pointed out in Smith's classic article [49], the cross-link of epoxy resin by polyamino-compound is accelerated by a large number of compounds capable of acting as hydrogen-bond donors, but retarded by molecules

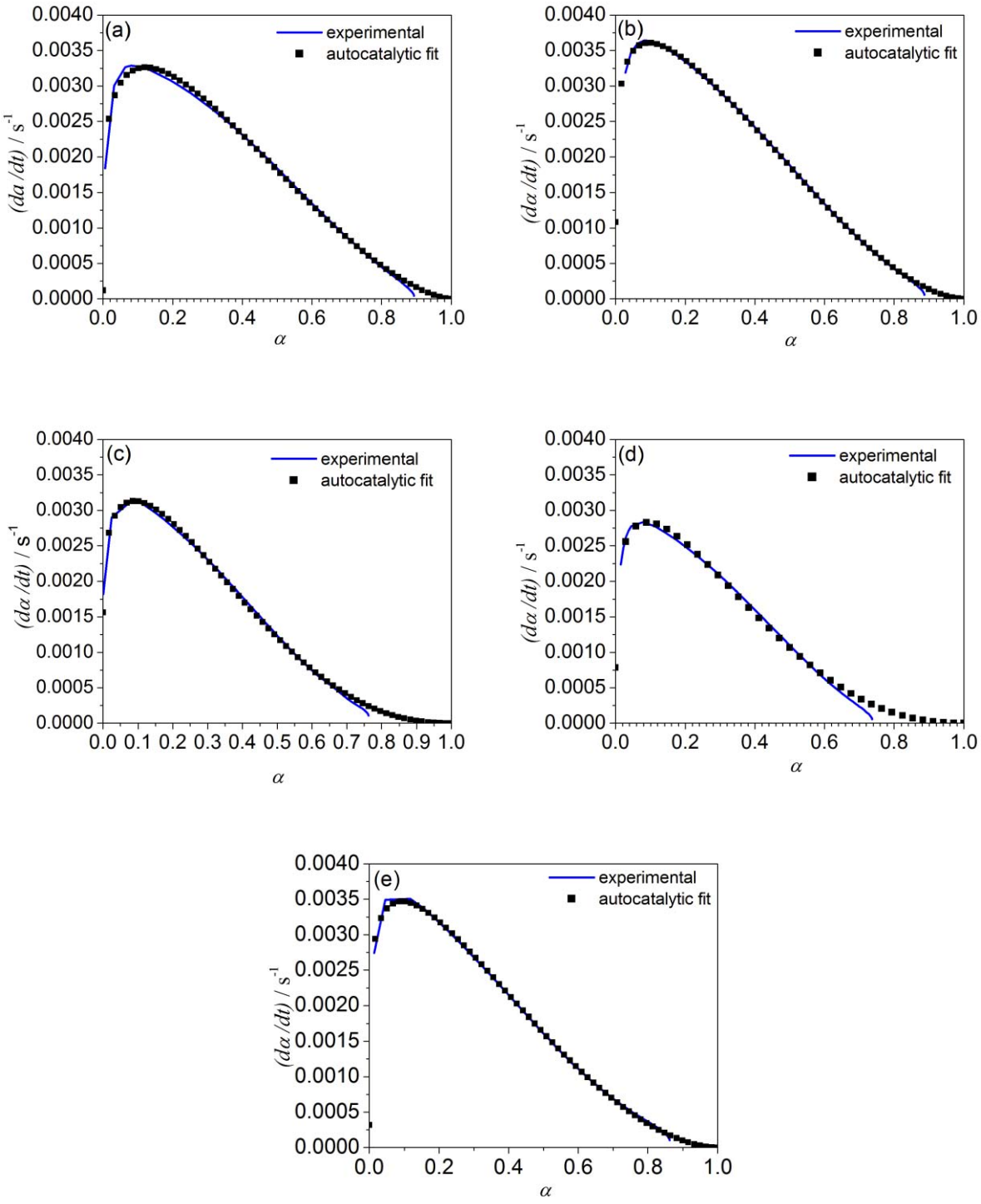

Figure 4.9. Comparison of experimental data with model predictions: rate versus conversion at 90°C for (a) pure epoxy, (b) epoxy + 10.0 phr of neat silica, (c) epoxy + 10.0 phr of silica-MAMS, (d) epoxy + 10.0 phr of silica-GPS and (e) epoxy + 10.0 phr of silica-MPS curing with cycloaliphatic amine.

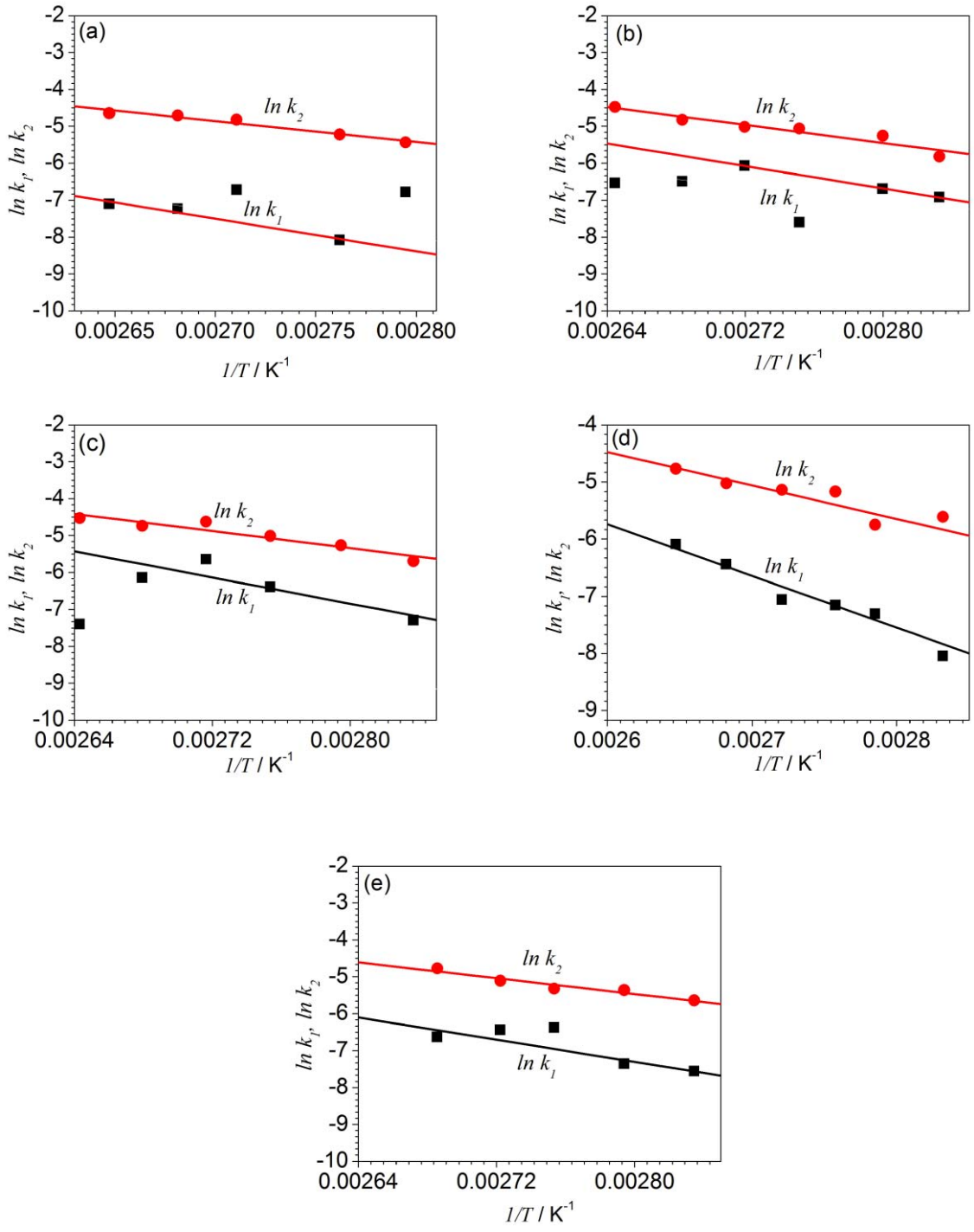

Figure 4.10. Temperature dependence of rate constant k_1 and k_2 in Kamal's equation (Equation 4.4) for (a) pure epoxy, (b) epoxy + 10.0 phr neat silica, (c) epoxy + 10.0 phr silica-GPS, (d) epoxy + 10.0 phr silica-MAMS and (e) epoxy + 10.0 phr silica-MPS curing with cycloaliphatic amine.

Table 4.6. Kinetic parameters k_1, k_2, m and n as determined from the autocatalytic kinetic model for epoxy + 10.0 phr silica at various curing temperatures.

T / °C	pure epoxy			epoxy + neat silica			epoxy + silica-GPS			epoxy + silica-MAMS			epoxy + silica-MPS		
	m	n	$m+n$	m	n	$m+n$	m	n	$m+n$	m	n	$m+n$	m	n	$m+n$
80.0	0.27	1.84	2.12	0.27	1.46	1.73	0.45	2.43	2.88	0.26	2.78	3.04	0.23	2.06	2.29
85.0	0.40	2.46	2.86	0.42	2.38	2.80	0.24	2.29	2.53	0.21	1.50	1.71	0.25	1.96	2.22
90.0	0.19	1.51	1.70	0.22	1.68	1.90	0.44	2.45	2.90	0.30	2.34	2.64	0.25	1.86	2.11
95.0	0.29	1.88	2.17	0.46	1.98	2.44	0.40	2.46	2.86	0.24	1.92	2.15	0.33	1.81	2.15
100.0	0.27	1.69	1.95	0.25	2.05	2.29	0.39	1.88	2.26	0.26	1.83	2.10	0.24	1.57	1.81
105.0	0.25	1.53	1.78	0.29	1.97	2.26	0.31	1.79	2.10	0.30	1.65	1.95	0.27	1.99	2.27

Table 4.7. Activation energy determined using isothermal scan method of pure epoxy resin and epoxy composites filled with different types of silica at 10 phr.

type of silica	E_{a1} / kJ/mol	E_{a2} / kJ/mol
neat silica	62.7	50.6
silica-GPS	73.4	48.3
silica-MAMS	75.1	48.6
silica-MPS	62.4	44.6
pure epoxy	73.5	47.3

capable of acting as hydrogen-bond acceptors. Thus, plausible explanations are as follows.

Hydroxyl (R-OH) and mercaptan (R-SH), which act as proton donors, form hydrogen bonds with epoxide groups with the following preferred arrangement—the hydrogen atom of the proton donor and lone pair electrons of the acceptor are in a straight line—as demonstrated in scheme 4.3. Thus, it is expected that a nucleophilic reagent (e.g. amine) reacts more readily with a hydrogen-bonded epoxide molecule than with a normal epoxide molecule. A mechanism for such a reaction is shown in scheme 4.4. On the other hand, an acrylate ester functional group, consisting of ester and double bond on the surface of silica-MAMS, acts as proton acceptors. Thus, the retardation of the reaction is observed. When silica-GPS is added to the epoxy, no change in E_{a1} is found. This is because of the similarity of functional groups (glycidyl groups) at the surface of silica to the reactive group of epoxy resin. Thus, neither acceleration nor retardation is observed.

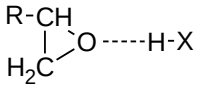

where H-X is any hydrogen-bond donor molecules

Scheme 4.3. The arrangement of a hydrogen-bonded epoxide molecule.

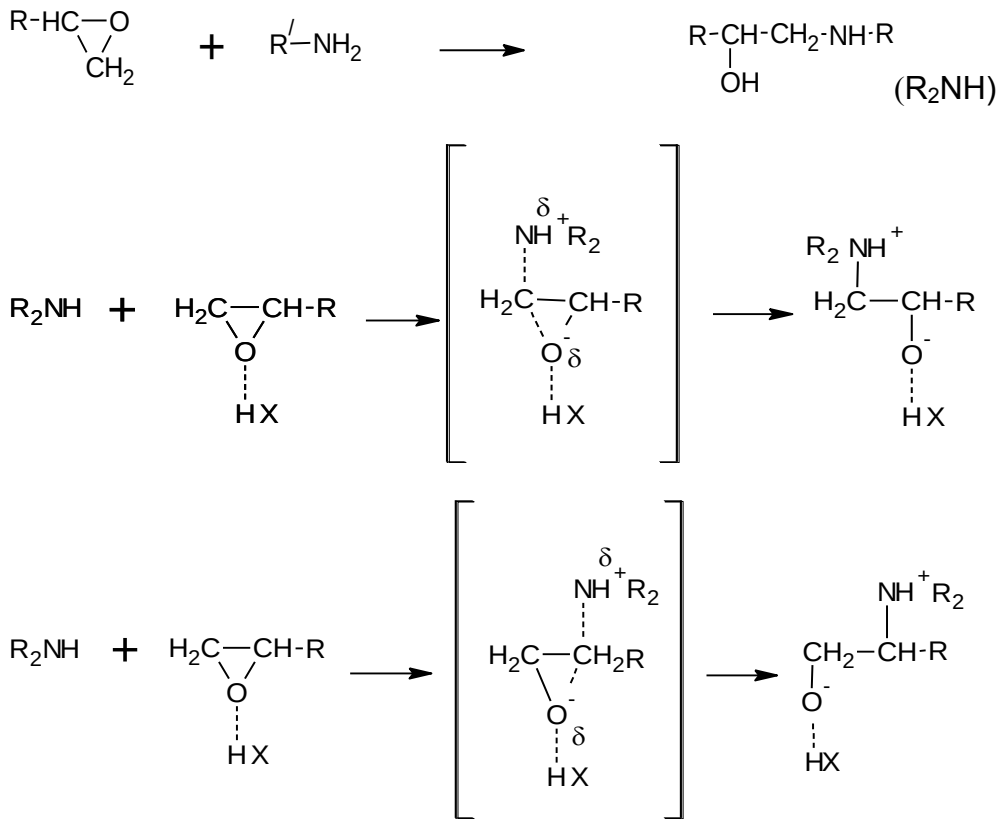

Intermediate compound

Scheme 4.4. Possible mechanisms of epoxy-amine reactions.

Incidentally, E_{a2} of epoxy systems show only slight changes when silica particles are added, compared with the changes found in E_{a1}. Neat silica, silica-MAMs and silica-GPS cause E_{a2} to increase to 3.3, 1.6 and 1.0, respectively. The steric hindrances and/or heat absorption due to the presence of neat silica on the system contribute to the increase in E_{a2} for the epoxy + neat silica [42]. Due to a small change in E_{a2} compared to the pure epoxy, an explanation similar to that for E_{a1} should apply for epoxy + silica-GPS. For the silica-MAMS, the acrylate ester function group, present on the surface of silica, can react with amine curing agent. This reaction results in a bulky secondary amine, which obstructed the further reaction of amine and epoxide groups rather than

readily promoting the reaction as usual. The heat, generated from the reaction of acrylate ester with amine curing agent, contributes to the total heat of reaction of the system, causing somehow a decrease in E_{a2} compared to the epoxy composites filled with neat silica.

It is found only in case of epoxy with silica-MPS that E_{a2} is lower than that of pure epoxy. E_{a2} is the activation energy for the reaction catalyzed by proton donors which are produced during curing. Possible explanations are as follows. Mercaptan on the surface of silica can react with an epoxide group (see scheme 4.2) and form the product containing the proton donor (hydroxyl group), which serves as a catalyst. In addition, the reaction rate of mercaptan and epoxy group was reported to be faster than that of the epoxy-amine reaction [42].

C. General remarks.

The cure kinetics of the pure epoxy and the epoxy composites using the cycloaliphatic amine (AMICURE®PACM) as hardener was investigated by means of DSC both isothermally at various temperatures and dynamically at various heating rates. The silica molecules interfere with functional groups of reacting monomers; maximum conversions are found to be reduced when 10.0 phr of any type of silica particles are added. The activation energy of overall reactions determined using the Kissinger and Ozawa methods are affected by addition of silica-MAMS and MPS whose functional groups could react with amine and epoxy, respectively.

The kinetic parameters obtained from the dynamic experiments are inconsistent with isothermal experiments, like those results found by Riccardi et al. [50] who investigated the differences between isothermal and dynamic scan DSC measurements for a

diglycidyl ether curing with ethylenediamine systems. One should keep in mind that, unlike the autocatalytic isothermal analysis, the dynamic DSC analysis does not separate the different types of reaction mechanisms. Values obtained from both the Kissinger and Ozawa methods are an overall value representing all complex reactions that occur during cure. The mechanisms of epoxy + silica curing with cycloaliphatic amines are complex; several side reactions and many paths of reactions occur.

4.8 References

[1] Shechter L, Wynstra J, Kurkjy RP. Ind Eng Chem 1956;48:94-97.

[2] Lui H, Uhlherr A, Varley RJ, Bannister MK. J Polym Sci Polym Chem 2004;42:3143-3156.

[3] IUPAC Compendium of chemical terminology, electronic version, http://goldbook.iupac.org/R05141.html. (06/17/2007),

[4] Prime RB. Thermosets. In: Turi EA, editor. Thermal characterization of polymeric materials
New York: Academic Press, 1981. p 972.

[5] Horie K, Hiura H, Sawada M, Mita I, Kambe H. J Polym Sci A-1 1970;8:1357-1372.

[6] Kamal AR, and Sourour, S. Polym Eng Sci 1973;13:59-64.

[7] Kamal MR. Polym Eng Sci 1974;14:231-239.

[8] Sourour S, Kamal MR. Thermochim Acta 1976;14(1-2):41-59.

[9] Lee SN, Chiu MT, Lin HS. Polym Eng Sci 1992;32:1037-1046.

[10] Zvetkov VL. Polymer 2001;42(16):6687-6697.

[11] Ozawa T. J Thermal Anal 1970;2:301-324.

[12] Fava RA. Polymer 1968;9:137-151.

[13] Brown ME, Maciejewski M, Vyazovkin S, Nomen R, Sempere J, Burnham A, Opfermann J, Strey R, Anderson HL, Kemmler A, Keuleers R, Janssens J, Desseyn HO, Li C-R, Tang TB, Roduit B, Malek J, Mitsuhashi T. Thermochim Acta 2000;355(1-2):125-143.

[14] Malek J, Criado JM. Thermochim Acta 1994;236:187-197.

[15] Vyazovkin S. Thermochim Acta 1994;236:1-13.

[16] Vyazovkin S. Thermochim Acta 1992;200:461-466.

[17] Vyazovkin S, Linert W. Thermochim Acta 1995;269-270:61-72.

[18] Vyazovkin SV, Lesnikovich AI. Thermochim Acta 1988;128:297-300.

[19] Miller RL, Oebser MA. Thermochim Acta 1980;36(2):121-131.

[20] Dutta A, Ryan ME. J Appl Polym Sci 1979;24:635-649.

[21] Lem KW, Han CD. J Appl Polym Sci 1983;28:3185-3206.

[22] Harsch M, Karger-Kocsis J, Holst M. Eur Polym J 2007;43(4):1168-1178.

[23] Macan J, Ivankovic H, Ivankovic M, Mencer HJ. Thermochim Acta 2004;414(2):219-225.

[24] Serier A, Pascault JP, My LT. J Polym Sci Polym Chem 1991;29(2):209-218.

[25] Barral L, Cano J, Lopez AJ, Lopez J, Nogueira P, Ramirez C. Thermochim Acta 1995;269-270:253-259.

[26] Barral L, Cano J, Lopez J, Lopez-Bueno I, Nogueira P, Ramirez C, Torres A, Abad MJ. Thermochim Acta 2000;344(1-2):137-143.

[27] Punchaipetch P, Ambrogi V, Giamberini M, Brostow W, Carfagna C, D'Souza NA. Polymer 2001;42(5):2067-2075.

[28] Thomas R, Durix S, Sinturel C, Omonov T, Goossens S, Groeninckx G, Moldenaers P, Thomas S. Polymer 2007;48(6):1695-1710.

[29] Abuin SP, Pellin MP, Nunez L. J Appl Polym Sci 1990;41:2155-2167.

[30] Abuin SP, Pellin MP, Nunez L, Gandara JS, Losada PP. J Appl Polym Sci 1993;47:533-541.

[31] Carrozino S, Levita G, Rolla P, Tombari. Polym Eng Sci 1990;41:2155-2161.

[32] Boey FYC, Qiang W. Polymer 2000;41(6):2081-2094.

[33] Flammersheim HJ, Horhold HH, Bellstedt K, Klee J. Makromol Chem 1983;184:113-121.

[34] Scott EP, Saad Z. Polym Eng Sci 1993;34:1165-1169.

[35] Spacek V, Pouchly J, Biros J. Eur Polym J 1987;23:377-382.

[36] Zvetkov VL. Polymer 2002;43(4):1069-1080.

[37] Barral L, Cano J, Lopez J, Lopez-Bueno I, Nogueira P, Abad MJ, Ramirez C. Polymer 2000;41:2657-2666.

[38] Barral L, Cano J, Lopez J, Lopez-Bueno I, Nogueira P, Torres A, Ramirez C, Abad MJ. Thermochim Acta 2000;344(1-2):127-136.

[39] Montserrat S, Martin JG. Thermochim Acta 2002;388(1-2):343-354.

[40] Marsella JA, Starner WE. J Polym Sci Polym Chem 2000;38:921-930.

[41] Matynai T, Gawdzik B. J Appl Polym Sci 1997;65(8):1525-1531.

[42] McAdams LV, Gannon JA. Epoxy resin. In: Mark HF, editor. Encyclopedia of polymer science and engineering, vol. 6. New York: Wiley, 1985.

[43] Catalani A, Bonicelli MG. Thermochim Acta 2005;438(1-2):126-129.

[44] Pascault JP, Sautereau H, Verdu J, Willaims RJJ. Thermosetting polymers, NY: Marcel Dekker, 2002.

[45] Barral L, Cano J, Lopez AJ, Lopez J, Nogueira P, Ramirez C. J Appl Polym Sci 1995;56:1029-1037.

[46] Kenny JM. J Appl Polym Sci 1994;51:761-764.

[47] Moroni A, Mijovic J, Pearce E, Foun CC. J Appl Polym Sci 1986;32:3761-3773.

[48] Tutorial manual, Origin 6; Microcal Software: Northampton, 1999.

[49] Smith LT. Polymer 1961;2:95-108.

[50] Riccardi CC, Adabbo HE, Willaims RJJ. J Appl Polym Sci 1984;29:2481-2492.

CHAPTER 5

CONCLUDING REMARKS

In this dissertation, two different approaches have been used to modify a commercial epoxy resin for improving its tribological performance. One is the incorporation of an inorganic filler, namely silica particles, into a commercial epoxy resin by a conventional blending method. The other is the incorporation of fluorine-modified epoxy oligomer, diglycidyl of trifluoromethyl aniline (DGTFA), into a commercial epoxy.

For the first approach, the effects of silica loading, as well as the silica surface treatment, were studied for not only the changes in tribological properties but also the properties related. The results of this study indicate that epoxy composites with silica exhibit different mechanical and tribological properties from the pure epoxy resin. Depending on the types of silane coupling agents used for silica surface treatment, the optimum silica content for the improved thermal, mechanical and tribological properties in each epoxy composite is different. Specific conclusions can be drawn as follows:

1. The activation energy of overall reactions is affected by the addition of silica-MAMS and silica-MPS whose functional groups could react with amine and epoxy, respectively. It is shown that silica-MPS accelerates the curing reaction of the epoxy DGEBA + cycloaliphatic amine system while silica-MAMS tends to retard the reaction.
2. Silica particles cause a slight improvement in thermal stability of epoxy resin. However, this behavior depends on the types of silica powder. The epoxy composites filled with silica-GPS show the highest thermal stability. Low cross-link density of the epoxy composites and high thermal resistance of

inorganic silica contribute to changes in thermal stability of epoxy composites filled with silica.

3. Chemical surface treatment of silica affects the change in the dynamic mechanical parameters and tensile properties of epoxy. Regardless of the agglomeration of silica at high silica content, interfacial interaction between silica and epoxy matrix increases stiffness of epoxy composites filled with surface-treated silica whereas lower degree of cross-link density decreases their stiffness. Regardless of the types of silane-treated silica, strain at break and tensile strength decrease with increasing silica content. However, due to higher interfacial interaction, the surface-treated silica provides strain at break and strength higher than the neat silica.
4. Even though changes in wear mechanisms as a function of silica content and the siliane-surface treatment still have not been fully understood, it is found from this study that the tribological behavior at high silica loading varies for a variety of reasons, including cross-link density, interface layer between particle surface adherence and epoxy, weakening of bulk epoxy, abrasive action of hard particles and the agglomeration of particles. Moreover, this study clearly shows that the homogeneous and tenacious transfer film contributes to the improvement in the wear resistance and friction coefficient of epoxy composites filled with silica.
5. The improvement in tribological properties, namely low friction coefficient and low wear rate, are observed in silica + epoxy composites; these properties depend on the type of silica in epoxy. The epoxy composites filled with silica-

MPS provide the best tribological properties, compared to other systems. The optimum silica content for the improvement both in wear resistance and in friction coefficient is about 10.0 phr for the epoxy composites filled with neat silica, about 5.0 phr for the composites filled with silica-MAMS, about 10.0 phr for the composites filled with silica-GPS, and about 15.0 phr for the composites filled with silica-MPS.

6. The mechanical properties cannot alone account for the observed differences in tribological behavior at a high pv condition—the improvement in wear resistance is found despite a measured deterioration in mechanical properties. There is no such a correlation of the bulk mechanical properties and wear resistance found in the epoxy composites filled with silica.

For the second approach, the effects of DGTFA content are investigated. The results indicate that DGTFA affects the thermal stability, mechanical and tribological properties as well as the curing kinetics of the of commercial DGEBA epoxy. The specific conclusions can be drawn as follows:

1. Due to the catalytic effect of DGTFA whose molecular backbone contains tertiary amine functional groups, the curing reaction of epoxy with polyamine is accelerated when DGTFA is added. Eventually, due to the bulky long chains, this acceleration effect reduces when a large amount of DGTFA (more than 15.0 phr) is added. Moreover, it is shown in the TGA analysis that the incorporation of tertiary amines into the system results in a reduction in thermal stability of commercial epoxy.

2. The storage modulus in glassy state increases significantly as a function of DGTFA content due to the antiplasticization effect. Provided that the direct plasticization effects (decrease of T_g) are acceptable, this system could be interesting for certain applications.
3. Tribological properties, both high wear resistance and low friction coefficient, are achieved by incorporation of DGTFA into the commercial epoxy. At least for the range of this study, while increasing the amount of DGTFA, both wear rate and friction coefficient are reduced. It is found that the increase in toughness of bulk material together with the formation of transfer film contributes to the reduction in friction coefficient and wear rate for this system. Moreover, the product of flexural strength and strain at deflection point, which is used to indicate the toughness of materials, is found to correlate with the reduction in wear rate.

APPENDIX A

CONTACT AREA, MAXIMUM CONTACT PRESSURE AND AVERAGE CONTACT PRESSURE

The evaluation of contact parameters is essential in many practical engineering applications. The most frequently used contact parameters are: the contact area dimensions, maximum contact pressure and average contact pressure. The contact area and contact pressure depend on the geometry of the contacting bodies, load and material properties. In the present studies, a flat surface (an epoxy resin) is in contact with a convex surface (a Si_3N_4 ball). The contact area between a sphere and a plane surface is circular. The geometry of these two contact surfaces is shown in Figure I. The contact parameters can be calculated as follows [1]:

Radius of the contact area (m), $a = \left(\frac{3WR^*}{E^*}\right)^{1/3}$ (1)

Average contact pressure (Pa), $p_{average} = \frac{W}{\pi a^2}$ (2)

Maximum contact pressure (Pa), $p_{max} = \frac{3W}{2\pi a^2}$ (3)

where W is the normal load (N), E^* is the reduced modulus (Pa) and R^* is the reduced radius of curvature (m).

The reduced radius of curvature is defined as:

$$\frac{1}{R^*} = \frac{1}{R_X} + \frac{1}{R_y} = \frac{1}{R_{Ax}} + \frac{1}{R_{Ay}} + \frac{1}{R_{Bx}} + \frac{1}{R_{By}} \quad (4)$$

The radii of the curvature of a plane surface are infinite, and symmetry of the sphere applies. The $R_{Bx} = R_{By} = \infty$ and $R_{Ax} = R_{Ay} = R_A$. Thus, the reduced radius of curvature is given by:

$$\frac{1}{R^*} = \frac{2}{R_A} \quad (5)$$

The reduced Young's modulus is defined as:

$$\frac{1}{E^*} = \frac{1}{2}\left[\frac{1-\nu_A^2}{E_A} + \frac{1-\nu_B^2}{E_B}\right] \quad (6)$$

[1] Stachowiak G, Batchelor AW. Engineering tribology. 3rd ed.; New York: Elsevier, 2005.

where ν_A and ν_B are Poisson's ratios of the contacting bodies A and B, respectively. E_A and E_B are Young's moduli of the contacting bodies A and B, respectively.

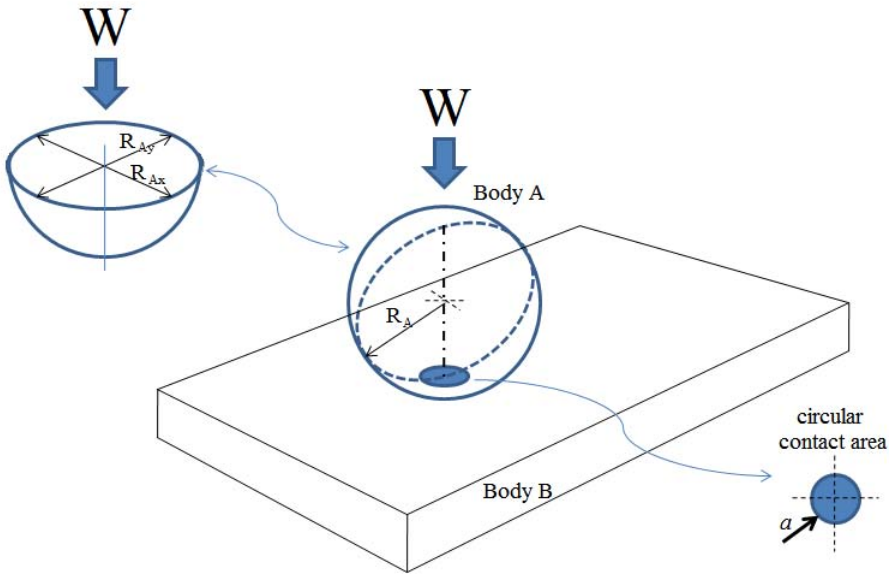

Figure A.I. Contact between a sphere and a flat surface.

In case of the epoxy curing with cycloaliphatic amine, the following parameters are used: the normal force is W = 5 N, radius of the ball is R_A = 1.6 mm, the modulus for Si_3N_4 ball is E_A = 320 GPa, the modulus for epoxy curing with cycloaliphatic amine is E_B = 1536 MPa and Poisson's ratios for Si_3N_4 ball and epoxy resin are ν_A = 0.27 and ν_B = 0.35, respectively. The obtained contact area a, average contact pressure $p_{average}$ and maximum contact pressure p_{max} are 151 μm, 70 MPa and 105 MPa, respectively.

In case of the epoxy curing with polyamine, the modulus for epoxy curing with polyamine is 459 MPa. Apart from that, the same conditions and parameters are used to estimate the contact parameters. The obtained a, $p_{average}$ and p_{max} are 226 μm, 31 MPa and 47 MPa, respectively.

APPENDIX B

MOVING HEAT SOURCE

In order to investigate the temperature distribution of the contact, the speed of a heat source needs to be quantified. Peclet number, Pe, is a non-dimensional measure of the sliding speed at which the heat source moves. This number can be interpreted as the ratio of the speed of the surface to the rate of thermal diffusion into the solid. It is defined as [2]:

$$Pe = Ua/2\kappa \quad (7)$$

where U is the velocity of a solid (m/s), a is the contact radius and κ is the thermal conductivity (W/mK).

This number is used as an indicator of the heat penetration into the bulk solid or time for the heat at sliding contact to diffuse into the stationary solid. The heat transfer between two contact-surfaces thus varies with the range of Pe as follows:

1. A small value, Pe< 0.1 means that one surface moves very slow relative to the other. There is sufficient time for the temperature distribution of the contact to be established in the stationary body.
2. An intermediate value, 0.1< Pe< 5 means that one surface moves faster than the other, and a slowly moving heat source model is assumed.
3. A large value, Pe> 5 means that one surface moves very fast relative to the other, and the flash temperature is modeled as a fast moving heat source. There is insufficient time for the temperature distribution at the contact to be established in the stationary body.

In the studies, the sliding velocity is 4.19 mm/s and the thermal conductivity of epoxy is assumed to be 0.255 W/mK [3]. Thus, the Pe for the epoxy curing with

[2] William J. Engineering tribology, New York: Cambridge University Press, 2004.
[3] Moisala A, Li Q, Kinloch IA, Windle AH. Compos Sci Technol 2006;66:1285-1288.

cycloaliphatic amine and the Pe for the epoxy curing with polyamine are 31.6 and 47.3, respectively.

APPENDIX C

FLASH TEMPERATURE IN CIRCULAR CONTACT

It is known that the energy dissipation during the process of friction is converted to heat. This frictional heat causes a local surface temperature to rise. For any specific part of the sliding surface, the frictional temperature increases last very short durations and the temperature generated is called flash temperature. It is important to know the expected number of this temperature because it can affect the friction and wear mechanisms through the alteration of the surface properties. Evaluation of the flash temperature is basically a heat transfer problem where the frictional heat generated in the contact is modeled as a heat source moving over the surface. Several assumptions are made for the analysis: the independence of thermal properties of the contacting bodies on temperature, a single area of contact as a plane source of heat, the uniformity of the frictional heat generated and the steady state condition. In case of the fast moving heat source, the average flash temperature for a circular contact due to friction is given by [1]

$$T_{fa} = 0.308 \frac{\mu W |U_A - U_B|}{Ka} \left(\frac{\chi}{Ua}\right)^{0.5} \quad (8)$$

where T_{fa} is the average flash temperature (^{o}C), μ is friction, W is the normal load (N), U_A and U_B are the surface velocities of solid A and solid B, respectively (m/s), a is the radius of the contact circle (m), χ is the thermal diffusivity (m^2/s) and K is the thermal conductivity (W/mK).

In the studies, the thermal diffusivity χ is assumed to be 1×10^{-7} m^2/s [4-5]. Thus, the tentative values of the average flash temperature are about 114^{o}C for the epoxy curing with cycloaliphatic amine and about 40^{o}C for the epoxy curing with polyamine.

[4] Morikawa J, Kurihara T, Hashimoto T, Sherbelis G. Thermochim Acta 1997;299:95-100.
[5] D'almeida JRM, Cella N, Monteiro SN, Miranda LCM. J Appl Polym Sci 1997;69:1335-1341.

APPENDIX D

AVERAGE ROUGHNESS PARAMETERS

Surface roughness most commonly refers to the variation in the height of the surface relative to a reference plane. It is usually characterized by the center-line average (R_a) and the root mean square average (R_q), skewness (Sk) and kurtosis (K).

In this study, only R_a and R_q were reported. The definitions of each parameter are given as follows [6]:

$$R_a = \frac{1}{L}\int_0^L |z - m| dx \tag{9}$$

$$m = \frac{1}{L}\int_o^L z dx \tag{10}$$

$$R_q^2 = \frac{1}{L}\int_0^L Z^2 dx \tag{11}$$

$$R_q = \sqrt{\frac{1}{L}\int_0^L Z^2 dx} \tag{12}$$

From the equation above, R_a is the arithmetic mean of the absolute values of vertical deviation from the mean line through the profile, while R_q is the root mean square of the arithmetic mean of the square of the vertical deviation from the reference line (see Figure II).

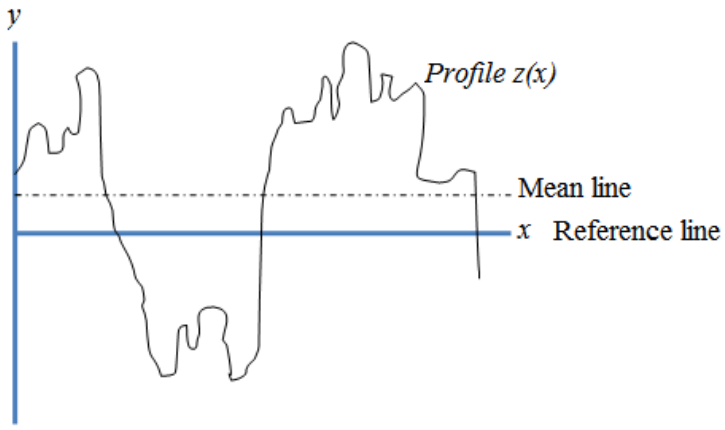

Figure A.II. Schematic of a surface profile.

[6] Bhushan B. Introduction to tribology, New York: Wiley, 2002.